SCHOOL OF MOLECULAR AND CELL BIOLOGY
UNIVERSITY OF THE WITWATERSRAND

Written research report

shRNAs targeting LRP mRNA as alternative therapeutic tools for Alzheimer's disease treatment

Danielle Gonsalves

Supervisor: Prof. S.F.T. Weiss
Co-supervisor: Prof. R. Veale

A dissertation submitted to the Faculty of Science, University of the Witwatersrand, Johannesburg, in the fulfillment of the requirements for the degree of Master of Science.

DECLARATION

I declare that this dissertation is my own, unaided work. It is being submitted for the Degree of Master of Science at the University of the Witwatersrand, Johannesburg. It has not been submitted before for any degree or examination in any other University.

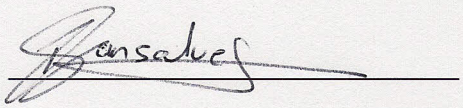

Danielle Gonsalves

4th day of March 2013

Dripping water hollows out stone, not through force but through persistence
-Ovid

ABSTRACT

Alzheimer's disease (AD) is the most prevalent neurodegenerative disease affecting in excess of 26.6 million individuals globally. The neuropathological features of AD include extracellular deposition of amyloid beta (Aβ) plaques and intracellular neurofibrillary tangle formation. The cellular prion protein (PrP^C) regulates the amyloidogenic cleavage pathway involved in Aβ shedding and interacts with the Aβ peptide. Given these interactions, the aim of this study was to investigate the influence of the 37kDa/67kDa laminin receptor (LRP/LR)- the cellular receptor for prion proteins- on Aβ shedding. Transfection of HEK293 cells with short hairpin RNAs (shRNAs) directed against LRP mRNA significantly decreased LRP levels in addition to Aβ shedding. Flow cytometric analysis revealed unchanged cell surface levels of the amyloid precursor protein (APP), β-secretase and γ-secretase after transfection of cells with shRNAs, suggesting a role of LRP/LR in Aβ shedding via a mechanism independent of gene-expression modulation of these key proteins. LRP-shRNA treatment significantly reduced sAPPβ expression, implicating LRP/LR in APP processing specifically via augmenting the activity of β-secretase. Co-localisation of LRP/LR with APP, β- and γ-secretase, respectively, alludes to a possible interaction between said proteins. Therefore, LRP-shRNAs are suggested as alternative therapeutic tools for AD treatment.

RESEARCH OUTPUTS

Original Publications

K. Jovanovic*, D. Gonsalves*, B. Da Costa Dias, K. Moodley, U. Reusch, S. Knackmuss, M. Little, C. Penny, M. Weinberg & S.F.T Weiss, The 37 kDa/67 kDa laminin receptor contributes to amyloid beta shedding in Alzheimer's Disease. *(under revision: Scientific Reports).*
* These authors contributed equally to this work.

B. Da Costa Dias, K. Jovanovic, D. Gonsalves, U. Reusch, S. Knackmuss, C. Penny, M. Little & S.F.T Weiss, Anti-LRP/LR specific antibody IgG1-iS18 rescues cells from $A\beta_{42}$ induced cytotoxicity. *(under revision: Scientific Reports).*

Reviews

A. Omar, K. Jovanovic, B. Da Costa Dias, D. Gonsalves, K. Moodley, R. Caveney, V. Mbazima, S.F.T. Weiss, Patented biological approaches for the therapeutic modulation of the 37 kDa/67 kDa laminin receptor. Expert Opin Ther Pat 21 (2011) 35-53.

B. Da Costa Dias, K. Jovanovic, D. Gonsalves, S.F. Weiss, Structural and mechanistic commonalities of amyloid-beta and the prion protein. Prion 5 (2011) 126 – 137.

Meeting reports

D. Gonsalves, K. Jovanovic, B. Da Costa Dias and S.F.T Weiss, Meeting Report: Global Alzheimer's Summit, Present and Future of Alzheimer's Disease Research. Prion 6 (2012) 1-4.

Patents

Patent Title: Treatment of Alzheimer's Disease
Inventors: Stefan Franz Thomas Weiss, Katarina Jovanovic, Danielle Gonsalves, Bianca Da Costa Dias, Stefan Knackmuss, Uwe Reusch, Melvyn Little
PCT Application number: PCT/IB2012/054918

Conferences

Mini Cell and Developmental Symposium
Wits Medical School
22 May 2011
Poster presentation
Title: The 37kDa/67kDa Laminin receptor specific antibody IgG1-iS18 impedes Aβ shedding in Alzheimer's Disease.
Authors: Katarina Jovanovic, Danielle Gonsalves, Bianca Da Costa Dias and Stefan F.T. Weiss

Global Alzheimer's Summit - Present and Future Alzheimer's Research
Palacio de Congresos de Madrid, Madrid, Spain
September 22-23, 2011
Poster presentation
Title: Antibodies targeting the 37kDa/67kDa Laminin receptor impede amyloid beta shedding in Alzheimer's Disease
Authors: Katarina Jovanovic, Danielle Gonsalves, Bianca Da Costa Dias, Stefan Knackmuss, Uwe Reusch, Melvyn Little and Stefan F.T. Weiss

Molecular Biology Research Thrust (MBRT) Research Day
Wits Professional Development Hub, Empire Road, Johannesburg
7 December 2011
Poster presentation
Title: The 37kDa/67kDa laminin receptor plays a role in amyloid beta shedding in Alzheimer's Disease
Authors: Katarina Jovanovic, Danielle Gonsalves, Bianca Da Costa Dias, Stefan Knackmuss, Uwe Reusch, Melvyn Little and Stefan F.T. Weiss

SASBMB/FASBMB Congress 2012
Champagne Sports Resort, Drakensberg, KwaZulu-Natal, South Africa
29 January – 1 February 2012
Poster presentation
Title: Antibodies targeting the 37kDa/67kDa laminin receptor impede amyloid beta shedding in Alzheimer's Disease
Authors: Katarina Jovanovic, Danielle Gonsalves, Bianca Da Costa Dias, Stefan Knackmuss, Uwe Reusch, Melvyn Little and Stefan F.T. Weiss

3rd Annual Alzheimer's SA, Gauteng, One-day seminar 'Dementia: Living together'
Linder Auditorium, 27 St Andrews Road, Parktown, Johannesburg
12 September 2012
Attendance only

WITS Faculty of Health Science: Research day and Postgraduate expo
University of the Witwatersrand, Medical School
19 September 2012
Attendance only

4th Cross-faculty symposium, 2012
Wits Professional Development Hub, Empire Road, Johannesburg
19 and 22 September 2012
Poster presentation
Title: shRNA targeting LRP mRNA impede amyloid beta shedding in Alzheimer's disease
Authors: Daniele Gonsalves, Clement Penny, Marco Weinberg and Stefan F.T. Weiss.

Molecular Biosciences Research Thrust (MBRT), 2012
Wits Professional Development Hub, Empire Road, Johannesburg
5 December 2012
Oral presentation
Title: shRNA direct against LRP mRNA as an alternative therapeutic tool for Alzheimer's treatment

ACKNOWLEDGEMENTS

I would like to thank my supervisor, Prof. S.F.T. Weiss for his guidance and support throughout the year, and reminding me that 'science takes time'. My thanks to Prof. M. Weinberg for his assistance with the shRNA design and production. To Dr. C. Penny, my gratitude for all of his assistance with the immunofluorescence microscopy.

To all the GERMANators of GH614, a big thank-you for always making me laugh. Without you science would have definitely 'eaten my soul.' Above all I would like to thanks my family and friends for all their encouragement, and pretending to be interested when 'I talk science'.

My sincere appreciation to the University of the Witwatersrand postgraduate merit fund and National Research Foundation (NRF), Republic of South Africa (RSA). Without you funding, this MSc would not have been possible.

TABLE OF CONTENTS

LIST OF FIGURES

LIST OF TABLES

ABBREVIATIONS

AAV	Adeno-associated virus
AD	Alzheimer's disease
ADAMs	A disintegrin and metalloproteinases
Ago2	Argonaut 2
AICD	Amino-terminal APP intracellular domain
APH	Anterior pharynx defective
APOE	Apolipoprotein E
APP	Amyloid precursor protein
ATCC	American Type Culture Collection
Aβ	Amyloid-β peptide
BACE1	β-site APP cleaving enzyme
BCA	Bicinchonininic acid
BSA	Bovine serum albumin
BSE	Bovine spongiform encephalopathy
C-terminus	Carboxy-terminus
CJD	Creutzfeldt-Jakob disease (CJD)
CSF	Cerebrospinal fluid
DMEM	Dulbecco's modified eagle medium
DNA	Deoxyribonucleic avid
dNTP	Deoxyrhibonucelotide triphosphate
ECACC	European Collection of Cell Culture
EDTA	Ethylenediaminetetra-acetic acid
EGCG	Epigallocetechin-3-gallate
ELISA	Enzyme Linked Immunosorbent Assay
EO-FAD	Early-onset familial Alzheimer's disease
ER	Endoplasmic reticulum
FCS	Fetal calf serum
FDA	Food and Drug Administration
GAG	Glycosaminoglycan
GFP	Green fluorescent protein
HBS	HEPES buffered saline
HRP	Horse Radish Peroxidase
HSPG	Heparan sulphte proteoglycan
kDa	Kilo Dalton
LOAD	Late-onset Alzheimer's disease
LR	Laminin receptor
LRP	Laminin receptor precursor
LTP	Long-term potentiation
mRNA	Messenger RNA
N-terminus	Amino-terminus
NCT	Nicastrin
NEAA	Non-essential amino acids
NFTs	Neurofibrillary tangles
NRG1	Neuregulin-1
PAGE	Polyacrylamide gel electrophoresis
PBS	Phosphate buffered saline
PCR	Polymerase Chain Reactin
PEN2	Presenilin enhancer 2

PHF	Paired helical filaments
PrP	Prion protein
PrP^{C}	Cellular prion protein
PrP^{Sc}	Infectious prion protein
PS	Presenilin
PVDA	Polyvinylidene fluoride
RISC	RNA-induced silencing complex
RLC	RISC loading complex
RNA	Ribonucleic acid
RNAi	Ribonucleic acid interference
SDS	Sodium dodecyl sulphate
shRNA	Short hairpin ribonucleic acid
siRNA	Small interfering ribonucleic acid
TRBP	TAR RNA binding protein
TSE	Transmissible spongiform encephalopathies
VEE	Venezuelan equine encephalitis virus
α	Alpha
β	Beta
γ	Gamma

CHAPTER 1

1. Introduction

1.1. Alzheimer's disease: An introduction

Alzheimer's disease (AD), also referred to as Alzheimer's dementia, Morbus Alzheimer's or simply Alzheimer's, is a progressive neurodegenerative disorder that is by far the most common form of dementia globally[1]. Initially, patients with the disease present with symptoms including disruptions in short-term memory, attention, language, personality and spatial orientation, in association with confusion and erratic mood changes[2]. These memory and other cognitive functions progressively become impaired over a time period of 8 to 10 years, resulting in characteristic neurodegenerative changes and the complete dependency and ultimate death of the patient[3]. Neurodegeneration typically begins within the entorhinal cortex, spreading in a well-defined manner to other regions of the brain, in particular the parietal and temporal regions of the neocortex, as well as the hippocampus[3; 4; 5].

Mounting AD research has been driven not only due to unclear disease etiology, but also due to the rise in life expectancies and subsequent number of individuals at risk for the disease[6]. In spite of tireless research endeavors, no known cures or treatments are available to halt the degeneration of neuronal cells in AD. However, the U.S. Food and Drug Administration (FDA) has approved 5 palliative therapies that have been shown to slow the symptoms of AD for an average of a year in approximately 50% of all individuals on therapy[7]. It is estimated, that over 90 drugs are currently in clinical trials, aimed at slowing the advancement of the disease[7]. The further development of therapies and their potential ability in slowing the progression of neurodegenerative changes linked to AD is crucial for the effective management of the burden of the disease.

1.2. Epidemiology of AD

In 2010, the global number of dementia patients was reported to be 35.6 million, a figure expected to double every 20 years, to 65.7 million in 2030, and 115.4 million in

2050 (Alzheimer's disease interactional: World Alzheimer Report 2009). It is suggested that this increase can mainly be attributed to a rise in the number of dementia cases within low and middle-income countries. The worldwide incidence rate of AD is estimated to be approximately 0.5% per year among individuals aged 65-70 to 6-8% in individuals over 85 years of age[8]. Within South Africa, more than 250 000 individuals are currently afflicted by the disease (Statistics South Africa), while 5.4 million Americans of all ages are estimated to have Alzheimer's disease in 2012 (2012 Alzheimer's disease facts and figures). In the United States a new case of AD develops every 69 seconds - a time expected to accelerate to 33 seconds by 2050[8]. Moreover, in the United States in 2006, AD was reported to be the 7th most prevalent cause of death across all age groups, and the 5th leading cause of death amongst those 65 years of age and older[9].

Given the increasing lifespan of the population, the burden of AD will only grow more significant. In 2011, the first baby boomers will reach their 65th birthdays. By 2029, all baby boomers will be at least 65 years of age. This group aged 65 years and older will have a significant impact on the healthcare system[7]. According to the World Alzheimer Report 2010, the total estimated worldwide cost of dementia was US$604 billion in 2010, accounting for approximately 1% of the world's gross domestic product. Low-income countries were accountable for 1% of total global costs, in spite of a 14% prevalence rate, as opposed to middle and high-income countries that accounted for 10% (but 40% prevalence) and 89% (but 46% of the prevalence) of costs, respectively. Moreover, 58% of costs within low-income countries were attributed to informal care, compared to 65% and 40% in middle and high-income countries, respectively. Conversely, high-income countries accounted for approximately 50% of costs due to professional care equivalent of nursing homes, as opposed to 10% for lower income countries.

1.3. Genetics of AD

With the exception of age, family history is the greatest risk factor for AD, with twin and family studies estimating that 80% of all AD cases have a genetic link[10]. This disease is genetically dichotomous, with two main forms having been identified: (i) early-onset familial AD (EO-FAD) afflicting a small minority of (<5%) of all AD

patients, typically before the age of 60, and characterised by Mendelian inheritance, and (ii) late-onset AD (LOAD) which accounts for the vast majority of all AD cases and is influenced by both genetic variants and lifestyle choices[11; 12].

1.3.1. Early-onset familial AD

Rare mutations in three genes have been strongly linked to EO-FAD: Amyloid Precursor Protein (*APP*) on chromosome 21q21 and the presenilin encoding genes (*PSEN1* and *PSEN2*) located on chromosomes 14q24 and 1q31, respectively *(Table 1.1)*. To date, 24 mutations have been identified in *APP*, 185 in *PSEN1* and 14 in *PSEN2* (Alzheimer Disease and Frontotemporal Dementia Mutation Database; http://www.molgen.ua.ac.be/ADMutations). With the exception of one of the >200 EO-FAD linked mutations (PSEN2-N141I), all others are inherited in an autosomal-dominant manner and lead to a common phenotype: an increased $A\beta_{42}$:$A\beta_{40}$ ratio[11; 13]. The relative increase in $A\beta_{42}$ ultimately results in aggregation of the protein and early-onset of the disease, usually within the fourth or fifth decade of life[14]. *APP* mutations, which are typically of the missense type, accounts for less than 1% of all AD patients and influence APP proteolytic processing and/or aggregation due to their positioning either on or near the Aβ-coding exon[6]. By far, the most prevalent AD-related mutations are of the *PSEN* genes[15]. The vast majority of these mutations are single-nucleotide substitutions; however small insertions and deletions have also been identified[16]. γ-secretase-mediated cleavage of APP is affected by *PSEN* mutations, resulting in an increased $A\beta_{42}$:$A\beta_{40}$ ratio, alluding to a loss- rather than a gain-of-function[16].

Table 1.1| Early-onset familial AD genes and their resultant molecular phenotype

Gene	Protein	Chromosome	Mutations	Molecular phenotype
APP	Amyloid precursor protein	21q21	24 (duplication)	↑ $A\beta_{42}$:$A\beta_{40}$ ↑ Aβ production ↑ Aβ aggregation
PSEN1	Presenilin 1	14q24	185	↑ $A\beta_{42}$:$A\beta_{40}$
PSEN2	Presenilin 2	1q31	14	↑ $A\beta_{42}$:$A\beta_{40}$

*(Adapted from [16]).

1.3.2. Late-onset AD

As opposed to EO-FAD which is characterised as being autosomal dominant, displaying classical Mendelian inheritance, LOAD inheritance is genetically complex in which genetic factors together with environmental and lifestyle factors contribute to the lifetime risk for AD[12]. A single gene variant, the ε4 allele of the apolipoprotein E gene (*APOE*) located on chromosome 19q13, is the only LOAD-risk factor consistently reported to attribute to AD[17] *(Table 1.2)*. The three major alleles of *APOE* differ in terms of amino acid combinations at residues 112 and 158 (ε2: Cys_{112}/Cys_{158}; ε3: Cys_{112}:Arg_{158}; ε4: Arg_{112}/Arg_{158}). The *APOE* ε4 allele affects both risk as well as age of disease onset in a dose dependant manner, with risk profile increasing fourfold when inherited as a single copy and by more than 10-fold for a double-dose. The ε3 allele is considered neutral, neither enhancing nor reducing AD-risk profile, while the ε2 allele is protective in nature[6; 18]. APOE has a biological function in lipid metabolism and transport but is believed to function in Aβ clearance from AD brains[16]. In addition Genome Wide Association Studies (GWAS) have identified statistically significant AD variants in the following genes: *CD33, CLU, CR1, PICALM, BIN1, ABCA7, CD2AP, EPHA1, MS4A6A/MS4A4E* and *ATXN1*[16] *(Table 1.2)*. Functionally, these genes contribute to AD pathogenesis through (i) production, clearance and degradation of Aβ, (ii) lipid metabolism, (iii) innate immunity or, (iv) cell signaling[16].

Table 1.2: Late-onset AD genes and their proposed molecular mechanism

Gene	Protein	Chromosome	Risk change (%)	Molecular phenotype
APOE	Apolipoprotein E	19q13	400-1500	Aβ clearance; lipid metabolism
CD33	CD33	13q13.3	10	Innate immunity; Aβ degradation
CLU	Clusterin	8p21.1	10	Aβ clearance; innate immunity
CR1	Complement component (3b/4b) receptor 1	1q32	15	Aβ clearance; innate immunity
PICALM	Phosphatidylinsoitol binding clathrin assembly molecule	11q14	15	Aβ production and clearance; cell signaling
BIN1	Bridging integrator 1	2q14	15	Aβ production and clearance; cell signaling
ABCA7	ATP-binding cassette subfamily A member 7	19p13.3	20	Lipid metabolism; cell signaling
CD2AP	CD2-associated protein	6p12.3	10	Cell signaling
EPHA1	EPH receptor A1	7q34	10	Cell signaling; innate immunity
MS4A6A/MS4A4E	Membrane-spanning 4-domains, subfamily A, members 6A and 4E	11q12.1	10	Cell signaling
ATXN1	Ataxin 1	6p22.3	NA	Aβ production

*NA: Not applicable. (Adapted from [16]).

1.4. Neuropathological alterations in AD

The neuropathological hallmarks of AD include both 'positive' and 'negative' lesions. Typical 'positive' features consist of (i) amyloid plaques composed of extracellular deposits of the amyloid beta peptide (Aβ), (ii) neurofibrillary tangles (NFTs) comprised of a hyperphosphorylated form of the microtubule associated protein, tau, (iii) neuropil threads consisting of axonal and dendritic regions associated with aggregated tau, and (iv) dystrophic neuritis[19; 20; 21; 22; 23]. These features are generally accompanied by astrogliosis[24; 25] and microglial cell activation[25; 26], in addition to cerebral amyloid angiopathy (the deposition of Aβ in the meningeal arteries and cortical capillaries, particularly in posterior regions of the brain)[19]. Neuronal, neurophil and synaptic losses are classical 'negative' AD-associated lesions accompanying the aforementioned 'positive' features of AD[27; 28; 29; 30; 31; 32].

1.4.1. Neuritic plaques

At the microscopic level, one of the defining features of AD is neuritic plaque formation[33]. Plaques, which form predominately within the limbic and associated cortices, are composed of extracellular deposits of Aβ surrounded by dystrophic neurites, reactive astrocytes and microglia[33] *(Fig. 1.1)*. The Aβ peptide, which is constitutively produced and readily detectable in the cerebrospinal fluid (CSF), has a range of isoforms between 38 and 43 amino acids[34]. The two predominate isoforms, $A\beta_{42}$- the more fibrillary form with an increased propensity for aggregartion- and $A\beta_{40}$ occur at relative proportions of 1:9 respectively[35]. These proportions are altered in AD patients, such that the levels of $A\beta_{42}$ are higher than that of $A\beta_{40}$ [35].

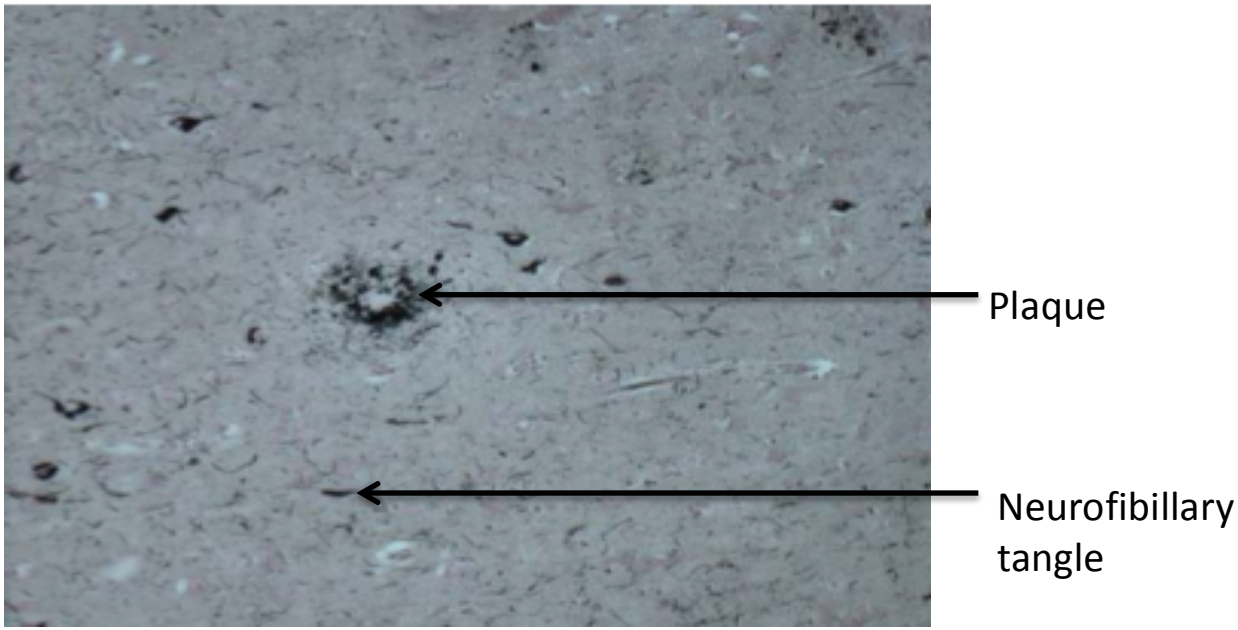

Fig. 1.1| Brain section showing AD related amyloid plaques and neurofibrillary tangles in the cerebral cortex. Plaques are composed of extracellular deposits of Aβ surrounded by dystrophic neurites, reactive astrocytes and microglia, whereas NFTs are composed of intracellular aggregates of the hyperphosphorylated microtubule-associated protein, tau (Adapted from [36]).

1.4.2. Amyloid cascade hypothesis

To date the amyloid cascade hypothesis remains the most favorable framework to explain AD pathogenesis *(Fig. 1.2)*. Although widely contested, this hypothesis is the most well studied and defined model for the cause of AD[37]. As originally described in the 1990's, the amyloid cascade hypothesis proposes that AD is a result of plaque formation due to either an increased production or decreased clearance of Aβ[38; 39]. Aggregated Aβ and subsequent plaque formation, triggers a cascade of neurological changes, the end result being neuronal death and associated dementia.

Several alterations, in terms of the pathogenic state of Aβ have arisen over time *(Fig. 1.3)*. The original hypothesis that states that plaques are the pathogenic agents responsible for AD *(Fig. 1.3a)* has lost credibility based on the following findings: (i) severity of dementia is poorly correlated to plaque load[31], (ii) many AD patients who present with severe cognitive decline and memory impairment do not display plaque formation upon post-mortem analysis, and (iii) *in vivo* neuroimaging techniques have revealed the presence of plaques in healthy individuals[40; 41]. The preceding evidence suggests that amyloid plaques are not the pathological species that trigger AD, but rather may be benign or protective in nature[42].

Subsequently, studies showing that mutations associated with familial AD increase $A\beta_{42}$ production, led to the hypothesis that increased $A\beta_{42}$ levels are the causative agent of AD[43] *(Fig. 1.3b)*. Yet another alternative of the amyloid cascade hypothesis states that it is not the level of $A\beta_{42}$ that is important for AD pathogenesis, but rather the ratio of $A\beta_{42}$:$A\beta_{40}$ [37] *(Fig. 1.3c)*. This alternative hypothesis is largely based on the inverse correlation between age of onset of AD and $A\beta_{42}$:$A\beta_{40}$ ratio[44]. However, several lines of investigative efforts now support the view that increased levels of soluble $A\beta_{42}$ oligomers, ranging in size from 2 to 12 subunits, lead to neurodegeneration and synaptic damage[45; 46; 47; 48; 49] *(Fig. 1.3d)*. *In vitro*, Aβ oligomers have been shown to inhibit long-term potentiation (LTP), damage neuronal spines and thwart activity-regulated cytoskeletal associated protein distribution[46; 50; 51; 52]. Similar Aβ oligomeric species have been identified in APP transgenic mouse models, as well as in the brains[53; 54; 55] and CSF of AD patients[56]; however, the

correlation between oligomer accumulation and severity of cognitive impairment remains evasive[53; 54; 55].

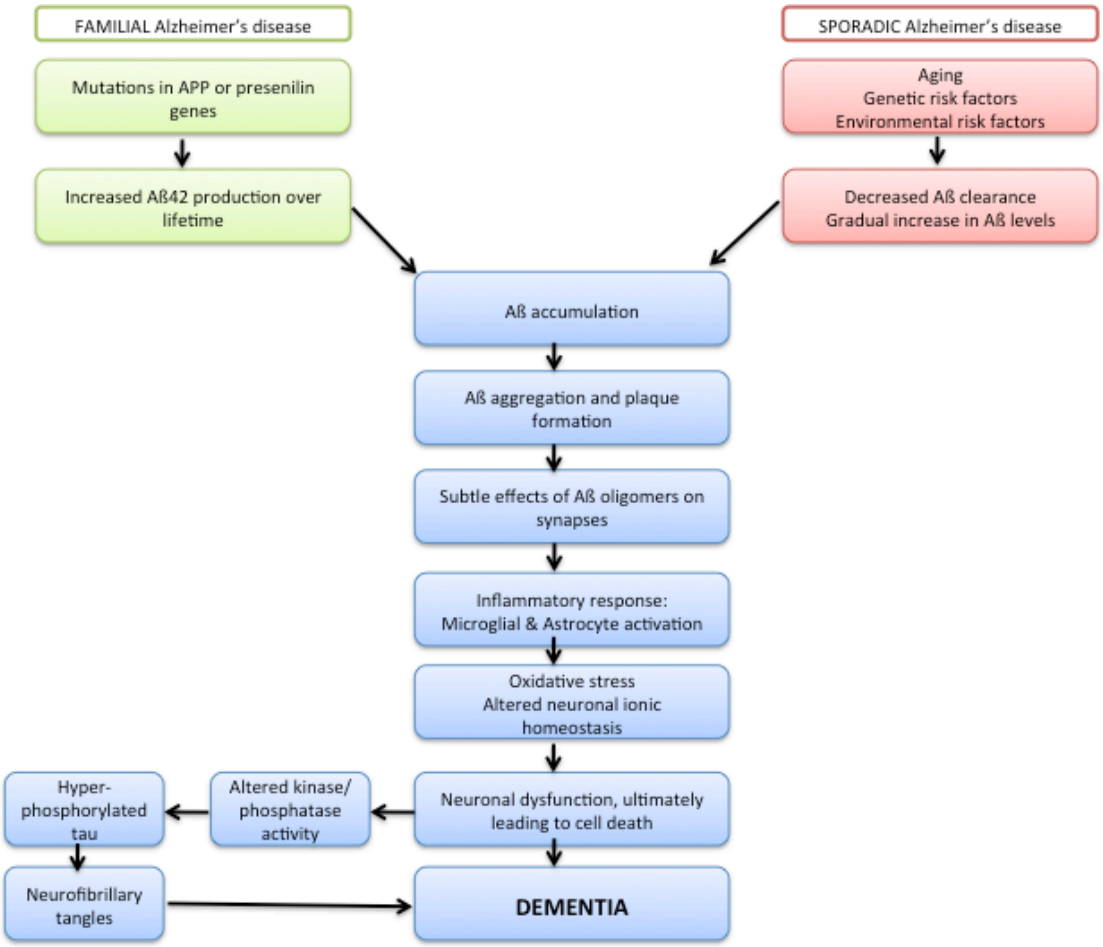

Fig. 1.2| Amyloid cascade hypothesis. According to the amyloid cascade hypothesis AD pathogenesis is the result of an increased production or decreased clearance of Aβ, ultimately leading to Aβ accumulation, aggregation and plaques formation. Aβ oligomers are believed to inhibit long-term potentiation and impair synaptic functioning, while aggregated and deposited Aβ has been linked to an inflammatory response and oxidative stress. These processes are believed to be responsible for neuronal and synaptic dysfunction, as well as neurotransmitter deficits, leading to the cognitive symptoms associated with AD. Although regarded as a down-steam event, tangle formation is thought to contribute to neuronal loss and cognitive decline (Adapted from [33]).

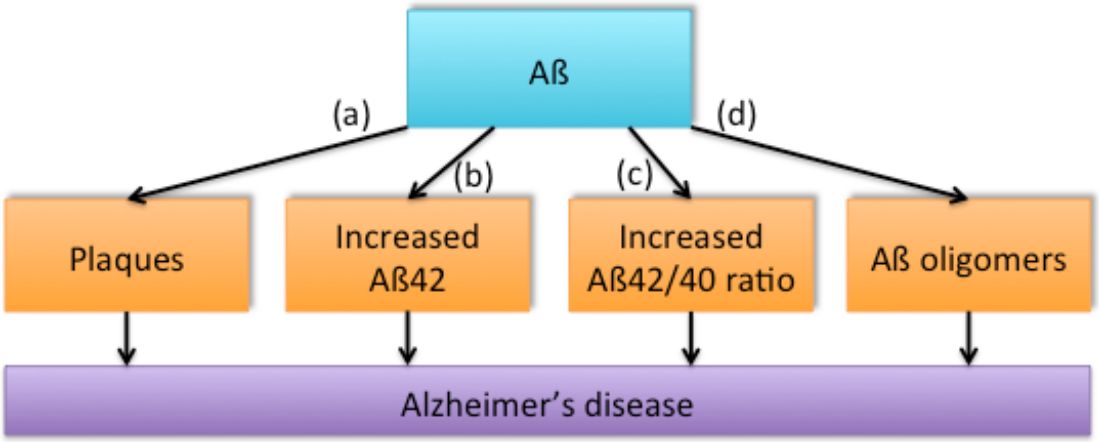

Fig. 1.3| Alternatives to the originally proposed amyloid cascade hypothesis. The primary claim of the amyloid hypothesis is that Aβ is largely responsible for AD pathogenesis. **(a)** It was originally proposed that increased levels of Aβ result in plaque formation, the latter being the agent responsible agent for causing AD. **(b)** Subsequent studies led to the hypothesis that increased levels of Aβ42 are the pathogenic species responsible for the disease. **(c)** Later it was proposed that the Aβ42:Aβ40 ratio, rather than the levels of Ab42, is important in disease pathogenesis. **(d)** However, recently it has been suggested that soluble Aβ oligomers are the toxic species responsible for AD development (Adapted from [37]).

1.4.3. Neurofibrillary tangles

In addition to neuritic plaque formation, numerous neurons that are typically affected in AD brains contain large, non-membranous bundles of insoluble filaments within the perinuclear cytoplasm[33]. These neurofibrillary tangles (NFTs) were shown to be composed of a hyperphosphorylated form of the microtubule-associated protein, tau[57; 58] assembled into paired helical filaments (PHFs); that is, fibrils of approximately 10nm in diameter that form pairs with a helical conformation at a regular periodicity of 65nm[59; 60; 61]. However, recent *in vitro* evidence has alluded to the presence of twisted ribbon-like assemblies of tau fibrils, thus disputing the PHF concept[62]. Nonetheless, tau, which functions in microtubule assembly and stability, is tightly regulated with respect to its degree of phosphorylation by various kinases (e.g. GSK-3ß and CDK5) and phosphatases (e.g. PP-1 and PP-2A)[63] *(Fig. 1.4)*. Disassembly of microtubules and the associated disruption in axonal transport, both of which result in synaptic dysfunction and neuronal death, are the consequence of hyperphosphorylated tau sequestration of normal tau and other microtubule-associated proteins[63]. The topographical progression of NFTs (and neurophil threads) occurs in a predictable manner, with tangle formation initially affecting the transentorhinal region, and then

spreading to the amygdala and hippocampus, and eventually to the neocortical areas of the brain[64; 65; 66; 67].

Whether NFT formation is a precursor of neuronal loss or merely a protective marker of other AD-related processes is still in question. However, multiple groups have established a strong correlation between the amount and distribution of NFTs with the severity of dementia[32; 68; 69; 70; 71]. In addition, the topographical distribution of NFTs is in accord with the hierarchical neuropsychological profile associated with AD, occurring prior to plaque deposition[19]. Nonetheless, these tangles are not only associated with AD pathology, but also a number of other neurodegenerative diseases and disorders, such as subacute sclerosing panencephalitis[72]. Although Aβ neuritic plaques have been described in the brains of healthy individuals not afflicted with AD, as well as patients suffering from dementia with Lewy bodies, it is not the primary lesion defining any disease other than AD[72]. Moreover, mutations within the tau gene results in the development of frontotemporal dementia (as opposed to AD)[73], while mutations resulting in an increased shedding of $A\beta_{42}$ are clearly linked to the development of familial AD[72]. As such, it is largely believed that Aβ is the primary causative agent in AD.

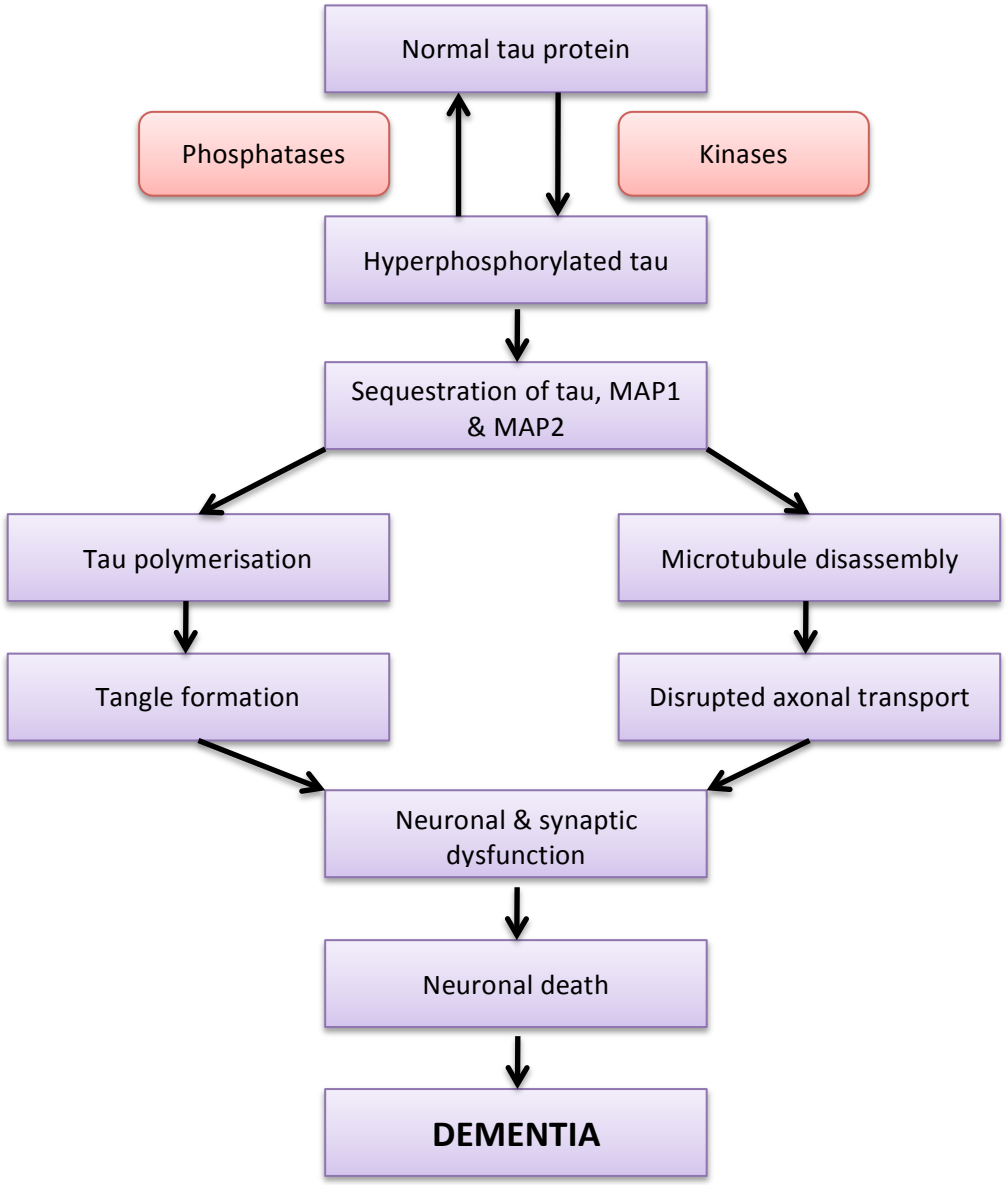

Fig. 1.4| Tau hyperphosphorylation and tangle formation in AD. The balance between normally phosphorylated and abnormally hyperphosphorylated tau is regulated by multiple kinases and phosphatases. Hyperphosphorylated tau sequesters normal tau and other microtubule-associated proteins, resulting in microtubule disassembly and disrupted axonal transport. Additionally, abnormally phosphorylated tau may aggregate into insoluble paired helical filaments and larger tangles. It is both tau polymerization and microtubule disassembly that is responsible for neuronal and synaptic dysfunction, ultimately leading to neuronal death and dementia (Adapted from [33]).

1.5. Origin of amyloid β-protein: Cell biology of APP

The realisation that Aβ was the main component of AD-associated plaques[74; 75] led to the subsequent need to elucidate the origins of this protein. It was found that Aβ was the derivative of the sequential proteolytic processing of the type I transmembrane protein, amyloid precursor protein (APP)[72] *(Fig. 1.5)*. APP is heterogenic in nature, the result of (i) alternate mRNA splicing, giving rise to three isoforms (695, 751 and

770 amino acid residues in length) and (ii) post-translational modifications including *N*- and *O*-linked glycosylation, phosphorylation and sulphation[76; 77; 78; 79]. APP_{751} and APP_{770} isoforms are ubiquitously expressed, predominantly within non-neuronal cells, while the APP_{695} isoform has largely been isolated from neuronal tissue[80]. The 37-43 amino acid Aβ peptide is located in part between the ecto- and transmembrane domain of APP[81]. Specifically, the Aβ sequence extends 28 residues into the extracellular domain and between 11 and 15 residues into the transmembrane domain, depending on the length of Aβ to be released[81]. Although APP maturation and trafficking occurs throughout the secretory pathway, it is proteolytically processed by three different secretases (α-, β- and γ-secretase) at various subcellular sites, with the sequential cleavage of β- and γ-secretase resulting in Aβ production.

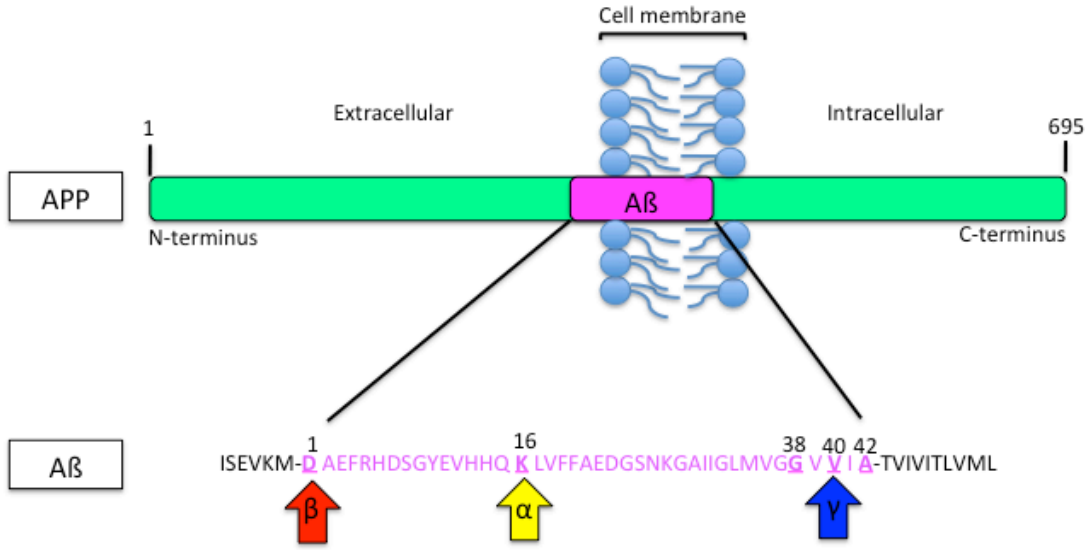

Fig. 1.5| Schematic representation of APP. APP is a type I transmembrane protein 695 amino acids in length. The Aβ sequence is shown in relation to APP, together with the α-, β-, and γ-secretase cleavage sites. β-secretase cleaves at residues 1 of the Aβ sequence, while γ-secretase cleaves at amino acid 16 of this same sequence. γ-secretase cleaves at residues 38, 40 or 42 depending on whether Aβ38, Aβ40 or Aβ42 is produced, respectively.
(Adapted from [36]).

1.5.1. Proteolytic processing of APP

APP is a transmembrane protein that is translocated to the endoplasmic reticulum (ER) co-translationally by its signal peptide, where it then undergoes post-translational modifications within the secretory pathway[72]. APP is cleaved differentially by α-, β- and γ-secretase giving rise to two APP cleavage pathways: (i) an Aβ synthesizing amyloidogenic pathway and (ii) a non-pathogenic, non-

amyloidogenic pathway *(Fig. 1.6)*. Although both of these pathways occur constitutively throughout the lifetime of an individual, the amyloidogenic processing of APP is favored in neuronal cells mostly due to high β-secretase expression levels[82]. The non-amyloidogenic processing of APP occurs predominantly in all other cell types[83; 84; 85; 86]. There is also some evidence supporting the competition between these two pathways, whereby enhanced γ-secretase activity decreases the shedding of Aβ and subsequent plaque formation[87; 88].

The non-amyloidogenic APP processing pathway involves the cleavage of APP at Lys16 within the Aβ region (or between amino acid residues 105 and 125 depending on the APP isoform) by α-secretase, and hence precludes Aβ formation[89; 90] *(Fig. 1.5/Fig. 1.6)*. This processing results in the release of the large, soluble ectodomain of APP, namely sAPPα, into the extracellular space[72; 82]. The resultant 83 residue long C-terminal portion of APP, designated C83, is retained within the membrane[72; 82]. The vast majority of sAPPα is formed by α-secretase cleavage of APP inserted within the plasma membrane[91; 92]. However, sAPPα can also be formed during the intracellular secretory processing of APP[93]. α-secretase activity is mediated by one or more enzymes belonging to the family of disintegrin and metalloproteinase domain proteins (ADAMs), where it has been hypothesised that ADAMs 9, 10, 17 and 19 are most likely responsible for α-secretase activity[94; 95; 96]. The C83 fragment undergoes subsequent cleavage by γ-secretase at amino acid residues 711 or 713 [72]. γ-secretase cleavage of C83 results in the generation of a 3kDa peptide called p3, as well as the amino-terminal APP intracellular domain (AICD)[84; 89] *(Fig. 1.6)*.

Some APP does not undergo cleavage by α-secretase, but is rather cleaved 16 residues N-terminal to the α-secretase cleavage site (or at the N-terminal of the Aβ region) by an enzyme referred to as β-secretase[97] *(Fig. 1.5/Fig. 1.6)*. This pathway that involves the formation of Aβ is referred to as the amyloidogenic pathway. Cleavage by β-secretase generates a slightly smaller ectodomain fragment, $sAPP_{ß}$, and the C-terminal fragment 99 residues in length (C99) that is retained within the cellular membrane[97; 98]. Although β-secretase cleavage predominantly occurs on the cell membrane, it also occurs to a smaller extent in the secretory trafficking of APP[93]. C99, which begins at residue 1 of the Aβ region, is subsequently cleaved by γ-

secretase at residues 38, 40 or 42 to release $A\beta_{38}$, $A\beta_{40}$ or $A\beta_{42}$, respectively[90; 99] *(Fig. 1.5/Fig. 1.6). In* addition to Aβ shedding, γ-secretase cleavage results in the remaining C-terminal fragment of APP referred to as AICD, being released into the cytoplasm[100; 101; 102].

Although γ-secretase cleavage of APP results in the release of Aβ and an AICD fragment 57 or 59 residues in length (C57 and C59, respectively), an additional cleavage site (ε-cleavage site) is located 7 to 9 amino acids towards the C-terminal end[101]. γ-secretase cleavage at the aforementioned site results in the formation of an AICD fragments 50 amino acids in length (C50)[101]. This 50 residue long fragment is the predominant AICD form, however, AICD fragments as short as 31 residues have been reported[101].

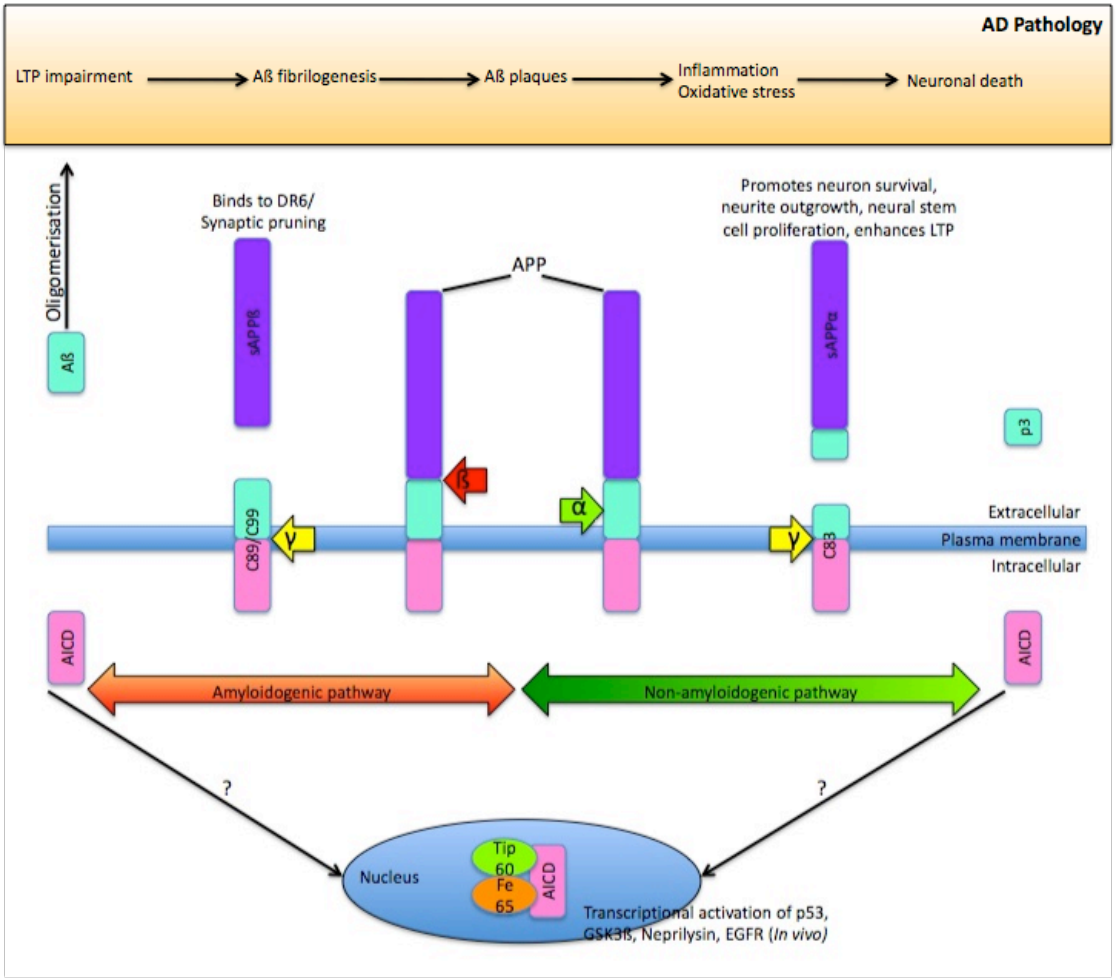

Fig. 1.6| APP processing and cleavage in AD pathogenesis. The non-amyloidogenic pathway *(right)* involves the sequencial cleavage by α- and γ-secretase, resulting in the formation of sAPPα and various C-terminal fragments (C83, p3 and AICD). The amyloidogenic pathway *(left)* involves the sequential cleavage by β- and γ-secretase generating $sAPP_{\beta}$ and the following C-terminal fragments: C89 or C99, Aβ, and AICD. Aβ fragment oligomerisation and fibrillation results in AD pathogenesis *(top panel)*. *α: α-secretase; β: β-secretase; γ: γ-secretase.* (Adapted from [101])

1.5.2. The amyloidogenic proteases: β- and γ-secretase

β-secretase

β-secretase is a membrane-bound enzyme displaying a high level of homology to the pepsin family of aspartyl proteases[103] and mediates the initial and rate-limiting step of the amyloidogenic pathway[104]. The predominant β-secretase within the central nervous system was identified as the β-site APP cleaving enzyme 1 (BACE1)[105]. BACE1 is the sole β-secretase involved in Aβ generation, as its knockout ablates Aβ shedding[106; 107]. BACE2, a homologue of BACE1, has also been identified[104] but found to exert an anti-amyloidogenic effect in non-neuronal cells[108; 109; 110; 111].

Although ubiquitously expressed, BACE1 levels are most prominent within brain and pancreatic tissues[82]. The concomitant high expression of APP within the brain provides an explanation for Aβ aggregation predominantly within neuronal tissue despite ubiquitous expression of both APP and BACE1[82].

The therapeutic targeting of BACE1 is substantiated as its blockage in activity is associated with a decrease in the shedding of Aβ and accumulation in the β-carboxy terminal fragment[112]. The later being an additional possible contributor of neurotoxic effects[82]. Although progress has been made towards the production of a successful BACE1 inhibitor[112], possible side-effects as a result of the inhibition of physiological BACE1 function have deterred the advancement of many clinical trials. Indeed, one of the physiological functions of BACE1 involves Schwann cell-mediated myelination via the Neuregulin-1 (NRG1) signaling pathway[113], with BACE1 knockout mice displaying a significant hypomyelination phenotype[114; 115].

γ-secretase

γ-secretase is an intramembranous multi-complex protein, consisting of four subunits: (i) presenilin (PS) 1 or 2 which contain two catalytic aspartyl residues within transmembrane domains 6 and 7 [116], (ii) PS enhancer 2 (PEN2)[117], (iii) nicastrin (NCT)[118] and (iv) anterior pharynx defective (APH)-1a or APH-1b[117]. While little is known about the physiological function of PEN2, NCT and APH-1, all four components are necessary for efficient γ-secretase activity[119]. It has been hypothesized that NCT plays a role as a size selecting substrate receptor[120; 121], yet recent evidence has challenged this view[122; 123]. PEN-2 has been proposed to mediate PS endoproteolysis and stabilization within the γ-secretase complex[124; 125], while APH-1 is thought to possibly act as a scaffold for NCT binding[126].

1.5.3. Functions of APP and its derivatives

It is difficult to ascertain a definite physiological function for APP, without considering its proteolytic cleavage derivatives[101]. Nonetheless, an overexpression of human APP has been linked to increased size of neurons within the cortex[127]. It is still unknown as to whether this increase in neuronal size is attributed to the full-length

APP or one of its cleavage derivatives[127]. Moreover, APP knockout mice display numerous altered phenotypes including a reduction in brain and body size, impairment in learning, increased propensity for seizures, as well as abnormal development of the corpus callosum[128; 129]. The extracellular domain of APP interacts with a variety of extracellular matrix molecules including heparin[130; 131], laminin[132] and collagen type I[133], implicating APP in cell adhesion. Moreover, APP has been identified as a novel class of synaptic adhesion molecules[129]. Evidence from numerous sources now implicates APP in neural- and synapto-trophic functions. The ablation or reduction in APP results in impaired neuronal viability *in vitro* and decreased synaptic activity *in vivo*[134; 135; 136].

Although the physiological function of sAPPα is still largely undetermined, it is believed that sAPPα is beneficial to neurons[101] *(Fig. 1.6).* sAPPα is thought to play a neuroprotective function against oxygen-glucose deprivation and excitotoxicity by stabilizing the resting membrane potential[137; 138]. sAPPα has also been implicated in the promotion of neurite outgrowth, cell adhesion and synapse formation[139; 140]. In contrast, sAPPβ is not associated with any of the neuroprotective effects as with sAPPα[138]. sAPPβ has been shown to be crucial in synaptic pruning during the development of neurons within the central and peripheral nervous system[141] *(Fig. 1.6).* sAPPβ has also been hypothesised to inhibit neuronal stem cell differentiation, while promoting the differentiation of glial cells[142].

The AICD has been shown to contain the consensus sequence, YENPTY. This sequence is believed to be vital in the functioning of AICD, as well as its binding to adaptor molecules, for example Fe65[143]. With regards to its signaling pathway, AICD has been found to bind to Fe65, followed by the sequestration of histone deacetylase TIP60, and its subsequent translocation into the nucleus[144; 145; 146] *(Fig. 1.6).* Here it acts as a transcriptional factor for p53[147], GSK3β[148; 149], neprilysin[150], EGFR[151], in addition to others[101; 129]. To date, the biological functions of the p3, C83, and C99 fragments have not been determined[101].

1.6. Prion proteins: An introduction

Prions (PrP or proteinaceous infectious particles) are the causative agent of transmissible spongiform encephalopathies (TSEs)[152]. This group of mammalian associated neurodegenerative diseases encompasses scrapie in sheep, bovine spongiform encephalopathy (BSE) in cattle, chronic wasting disease in cervids, and kuru, familial fatal insomnia, Creutzfeldt-Jakob disease (CJD), and Gerstmann-Sträussler-Scheinker syndrome in humans[153; 154; 155; 156; 157; 158; 159]. These TSEs are rare and have a prevalence rate (in humans) of approximately one per one million individuals[160]. TSEs may arise either spontaneously, through heritable mutations in the *PRNP* gene, or be transmitted via an infectious route[160]. Subsequent to an extended incubation period, those afflicted with the disease present with symptoms including cognitive and motor dysfunction, as well as cerebral ataxia[160]. Further, TSE diseased brains are characterized by astrogliosis, spongiform degeneration, and aggregates of misfolded protein[154; 156; 157].

It is generally accepted that the cellular isoform of PrP, PrP^{c}, is post-translationally misfolded into the infectious scrapie form of PrP, namely PrP^{Sc} [161]. According to the protein-only hypothesis, the oligomeric β-sheet rich PrP^{Sc} is propagated via binding to endogenous PrP^{c}- the interaction sufficient to cause the template-driven refolding into the infectious PrP^{Sc} isoform[71-77]. There is growing evidence in support of this hypothesis which explains that the transmission of TSEs do not require nucleic acids, but rather PrP^{Sc} alone is able to act as the infectious agent[160].

PrP^{c} is expressed in particularly high amounts on the neuronal cell surface, but is also expressed on the cell surface of a number of other cell types[161]. This glycosyl-phosphatidylinositol anchored protein consists of a flexible N-terminus and a globular C-terminus, mostly α-helical in nature[162]. The physiological role of PrP^{c} has yet to be fully elucidated but hypotheses include cell adhesion, ion channel activity, neurite outgrowth, neuronal excitability, cytotoxicity and cytoprotection[152]. Nonetheless, PrP-deficient mice have been shown to display only very mild phenotypic abnormalities; for example, changes in myelination[163] and olfactory function[164]. Proposed PrP^{c} binding partners are numerous, with it being suggested that some of these binding

partners are not only important to PrP^c function but also to the $PrP^c \rightarrow PrP^{Sc}$ conformation conversion process[165; 166; 167].

1.7. Linking prion proteins and Alzheimer's disease

A number of studies have provided both genetic and neuropathological similarities between AD and the PrP-linked TSEs. AD-associated pathology has been reported within individuals with CJD[168], while PrP^c has been shown to co-localise with Aβ in plaques[169]. It was further determined that patients with CJD, presenting with AD-associated pathology, often develop these Aβ-PrP^c co-localised plaques[170]. Both AD and CJD risk is enhanced by the *APOE4* allele and decreased by the *APOE2* allele. Moreover, APOE binds to numerous amyloidogenic proteins, including Aβ and PrP, with histological studies revealing APOE's association with Aβ and kuru-like plaques of AD and CJD brains, respectively. A possible role of PrP^c promotion of Aβ formation has also been suggested[171]. Studies have revealed *PRNP* as a potential AD susceptibility gene[172], with the Met/Val 129 polymorphism being linked to the early onset of AD[170; 173; 174], as well as long term memory[175] and early cognitive decline[176]. Total PrP levels within the CSF have been linked to increased disease severity in AD, in addition to other neurodegenerative disorders[177; 178]. In spite of these genetic and pathological links between AD and PrP, a definitive role of PrP in APP processing was identified only recently[179].

1.7.1. Regulatory role of prions in APP processing

In 2007, Parkin et al.[179] reported that PrP^c mediates a decrease in the amyloidogenic cleavage of APP, and hence a reduction in Aβ shedding. The initial results, produced in human neuroblastoma cell lines induced to overexpress PrP^c, revealed decreased levels of both $sAPP_\beta$ and Aβ[179]. Further, the siRNA-induced silencing or genetic knockout of PrP^c within murine neuroblastoma (N2a) cells resulted in increased Aβ levels[179]. Changes in the levels of $sAPP_\beta$ in response to PrP^c led to the conclusion that PrP^c is able to influence APP processing and hence Aβ shedding by decreasing cleavage of APP by BACE1[179]. Investigations by the same author revealed that PrP^c interacts directly with BACE1 since both are localised in cholesterol-rich, lipid rafts[179]-the site where β-secretase cleavage preferentially occurs[180; 181]. This interaction has been mapped to the BACE1 prodomain where it leads to slowed

BACE1 trafficking through the ER and trans-Golgi network, reducing BACE1 cell surface levels[182]. Hence it can be concluded that PrP^c has a regulatory role in Aβ shedding, possibly protecting against AD[183].

Later, Vincent et al. described a link between PrP^c and the catalytic subunit of γ-secretase, the presenilins[184]. Within this study it was revealed that the AICD, resulting from the γ-secretase cleavage of APP, regulates the transcription of PrP^c. It is believed that AICD, complexed to Tip60 and Fe65, translocates to the nucleus where it then acts as a transcription factor mediating the expression of p53[184]. p53, in turn, was shown to bind to the promoter region of *PRNP*, hence mediating PrP^c expression[184]. Moreover, it has been noted that AICD acts as transcription factor for the Aβ-degrading enzyme, neprilysin[150; 185].

The work of Parkin et al.[179], taken together with that of Vincent et al.[184] suggests that a possible feedback loop between AICD and PrP^c might exist[186] *(Fig. 1.7)*. It is believed that β-secretase mediates the inhibition of AICD and Aβ by PrP^c [186]. In turn, the amount of amyloidogenic processing of APP regulates the inhibition of PrP^c on BACE1 via the AICD, which regulates PrP^c expression[186]. Such a feedback loop is thought to keep the physiological levels of Aβ in balance, ensuring sufficient amounts to maintain normal function while preventing toxic effects that are the result of Aβ accumulation[186]. However, in AD, the level of Aβ is elevated due to either its increased production and/or decreased clearance. This in turn results in the increased assembly of Aβ into soluble oligomers, which exerts their toxicity via the interaction with PrP^c [186]. The Aβ-PrP^c interaction is believed to interfere with PrP^c regulation of BACE1, which subsequently leads to the increased processing of APP and hence Aβ levels.

Recently, however, through the use of transgenic mice, cell culture models and modulation of APP expression levels, no such link between PrP^c expression and AICD regulation has been proven, suggesting that the control of PrP^c levels by AICD is not as straightforward as originally proposed. Moreover, Calella et al. showed that altering the levels of PrP^c, in APP/PS1 transgenic mice, does not change the levels of Aβ[187]. However, it is argued that the PS1 mutation used in this study might change the

metabolic pathway which results in Aβ formation, and hence the effectiveness of PrP^c [188].

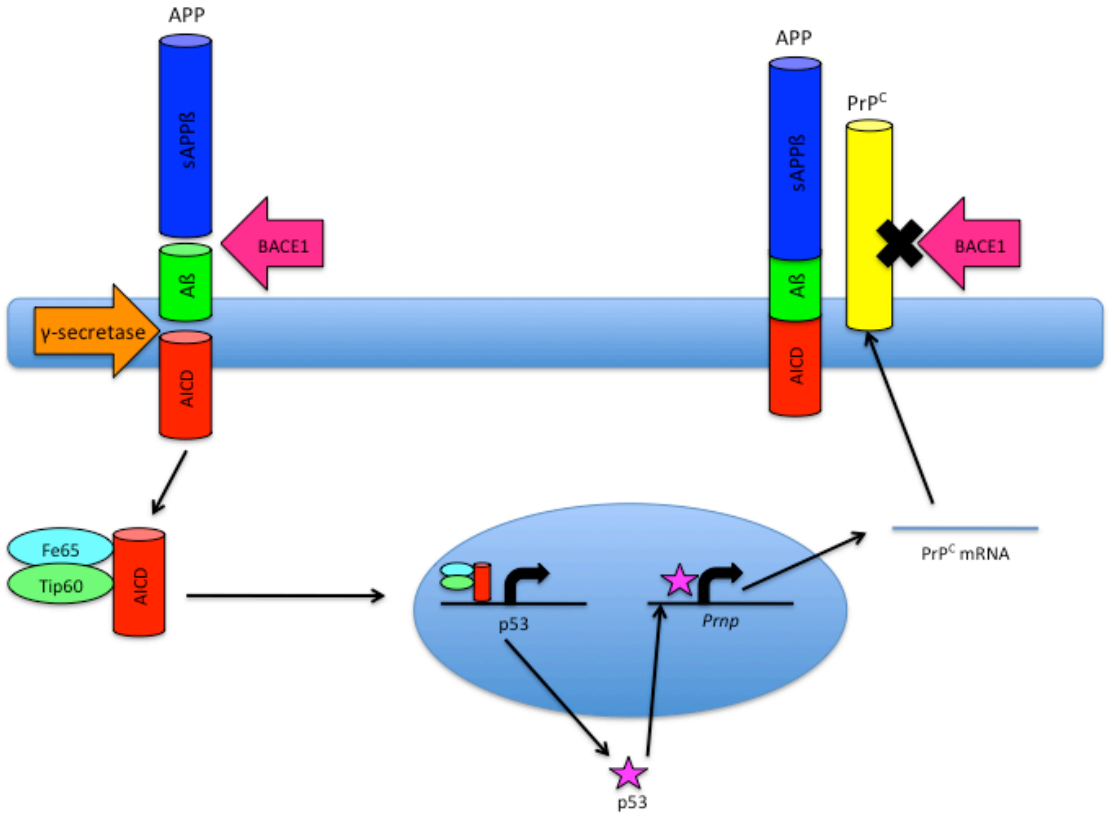

Fig. 1.7| A possible feedback mechanism for the regulation of APP processing by PrP^c. APP processing by β- and γ-secretase gives rise to sAPPβ, Aβ, and AICD *(left)*. AICD forms a complex with Fe65 and Tip60, where it then translocates to the nucleus and interacts with the p53 promoter, regulating its expression. The p53 protein in turn acts a regulator of the *PRNP* gene for PrP^c expression. PrP^c is transported to lipid rafts within the cell membrane, where it is able to inhbit the action of the β-secretase, BACE1 *(right)*. BACE1 inhibition results in decreased Aβ shedding and AICD release, hence downregulating the expression of PrP^c (Adapted from [186]).

1.7.2. The prion protein as a receptor for amyloid-ß

Evidence by Lauren et al.[189] has elucidated to PrP^c being the main receptor for Aβ oligomers, and responsible for mediating the neurotoxic effects of Aβ. Although Aβ oligomers are generally regarded as the pathogenic species responsible for AD-associated neurodegeration[48], the pathogenic mechanism activated by these oligomers remains unclear. Through binding studies, PrP^c was identified as a high affinity receptor for soluble Aβ oligomers, while long-term potentiation (LTP) and behavioral studies (*in vitro* and *in vivo*, respectively) revealed that the absence of PrP^c was able to prevent the toxic effects of Aβ oligomers[189].

While a high affinity interaction between Aβ oligomers and PrP^c has been confirmed, the role that this interaction plays in synaptic impairment has been excluded by several different studies[188]. Data obtained by Balducci et al.[190] using PrP knockout mice revealed that although $A\beta_{42}$ oligomers are the toxic species responsible for the AD pathogenicity, this effect occurs independently of PrP^c. Likewise, two additional studies found that PrP^c was not required for the impairment of synaptic plasticity by $A\beta_{42}$ oligomers[187; 191]. While possible explanations have been put forward to explain these apparent contradictory results[188], it becomes clear that the role of PrP in AD pathogenesis is still far from being fully elucidated[36].

1.8. Linking laminin and amyloid-β

Laminin, an 850 kDa extracellular matrix, glycoprotein complex, has been found to interact with heparan sulfate proteoglycans[192], heparin[193] and collagen type IV[194]. 11 isoforms of laminin has been identified, each composed of one of five different α-chains (200-400kDa) joined to β (220kDa) and γ (210kDa) polypeptide chains to form a cruciform-like structure[195]. Functionally, laminin has been shown to be a powerful inducer of neurite outgrowths[196; 197] and synapse formation[198]. Additionally, laminin production has been found to be stimulated in response to brain injury[199] and specifically co-localises with Aβ deposits in AD and Down's syndrome brains[200]. It has also been indicated that various isoforms of $sAPP_\beta$ bind to laminin, as well as other basement membrane components[201].

Thioflavin T fluorescence spectroscopy and electron microscopic examination revealed that laminin inhibits Aβ fibrillation[202]. Castillo et al.[203] later demonstrated that laminin not only binds Aβ with high affinity, but also acts as an inhibitor of Aβ fibrillogenesis. Within this same study, an Aβ binding site, located within the globular domain repeats on the laminin α chain, was identified[203]. In the presence of laminin, decreased amyloid neurotoxicity has been revealed in both rat primary hippocampal neurons and primary cortical cells[204]. These studies have led to laminin being investigated as a possible target for the inhibition of Aβ fibrillogenesis, and ultimately AD pathogenesis.

1.9. The 37kDa/67kDa high affinity laminin receptor

The 37kDa laminin receptor precursor (LRP) is believed to be the precursor of the 67kDa high affinity laminin receptor (LR), however this relationship is poorly understood[205]. Direct homodimerisation of the 37kDa LRP seems to be an implausible argument based on the fact that LRP is monomeric and is not able to interact with itself, as determined by yeast-two hybrid analysis and size exclusion chromatography[206]. Additionally, it has been hypothesised that a mature 67kDa LR heterodimeric structure might be stabilised by fatty acid-mediated interactions, with additional analyses suggesting a role of acetylation in LRP processing to give rise to the mature receptor[207; 208]. Nonetheless, both the 37kDa LRP and 67kDa LR have been isolated from the cellular surface[209]. Given the above, it is often difficult to make a distinction between LRP and LR, and within this dissertation the receptor is generally referred to as LRP/LR. Knockdown of LRP, for example, will ultimately result in subsequent LR downregulation, and as such downstream effects observed from LRP knockdown cannot exclusively be put down to altered LRP levels but must include the contribution of LR.

The LRP/LR is a non-integrin cell surface receptor that has been shown to have a high binding affinity for laminin, an extracellular matrix glycoprotein known to play a role in cell differentiation, movement, growth and attachment[210; 211; 212; 213]. The LRP/LR has two laminin binding domains located between amino acids 161-180 and 205-229 [214] *(Fig. 1.8)*. Furthermore, the high affinity laminin receptor has been implicated in laminin-induced tumour proliferation, metastasis and invasiveness[215; 216]. The overexpression of the 67kDa LR- found in many cancer types- is correlated with both the invasiveness and metastatic potential of the tumour[214; 217; 218]. Anti-LRP/LR specific antibodies have been shown to interfere with adhesion and invasion, key events in metastatic cancer[36; 205]. In addition to its role as a high affinity receptor for laminin, the 67kDa LR has also been shown to act as a receptor for other extracellular matrix molecules including elastin and carbohydrates[210].

Moreover, LRP/LR has been shown to act as a receptor for both cellular and infectious prion proteins[209; 219]. Two LRP/LR binding domains have been identified on PrP, one direct and the other indirect, located between amino acids 144-179 and

53-93, respectively[206]. Binding of LRP/LR to the indirect binding domain is dependent upon the presence of heparan sulphate proteoglycans (HSPGs)[206]. HSPGs, consisting of core polypeptides to which glycosaminoglycans (GAGs) are covalently attached, have been shown to act as initial receptors for various extracellular molecules[220; 221]. Moreover, a direct PrP binding domain on the 37kDa/67kDa LRP/LR has been identified between amino acids 161-180[206] *(Fig. 1.8)*. While a HSPG-dependant binding site on LRP/LR has yet to be identified, one is assumed to be located between amino acids 180 and 285[222]. In relation to AD, HSPGs are known to be associated with Aβ deposits[222].

It has recently been demonstrated that LRP/LR acts as a receptor for the green tea extract, epigallocatechin-3-gallate (EGCG), inducing anti-cancer and anti-allergic activity within human colon cancer cells[223]. In another study, LRP/LR was implicated in tumour viability. It was shown that the down-regulation of LRP/LR via the use of siRNAs (in Hep3B cells) led to the promotion of apoptosis[224]. LRP/LR has also been shown to act as a receptor for a number of different viruses including the Dengue virus serotypes 1, 2 and 3[225; 226], Sindbis virus[227], Venezuelan equine encephalitis (VEE) virus[228], and Adeno-associated virus (AAV) serotypes 2, 3, 8 and 9[229].

As mentioned above, the 37kDa/67kDa LRP/LR acts as a receptor on the cell surface. Furthermore, LRP/LR has been isolated from the cytoplasm and is associated in this subcellular compartment with the p40 ribosome and involved in 40S ribosomal subunit maturation[230; 231]. The 37kDa LRP has also been isolated from both the perinuclear compartment and nucleus, where it is in contact with PrP and histones, respectively[230; 232; 233]. The affinity between LRP and histones suggests a possible role for LRP in the maintenance of nuclear structures. Due to the fact that LRP/LR is found in various regions within the cells and has multiple functions, including a role in protein synthesis, cell viability and proliferation, the specific targeting of LRP/LR hold huge promise in the treatment of various human diseases.

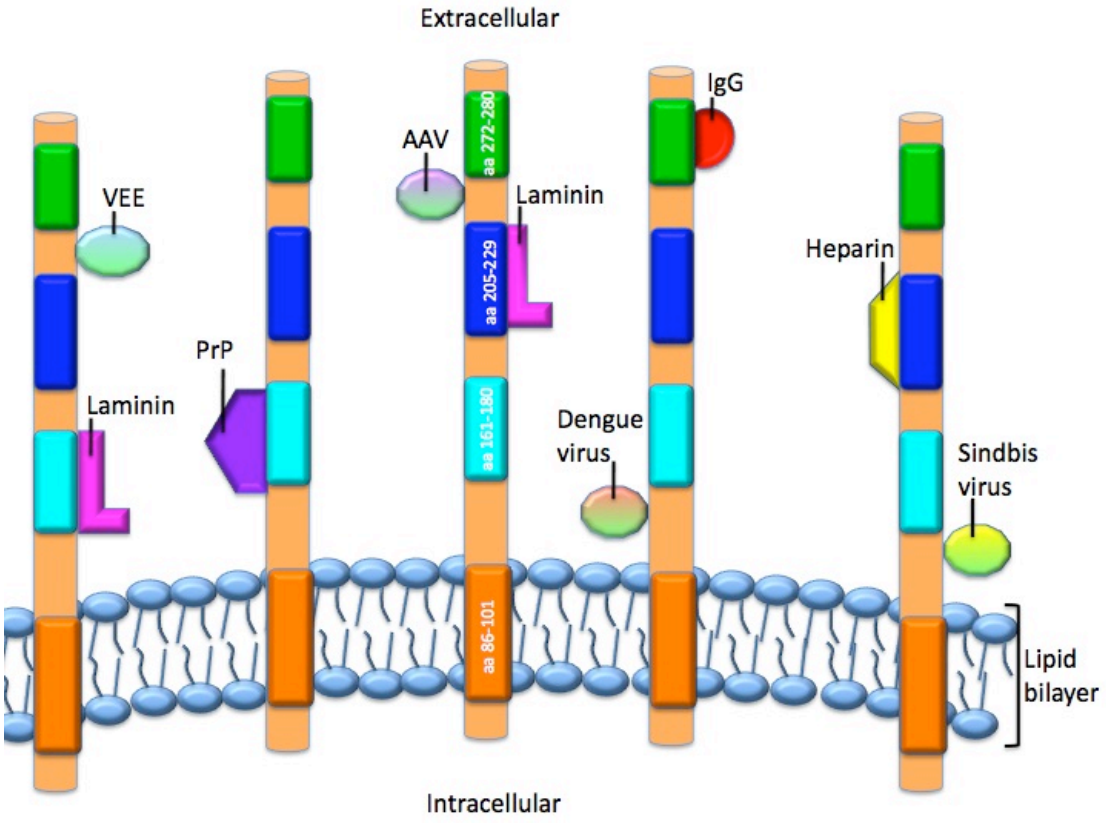

Fig. 1.8| Schematic representation of the 37kDa laminin receptor precursor (LRP). The 37kDa LRP is 295 amino acids (aa) in length and consists of four functional domains with its C-terminus exposed to the extracellular space. The transmembrane domain is located between amino acids 86-101, while a laminin/prion protein (PrP) binding domain has been found to be positioned between amino acids 161-180. Further, a heparin/laminin binding domain and a scFv/IgG1 antibody binding domain have been shown to be located at amino acid positions 205-229 and 272-280, respectively. Four viruses are known to bind to LRP/LR, namely Venezuelan Equine Encephalitis Virus (VEE), Adeno-associated virus (AAV), Dengue virus and Sindbis virus. However, the binding domains of these aforementioned viruses to LRP/LR as of this time remains unclear, and as such viral-LRP binding has been arbitrarily depicted within this diagram (Adopted from [36]).

1.10. Implications of LRP/LR in Alzheimer's disease

LRP/LR has been reported to be a receptor for the basement membrane protein, laminin[36]. Additionally, it has been shown that laminin inhibits Aβ fibrillation[202; 203]. Moreover, Gauczynski et al. have shown that the 37kDa/67kDa LRP/LR acts as a receptor for both infectious (PrP^{Sc}) and non-infectious prions (PrP^{c})[209; 219]. It is known that PrP^{c} inhibits Aβ shedding[179], while also acting as a high affinity receptor for Aβ oligomers[189]. Thus, a possible relationship between LRP/LR (the receptor for PrP^{c}/ PrP^{Sc} and laminin) and Aβ, whose shedding and fibrillation is regulated by PrP^{c} and laminin, respectively, is conceivable.

1.11. RNA interference (RNAi)

RNAi refers to the biological process by which a specific double-stranded RNA (ds-RNA) sequence knockdowns the expression of a particular gene target[234]. This process was originally observed in plants[235] but accurately described for the first time in *Caenorhabditis elegans* by Fire et al[236]. Shortly, the mechanism of RNAi involves the processing of the long ds-RNA into short or small interfering RNA (siRNA) by the endonuclease Dicer[234] *(Fig. 1.9)*. The processed siRNAs are approximately 21 nucleotides in length, of which 19 nucleotides form a helix and 2 nucleotides on each of the 3' ends are unpaired[234]. The ribonucleoprotein complex RISC (RNA-induced silencing complex) is then guided by the siRNA to its complementary mRNA target sequence[234]. The target mRNA is subsequently cleaved 10 nucleotides from the 5' end of the siRNA strand[237] by Argonaut 2 (Ago2) [238]. The cleaved mRNA target lacks a 5' end cap and 3' poly-A tail that is endogenously responsible for mRNA stability, and as a result the cleaved mRNA is rapidly degraded by RNases and translation of the coded protein is inhibited. In mammalian cells, the loading of the siRNA into the RISC is achieved by the RISC-loading complex (RLC)- the constituents of which include Dicer and TAR RNA binding protein (TRBP)[234]. Moreover, during RISC activation, the passenger or sense strand is degraded while the guide or anti-sense strand incorporates into the RISC[239; 240].

The use of plasmids expressing short hairpin RNAs (shRNAs) is a useful system by which siRNAs are continuously generated in cells. In this system the shRNA is converted into DNA sequences coding for a sense-strand, loop region and anti-sense strand[234]. The DNA template is designed to be transcribed from a vector under the control of the RNA polymerase III promoter (usually U6 or H1 promoter). During transcription, a self-complementary RNA is synthesized, referred to as an shRNA[234]. The resultant shRNA is processed by Dicer to form a siRNA, which mediates gene silencing as described above.

The ability of RNAi to modulate gene expression has dramatically enhanced the study of gene function, in addition to revolutionizing disease treatment. Inherent difficulties in blocking several desirable targets through the use of small molecule inhibitors or monoclonal antibodies for example, has led to the explosion of interest into RNAi-

based therapies[241]. Despite its attractiveness as an alternative therapeutic approach for the treatment of numerous diseases, several hurdles must be overcome to successfully introduce RNAi-based therapies into the clinical setting. Some of which include a safe and efficient delivery system and avoidance of off target effects[241].

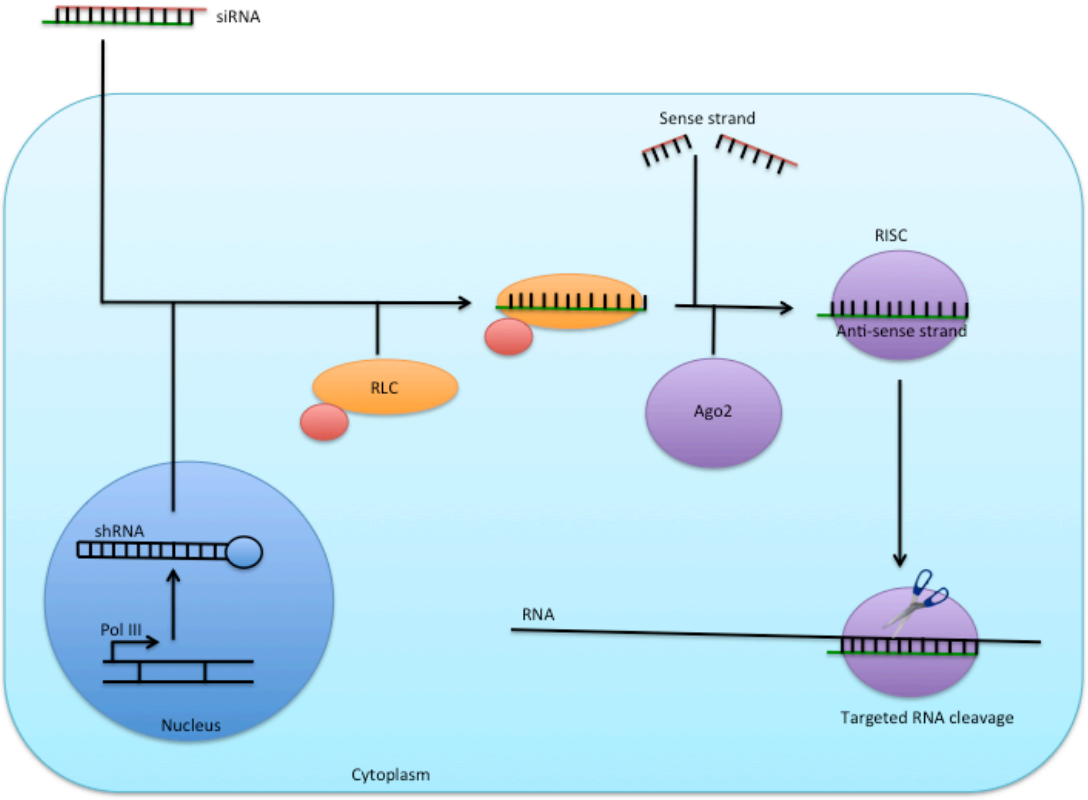

Fig. 1.9| RNAi mechanism. Subsequent to uptake of siRNAs into the mammalian cell, the siRNAs are loaded onto RISC by RLC. During this process, the sense strand is degraded. The anti-sense strand guides RISC to its complementary target RNA where Ago2 induces targeted cleavage of the mRNA. RNAi can also be accomplished through the intracellular expression of shRNA in a similar mechanism as described above (Adapted from [234]).

1.12. Aims and Objectives

1.12.1. Aim

The aim of this research was to ascertain a possible role of LRP/LR in the proteolytic processing of APP and hence shedding of Aβ.

1.12.2. Objectives

i. Assess the cellular distribution of the AD relevant proteins, namely APP, β- and γ-secretases in relation to LRP/LR using indirect immunofluorescence microscopy
ii. Determine, by enzyme-linked immunosorbent assay (ELISA), whether the shRNA-mediated downregulation of LRP/LR will significantly reduce the shedding of Aβ
iii. Determine the molecular mechanism underlying the possible reduction in Aβ shedding. That is, to determine the role of LRP/LR in APP processing, and specifically with β- and γ-secretase via:
    a. The shRNA-mediated downregulation of LRP/LR and Western blot detection for sAPPβ
    b. The determination of the cell surface levels of APP, β- and γ-secretase using flow cytometry on shRNA-treated cells

CHAPTER 2

2. Materials and Methods

2.1. Short hairpin ribonucleic acid (shRNA) production

2.1.1. shRNA design

Prof. M. Weinberg (Department of Internal Medicine, University of the Witwatersrand) assisted with the design of shRNA constructs targeting human LRP mRNA (Appendix 1.1). The shRNA constructs were produced together with a fellow MSc student of the laboratory, Kiashanee Moodley. The target sequence for LRP-shRNA1 was identified based on the bioinformatic prediction tool, 'The RNAi Consortium' (http://www.broadinstitute.org/rnai/). LRP-shRNA7 and LRP-shRNA9 target sequences are the human homologues of the murine target sequences for pENTR siRNA-LRP7 and pENTR siRNA-LRP9, respectively[242] (Appendix 1.2). LRP-shRNA1, 7 and 9 were designed to be Polymerase Chain Reaction (PCR) amplified in two separate rounds using the H1 RNA Polymerase III promoter (pTI-H1, kindly donated by Prof. M. Weinberg) as a template, such that the complete expression cassette included a full length H1 promoter sequence. Further, cassettes were designed with the siRNA guide strand in the 3' arm of the shRNA and to include a ploy-T termination signal. The oligonucleotides used as the forwards and reverse primers were produced by Integrated DNA Technologies. A randomized/scrambled control (pTZ57R/T shRNAscr) that does not target any gene product was used as a negative control and kindly donated by Prof. M. Weinberg.

2.1.2. Nested PCR

First round of PCR

In a sterile, nuclease-free PCR tube the following was combined on ice: 10µl 5X Go Taq® Reaction buffer (Promega), 1µl deoxyrhibonucleotide triphosphate (dNTP) mix-10mM each (Promega), 0.25µl GoTaq® DNA Polymerase-5u/µl (Promega), 5µl 25mM $MgCl_2$ (Promega), 50pg pTI-H1 (template DNA), 0.5µM H1 F + XbaI (forward primer), 0.5µM reverse primer (see below), and nuclease-free water to a final volume of 50µl. Primers used were as follows:

Forward primer:

H1 F + XbaI

5’ GATCTCTAGAGCGAACGCTGACGTCATCAA 3’

Reverse primer:

LRP-shRNA1 R1

5’CCATTTGGGTCAGGAATGGCAACAATTGCACGAGCGGGTCCGAGTGGTC TCATAC3’

or

LRP-shRNA4 R1

5’CTTCCTGGGTCAGGAGAAGGCTGCCTGGATCTGGCGGGTCCGAGTGGTC TCATAC3’

or

LRP-shRNA7 R1

5’GAATTTGGGTCAGGAATTCCTCCTTGGTCACTGCCGGGTCCGAGTGGTCT CATAC3’

The reactions were placed in a thermal cycler (Biometra trio-thermoblock^{TM}), preheated to 95°C. The thermal cycling conditions included an initial denaturation step at 95°C for 3 min, followed by 32 cycles of denaturation at 95°C for 30 sec; annealing at 60°C for 30 sec; and extension at 72°C for 30 sec, with a final extension cycle at 72°C for 15 min. The first round of PCR products were visualized by electrophoresis (Cleaver scientific CS-300V) at 100V for approx. 45min on a 1% agarose gel (Appendix 1.3.1).

Second round of PCR

In a sterile, nuclease-free PCR tube the following was combined on ice: 10µl 5X Go Taq® Reaction buffer (Promega), 1µl deoxyrhibonucleotide triphosphate (dNTP) mix-10mM each (Promega), 0.25µl GoTaq® DNA Polymerase-5u/µl (Promega), 5µl 25mM $MgCl_2$ (Promega), 1µl PCR product from the first round of PCR (template DNA), 0.5µM H1 F + XbaI (forward primer), 0.5µM reverse primer (see below), and nuclease-free water to a final volume of 50µl. Primers used were as follows:

Forward primer: see above

Reverse primer:

LRP-shRNA1 R2

5’ AAAAAAGCTCGTGCAATTGTTGCCATTTGGGTCAGGAATG 3’

or

LRP-shRNA4 R2

5’ AAAAAAGCCAGATCCAGGCAGCCTTCCTGGGTCAGGAGAA 3’

or

LRP-shRNA7 R2

5’ AAAAAAGGCAGTGACCAAGGAGGAATTTGGGTCAGGAATT 3’

Thermal cycle conditions were as previously documented above. The second round of PCR products were visualized by electrophoresis (Cleaver scientific CS-300V) at 100V for approx. 45min on a 1% agarose gel (Appendix 1.3.1).

2.1.3. PCR Clean-up

The Wizard® SV Gel and PCR Clean-up System (Promega) was used to remove excess nucleotides and primers from the PCR products prior to ligation. This system is designed to extract and purify DNA fragments from standard agarose gels in either Tris acetate (TAE) or Tris borate (TBE). PCR products were separated by electrophoresis on a 1% agarose gel as previously described (see 3.1.2). A 1.5ml microcentrifuge tube for each PCR product to be isolated was weighed. The PCR product was excised in a minimal volume of agarose using a clean scalpel. The gel slice was transferred to the weighed microcentrifuge tube and the weight recorded. Membrane binding solution was added to the tube at a ratio of 10µg of solution per 10mg of agarose gel slice. The mixture was vortexed and incubated at 60°C for approximately 10min (or until the gel slice was completely dissolved). One SV Minicoloumn was placed in a collection tube for each dissolved gel slice. The dissolved gel mixture was transferred to the SV Minicolumn assembly and incubated at room temperature for 1min. The SV Minicolumn assembly was centrifuged at 16 000g for 1min (Eppendorf 5417C), followed by removal of the liquid in the collection tube. The column was washed by addition of 700µl Membrane Wash solution to the SV Minicolumn assembly and centrifuged at 16 000g for 1min (Eppendorf 5417C). The collection tube was emptied and the SV Minicolumn re-washed with 500µl Membrane Wash solution. The SV Minicolum assembly was centrifuged at 16 000g for 5min. The liquid from the collection tube was removed and the SV Minicolumn assembly re-centrifuged at 16 000g for 1min. The SV Minicoulmn was transferred to a clean 1.5ml microcentrifuge tube. 50µl of nuclease-

free water was added directly to the centre of the column without touching the membrane with the pipette tip. The system was incubated at room temperature for 1min and then centrifuged at 16 000g for 1min. The microcentrifuge tube containing the eluted DNA was stored at -20°C.

2.1.4. Ligation reaction

The cleaned product of the second round of PCR (see 3.1.3) was ligated into the pTZ57R/T plasmid using the InsTAclone™ PCR Cloning Kit (Fermentas). The ligation reaction was set up by combining the following components in a sterile microcentrifuge tube: 3µl vector pTZ57R/T (0.17pmol ends) (Fermentas), 6µl 5X ligation buffer (Fermentas), 68.5ng PCR product (0.52pmol ends), nuclease-free water to a final volume of 29µl and 1µl T4 DNA liagse (Fermentas). The mixture was mixed and incubated overnight at 4°C.

2.1.5. Preparation of competent bacteria

Preparation of competent *Escherichia coli* (*E.coli*) XL-1blue was achieved using the TransformAid™ Bacterial Transformation kit supplied as part of the InsTAclone™ PCR Cloning kit (Fermentas). The day before transformation, an overnight culture was seeded by inoculating 2ml of C-medium (Fermentas) with a single colony of *E.coli* XL-1blue. The culture was incubated overnight at 37°C with shaking at 200r.p.m (Labcon SPL15). The day of transformation, 1.5ml C-medium was pre-warmed to 37°C for 20min. 150µl of the overnight bacterial culture was added to 1.5ml warmed C-medium. The mixture was incubated for 20min at 37°C with shaking at 180r.p.m. The bacterial cells were pelleted by centrifugation for 1min at 3300g (Eppendorf 5417C). The supernatant was discarded and the cells resuspended in 300µl T-solution (Appendix 1.5.1) followed by incubation on ice for 5min. The mixture was centrifuged for 1min at 3300g, the supernatant discarded and the cell pellet resuspended in 120µl T-solution followed by incubation on ice for 5min.

2.1.6. Transformation

2.5µl of the ligation mixture (see 3.1.4) was placed in a microcentrifuge tube and chilled on ice for 2min. 50µl of the prepared *E.coli* XL-1blue (see 3.1.5) was added to the DNA-containing tube, mixed and incubated on ice for 5min. The mixture was plated onto pre-warmed LB-plates containing 50µg/ml ampicillin, 0.1mM IPTG and

40µg/ml X-Gal (Appendix 1.6.4) and incubated overnight at 37°C for blue/white screening.

2.1.7. Plasmid purification: mini-prep

4-6 white colonies were individually inoculated into 5ml LB medium (Appendix 1.5.2) containing 50µg/ml ampicillin. The cultures were grown at 37°C for 16h with constant shaking at 200r.p.m (Labcon SPL15). Plasmids were isolated using the NucleoSpin® Plasmid DNA Purification kit (Macherey-Nagel) according to the following protocol. 5ml of the saturated *E.coli* LB culture was centrifuged at room temperature for 30sec at 11 000g (Eppendorf 5417C). The supernatant was discarded and the cells resuspened in 250µl Buffer A1. 250µl Buffer A2 was added to the cell suspension, gently mixed by inverting the tube 6-8 times and incubated at room temperature for 5min. 300µl Buffer A3 was added to the tube and mixed thoroughly by inverting 6-8 times. Following centrifugation at room temperature for 5min at 11 000g, the supernatant was placed within a NucleoSpin® Plasmid Column in a 2ml Collection Tube. The column/tube was centrifuged for 1min at 11 000g. The flow-through was discarded and the column placed back into the collection tube. The silica membrane was washed with 600µl Buffer A4, followed by centrifugation for 1min at 11 000g. The flow-through was discarded and the column placed back into the collection tube. The silica membrane was dried by centrifugation for 2min at 11 000g. The column was placed in a 1.5ml microcentrifuge tube and 50µl Buffer AE added. Subsequent to an incubation period of 1min at room temperature, the plasmid DNA was eluted by centrifugation for 1min at 11 000g. The final DNA concentration in the sample was quantified with the Nanodrop® ND-1000 Spectrophotometer.

2.1.8. Plasmid DNA sequencing

The inserts of the isolated plasmid DNA (pTZ57R/T LRP-shRNA1, pTZ57R/T LRP-shRNA7 and pTZ57R/T LRP-shRNA9) were sequenced using standard M13/pUC sequencing primers by Inqaba biotec.

2.2. Cell lines

The Neuro-2a (or N2a) cell line is derived from the neuroblastoma of a strain A albino mouse and supplied by the American Type Culture Collection (ATCC). The cell line was cultured in 10cm tissue culture dishes (Corning) and maintained in a

humidified, 37°C, 5% carbon dioxide atmosphere. N2a cells were cultured in Opti-MEM Reduced Serum Medium (Gibco®) supplemented with 10% Foetal Calf Serum (FCS) (PAA Laboratories) and 1% Penicillin-Streptomycin antibiotic mixture (Gibco®). Sub-confluent cultures (70-80%) were split 1:10 to 1:20.

The human neuroblastoma cell line, SH-SY5Y, is a thrice-cloned sub-line of bone marrow biopsy-derived line SK-N-SH and was obtained from the European Collection of Cell Cultures (ECACC). The cell line was cultured in 10cm tissue culture dishes (Corning) and maintained in a humidified, 37°C, 5% carbon dioxide atmosphere. SH-SY5Y cells were maintained in F12 Nutrient Mixture: Eagles Minimal Essential Media (1:1) (Gibco®) supplemented with 2mM Glutamine (Gibco®), 1% Non-Essential Amino Acids (NEAA) (Gibco®), 15% FCS and 1% Penicillin-Streptomycin antibiotic mixture. Sub-confluent cultures (70-80%) were slit 1:10.

The HEK293 cell line is derived from human embryonic kidney cells transformed with adenovirus 5 DNA and was originally supplied by ATCC. Cell lines were cultured in 10cm tissue culture dishes (Corning) and maintained in a humidified, 37°C, 5% carbon dioxide atmosphere. HEK293 cells were cultured in Dulbecco's Modified Eagle Medium (DMEM) (Gibco®) supplemented with 10% FCS and 1% Penicillin-Streptomycin antibiotic mixture. Subculivation of 70-80% confluent cells occurred at a ratio of 1:10 to 1:20.

The subculturing procedure for the above mentioned cell lines are as follows: the culture medium was aspirated and the monolayer of cells rinsed with Dulbecco's Phosphate-buffered saline (D-PBS) (Gibco®). 1ml of 0.25% (w/v) Trypsin- 0.53mM ethylenediaminetetra-acetic acid (EDTA) solution (Gibco®) was added to the cell culture dish and incubated at 37°C for approximately 5min (or until the cell layer was dispersed when viewed under an inverted microscope). The cells were resuspended in 9ml of the appropriate complete growth medium (see above). Aliquots of the cell suspension were added to new culture vessels, while subcultivation occurred at the ratios listed above.

2.3.Plasmids

For the downregulation of LRP mRNA levels in murine cells (N2a), the following plasmid contructs were employed: pENTR siRNA-LRP4, pENTR siRNA-LRP7 and pENTR siRNA-LRP9[242] (Appendix 1.2). It is important to note that although the aforementioned plasmids are designated as siRNA constructs, they are in fact shRNA constructs. pTZ57R/T LRP-shRNA1 and pTZ57R/T LRP-shRNA7 (see 3.1) (also referred to as LRP-shRNA1 and LRP-shRNA7) were used to downregulate LRP mRNA levels in the human cell line, HEK293. pTZ57R/T shRNAscr (also referred to as LRP-shRNAscr) does not target any gene product and was used as a negative control. pCIneo-GFP, a plasmid encoding the Green Fluorescent Protein (GFP) was used to assess the transfectability of HEK293 and N2a cells (see 3.7.1, 3.7.2 and 3.8.1). Both pTZ57R/T shRNAscr and pCIneo-GFP were kindly donated by Prof. M. Weinberg.

2.4.Preparation of competent bacteria for heat-shock transformation

A colony of *E.coli* XL-1blue cells was inoculated into 2ml LB medium (Appendix 1.5.2) and incubated at 37°C overnight with shaking at 180r.p.m (Labcon SPL15). 1ml of the overnight culture was inoculated into 100ml LB medium (Appendix 1.5.2) and incubated at 37°C and 180r.p.m (Labcon SPL15) to an OD_{600} value of approximately 0.5. The culture was chilled on ice for 15min and centrifuged for 10min at 3300g at 4°C (Heraeus sepatech RF). The supernantant was discarded and the cells resuspended in 30ml ice cold 0.1M$CaCl_2$, followed by incubation on ice for 30min. The cells were centrifuged for 10min at 3300g at 4°C. The supernatant was removed and the cell pellet resuspended in 6ml ice cold 0.1M $CaCl_2$/15% glycerol solution. 50µl of the cell suspension was aliquoted into sterile 1.5ml microcentrifuge tubes, rapidly frozen in liquid nitrogen (10sec) and stored at -70°C.

2.5.Heat-shock transformation

The competent XL-1blue *E.coli* cells prepared above (see 3.4) were thawed on ice for approximately 5min. 100ng of plasmid DNA (see 3.3) was added to 50µl of the competent cells in a sterile microcentrifuge tube. The contents were mixed, placed on ice for 30min, and heat-shocked at 42°C for 45sec. The tube was placed back on ice for 2min and 900µl of pre-warmed SOC medium (37°C) (Appenidx 1.6.6) was added to the mixture. The contents were incubated at 37°C for 60min with shaking at

220r.p.m (Labcon SPL15). 100µl of pENTR siRNA-LRP4, pENTR siRNA-LRP7 and pENTR siRNA-LRP9 transformation mixtures were inoculated onto LB-plates containing 50µg/ml kanomycin (Appendix 1.6.7), which were incubated overnight at 4°C. 100µl of the pTZ57R/T LRP-shRNA1, pTZ57R/T LRP-shRNA7, pTZ57R/T shRNAscr and pCIneo-GFP transformation mixtures were inoculated onto LB-plates containing 50µg/ml ampicillin (Appendix 1.6.3), which were incubated overnight at 37°C.

2.6. Plasmid purification: Maxi-prep

The endotoxin-free plasmid DNA purification kit, NucleoBond® Xtra Maxi Plus EF (Macherey-Nagel), was used to extract sufficient amounts (up to 500µg) of purified plasmid from transformed competent bacteria. A starter culture was prepared by inoculating 5ml of LB medium containing the appropriate selective antibiotic with a single colony picked from the transformed bacterial plate. The following plasmids were grown in LB medium (Appendix 1.5.2) containing 50µg/ml kanomycin: pENTR siRNA-LRP4, pENTR siRNA-LRP7 and pENTR siRNA-LRP9. pTZ57R/T LRP-shRNA1, pTZ57R/T LRP-shRNA7, pTZ57R/T shRNAscr and pCIneo-GFP were grown in LB medium (Appendix 1.5.2) containing 50µg/ml ampicillin. The starter cultures were incubated at 37°C for 8h with shaking at 300r.p.m (Labcon SPL15). A large overnight culture was prepared by diluting the starter culture 1:1000 into 300ml of LB medium containing the appropriate selective antibiotic. Cultures were grown at 37°C for approximately 16h at 300r.p.m until an OD_{600} of 4 was reached. The cells were pelleted by centrifugation at 4°C for 10min at 6 000g (Heraeus sepatech RF). The supernatant was discarded and the cell pellet resuspended in 12ml Resuspension Buffer RES-EF + RNase A. 12ml Lysis Buffer LYS-EF was added to the suspension and the tube gently mixed by inverting 5 times. The mixture was incubated at room temperature for 5min. 12ml Neuralisation Buffer NEU-EF was added to the suspension and the lysate mixed by inverting the tube 10-15 times, followed by incubation on ice for 5min. The NucleoBond® Xtra Column together with the inserted column filter was equilibrated with 35ml Equilibration Buffer EQU-EF and allowed to empty by gravity flow. The lysate was applied to the equilibrated NucleoBond® Xtra Column Filter and allowed to empty by gravity flow. The NucleoBond® Xtra Column and Filter was washed with 10ml Filter Wash Buffer FIL-EF. The column filter was discarded and the NucleoBond® Xtra Column washed with 90ml Wash

Buffer ENDO-EF. The column was washed a third time with 45ml Wash Buffer WASH-EF and the plasmid DNA eluted with 15ml Elution Buffer EF.

The plasmid DNA was concentrated with the NucleoBond® Finalizer (supplied as part of the NucleoBond® Xtra Maxi Plus EF kit (Macherey-Nagel)) according to the following protocol: The DNA was precipitated with 0.7 volumes of isoporpanol, followed by vortexing and incubation at room temperature for 2min. The plunger from a 30ml syringe was removed and the NucleoBond® Finalizer attached to the outlet. The precipitation mixture was filled into the syringe, the plunger reinserted and the mixture slowly pressed through the finalizer. The NucleoBond® Finalizer was washed with 5ml 70% ethanol and the filter membrane of the finalizer dried by pressing through air using the syringe and plunger. The finalizer was attached to the outlet of a 1ml syringe and 500µl of Redissolving Buffer TE-EF added to the syringe. The plasmid DNA was eluted from the finalizer by inserting the plunger into the syringe. The first eluate was transferred back into the syringe and passed a second time through the finalizer. The DNA yield was quantified with the Nanodrop® ND-1000 Spectrophotometer.

2.7. Transient transfections

2.7.1. HEK293 cells

In order to assess the transfectability of HEK293 cells using *Trans*IT®-LT1 Transfection Reagent (Mirus), the cells were transfected with pCIneo-GFP followed by immunofluorescence microscopy. The day before transfection, $3x10^5$ HEK293 cells were seeded in complete growth medium (see 3.2) onto a microscope slide within each well of a 6-well plate (Corning). The cell cultures were incubated overnight in a humidified, 37°C, 5% carbon dioxide atmosphere. On the day of transfection, the complete growth medium was replaced by 2.5ml antibiotic-free complete growth medium. 250µl of serum-free DMEM (Gibco®) was placed in a sterile microcentrifuge tube to which 7.5µl of *Trans*IT®-LT1 Transfection Reagent (pre-warmed to room temperature) was added. 2.5µg plasmid DNA was added to the diluted *Trans*IT-LT1 Reagent, the solution mixed and incubated at room temperature for 30min. The *Trans*IT-LT1 Reagent-DNA complex was added dropwise to the cells and the culture vessel rocked back and forth and from side to side to evenly distribute the *Trans*IT-LT1 Reagent-DNA complexes. Cells were incubated in a humidified,

37°C, 5% carbon dioxide atmosphere for 24h prior to slide preparation for immunofluorescence.

In order to downregulate the LRP mRNA levels in HEK293 cells, cells were transfected with pTZ57R/T LRP-shRNA1, pTZ57R/T LRP-shRNA7 and pTZ57R/T shRNAscr (control) using *Trans*IT®-LT1 Transfection Reagent (Mirus). The day before transfection, $3x10^5$ HEK293 cells were seeded in 2.5ml complete growth medium (see 3.2) in each well of a 6-well plate (Corning). Transfection was carried out as detailed above, however, a transfection incubation period of 72h (as opposed to 24h) was allowed prior to analysis.

2.7.2. N2a cells

In order to assess the transfectability of N2a cells using GenePORTER® 2 Transfection Reagent: QuikEase™ Single-Use Tubes (Genlantis), the cells were transfected with pCIneo-GFP followed by immunofluorescence microscopy. The day before transfection, $6x10^5$ cells were seeded in antibiotic-free complete growth medium (see 3.2) onto a microscope coverslip within each well of a 6-well plate (Corning). 4µg of plasmid DNA was diluted with 100µg DNA Diluent and incubated at room temperature for 5min. Serum-free Opti-MEM Reduced Serum Medium (Gibco®) was added to the diluted DNA to a final volume of 250µl. The Gene PORTER 2 reagent was hydrated with the DNA solution, pipetted up and down 5 times and incubated at room temperature for 20min. The GenePORTER 2/DNA complexes were added directly to the N2a cells growing in 750µl antibiotic-free complete growth medium. The culture vessels were incubated in a humidified, 37°C, 5% carbon dioxide atmosphere for 24h prior to slide preparation for immunofluorescence.

In order to downregulate the LRP mRNA levels in N2a cells, cells were transfected with pENTR siRNA-LRP4, pENTR siRNA-LRP7, pENTR siRNA-LRP9 and pTZ57R/T shRNAscr (control) using GenePORTER® 2 Transfection Reagent: QuikEase™ Single-Use Tubes (Genlantis). The day before transfection, $6x10^5$ N2a cells were seeded in antibiotic-free complete growth medium (see 3.2) in each well of a 6-well plate (Corning). Transfection was carried out as detailed above, however, a

transfection incubation period of 72h (as opposed to 24h) was allowed prior to analysis.

2.7.3. SH-SY5Y cells

Thermo Scientific Dharmacon® Accell® siRNA Reagents is specially modified for use without a transfection reagent and works at a higher concentration than conventional siRNA with minimal disruption of the expression profile. When used with Accell® siRNA® delivery media, little to no delivery optimization is required. This system is particularly useful for difficult-to-transfect cell lines such as SH-SY5Y cells [243]. Accell® siRNA®-human LAMR1 (Thermo Scientific Dharmacon), targeting a single open reading frame of the LRP sequence, together with Accell® siRNA® Delivery media (Thermo Scientific Dharmacon) was used to downregulate LRP/LR expression levels in SH-SY5Y cells.

The day before transfection, $3.3x10^5$ SH-SY5Y cells were plated in complete growth medium (see 3.2) in each well of a 6 well plate (Corning). On the day of transfection, 5x siRNA buffer (Thermo Scientific Dharmacon®) was diluted to 1x siRNA buffer with RNase-free water (Thermo Scientific). 100µM siRNA®-human LAMR1 solution (Thermo Scientific Dharmacon) in 1x siRNA buffer was prepared and stored in aliquots at -20°C until use. In a separate sterile microcentrifuge tube, 20µl of 100µM siRNA solution was mixed with 1980µl Accell® siRNA® Delivery media (Thermo Scientific Dharmacon) to a final concentration of 1µM. The growth media from the cells was removed and replaced with the Accell siRNA-delivery media mixture. The cells were incubated in a humidified, 37°C, 5% carbon dioxide atmosphere for 72h.

2.8. Immunofluorescence microscopy

2.8.1. Transfectability of HEK293 and N2a cells

HEK293 and N2a cells transfected with pCIneo-GFP (see 3.7.1 and 3.7.2, respectively) were tested for their transfectability with their respective transfection reagents. The microscope coverslips onto which the cells were grown and transfected, were fixed in 4% paraformaldedye (Appendix 1.7.1) for 15min. The cells were rinsed four times in PBS (Appendix 1.7.2), blocked and permeabilised in 0.25% Triton X-100 + 0.5% Bovine serum albumin (BSA) solution (Appendix 1.7.4) for 10min,

followed by an additional wash in PBS. 100µl of a 1:100 dilution of Hoechst 33342 stain (2mg/ml, Sigma-Aldrich) in PBS was prepared and placed onto the coverslip for 10min. The cells were rinsed in PBS and mounted onto a clean microscope slide with 50µl Fluoromount™ Aqueous Mounting Medium (Sigma-Aldrich). The prepared slides were allowed to dry for at least 1h in the dark and subsequently stored at 4°C until ready to be viewed. Cells were visualised using the Olympus IX71 Immunofluorescence Microscope and AnalySIS getIT Software. (Hoechst: λ_{ex} = 346nm, λ_{em} = 460nm; GFP: λ_{ex} = 488 nm, λ_{em} = 509nm).

2.8.2. Indirect immunofluorescence microscopy

Indirect immunofluorescence microscopy was employed to assess the cellular distribution of APP, β- and γ-secretase in relation to LRP/LR on the cell surface. HEK293 cells were cultured on microscope coverslips placed within the wells of a six-well plate (Corning). Following incubation in a humidified, 37°C, 5% carbon dioxide atmosphere for 24 hours, cells were fixed in 4% paraformaldehyde (Appendix 1.7.1) at room temperature for 15min. Cultures were rinsed four times in PBS (Appendix 1.7.2), blocked in 0.5% BSA solution (Appendix 1.7.3) for 10min, followed by an additional wash in PBS. 100µl of the primary antibody diluted 1:150 in 0.5% BSA solution (Appendix 1.7.3) was placed on the coverslip and incubated overnight at 4°C. LRP/LR was detected with IgG1-iS18 (Affimed Therapeutics). APP was detected with anti-APP (rabbit polyclonal IgG) (Abcam). β-secretase was detected using anti-BACE (M-83) (rabbit polyclonal IgG) (Santa Cruz Biotechnology). γ-secretase was detected by anti-PEN-2 (FL-101) (rabbit polyclonal IgG) (Santa Cruz Biotechnology). VLA6 (negative control) was detected by anti-very late antigen-6 (VLA6) CD49-f (rabbit monoclonal IgG) (Immunotech). Following incubation in primary antibody, the cells were rinsed three times in 0.5% BSA solution. 100µl of the appropriate secondary antibody diluted 1:350 in 0.5% BSA solution, was added to the cells and incubated in the dark at room temperature for 60min. VLA6, APP, β- and γ-secretase were indirectly labelled with Alexa Fluor® 633 (Life Technologies™) , while an anti-human fluorescein isothiocyanate (FITC) coupled antibody (Cell Lab) was used to label LRP/LR. The cultures were rinsed three times in PBS and mounted onto clean microscope slides with 50µl Fluoromount™ Aqueous Mounting Medium (Sigma-Aldrich). The prepared slides were allowed to dry for at least 60min in the dark and subsequently stored at 4°C until

ready to be viewed. Cells were visualised using the Olympus IX71 Immunofluorescence Microscope and AnalySIS getIT Software. 2D-cytofluorograms were acquired using CellSens Software. (Alexa Fluor® 633: λ_{ex} = 633nm, λ_{em} = 647nm; FITC: λ_{ex} = 494 nm, λ_{em} = 518nm).

2.9. Cell lysate preparation

Following the transfection of HEK293, N2a and SH-SY5Y cells (see 3.7), the culture medium was aspirated and the cells rinsed in D-PBS (Gibco®). 100µl of lysis buffer (Appendix 1.8.1) was added to the cells that were subsequently scraped from the culture dish and added to a microcentrifuge tube. The cell lysates were incubated on ice for 15min, followed by centrifugation for 2min at 20 000g (Eppendorf 5417C). The supernatant was collected, transferred to a new microcentrifuge tube and stored at -20°C.

2.10. Protein quantification

The bicinchoninic acid (BCA) assay is based upon the reduction of Cu^{2+} ions in the presence of peptides, with the amount of Cu^{1+} being formed directly proportional to the concentration of protein. The bicinchoninic acid chelates the $Cu^{1+,}$ forming a deep purple complex that absorbs light at a wavelength of 562nm. 0, 0.2, 0.4, 0.6, 0.8 and 1mg/ml BSA standards were prepared and 25µl of each of the BSA-standards were added to a 96 well plate (Corning). 1:5 dilutions of crude cell lysates (see 3.9) were prepared and added to the plate. 200µl of BCA reagent (Sigma-Aldrich) (Appendix 1.9.1) was added to the wells containing the BCA standards and diluted cell lysates. The plate was incubated at 37°C for 30min and the absorbance measured at 562nm (Tecan Sunrise Microtitre plate).

2.11. Immunoblot analysis

LRP/LR levels within the crude cell lysate of HEK293, N2a and SH-SY5Y transfected cells were determined by Western blot analysis. Additionally, the shedding of sAPPβ within the cell culture medium of transfected HEK293 cells was investigated by the same methodology. The crude cell lysate/cell culture medium was mixed with 5x Laemmli sample buffer (Appendix 1.10.1) and denatured by heating at 95°C for 5min. 30µg of protein per lane (for LRP/LR detection) and 220µg of protein

per lane (for sAPPβ detection) was resolved on a 12% SDS-PAGE gel (Appendix 1.10.2) according to Laemmli[244] at constant voltage (200V) with electrophoresis buffer (Appendix 1.10.3) (Biorad Mini PROTEAN® Tetra cell and PowerPac™ HC). Samples were electroblotted onto polyvinylidene fluoride (PVDF) transfer membrane (PALL Life Sciences), using the PerfectBlue `semi-dry` electro blotter 52-2020 (PeQLab) at 350mA for 45min in Western blot transfer buffer (Appendix 1.11.1). The membrane was blocked in blocking buffer (Appendix 1.11.3) for 60min and incubated with either IgG1-iS18 (1: 5000, for the detection of LRP/LR) (Affimed Therapeutics) or anti-sAPPβ-wild type (1:1000) (Immuno-Biological Laboratories) diluted in blocking buffer, overnight at 4°C. Washing was performed three times at 10min intervals with PBS-Tween (Appendix 1.11.2). The membrane was incubated in a horse-radish peroxidase (HRP) coupled secondary antibody diluted 1:10 000 in blocking buffer for 60min (Rabbit anti-human IgG-HRP (Santa Cruz Biotechnology) for LRP/LR; goat anti-rabbit IgG-HRP (CellLab) for sAPPβ detection). Following incubation in the appropriate secondary antibody, membranes were washed six times at 5min intervals with PBS-Tween, before being exposed to the SuperSignal West Pico Chemiluminescent Substrate kit: working solution (Pearce) (Appendix 1.11.4). Blots were sealed in polyethylene wrap and exposed to CL-X Posure™ Film (Thermo Scientific) for 10min. The film was developed using GBX developer and replenisher (Kodak), briefly rinsed in water, before being fixed in GBX fixer and replenisher (Kodak). The film was rinsed in water before being allowed to dry. The GS-800™ Calibrated Densitometer (Biorad) and Quantity One® 1D Analysis Software (Biorad) was used for densitometric analysis of western blots.

2.12. Enzyme-Linked Immunosorbent Assay (ELISA)

Human Amyloid β(1-x) Assay kit (Immuno-Biological Laboratories) was used to assess the concentration of Aβ shed within the cell culture medium of transfected HEK293 cells. The assay was performed as per manufacturer's instructions. Shortly, human Aβ(1-40) standard solutions containing 0.00, 7.81, 15.63, 31.25, 62.50, 125.00, 250.00 and 500.00pg/ml were prepared. 100µl of each of the standards and transfected HEK293 cell culture medium was added to the wells of the ELISA plate and incubated overnight at 4°C. Each well was washed seven times with wash buffer, before adding 100µl of labeled antibody and incubating at 4°C for 60min. The wells

were washed an additional nine times with wash buffer and 100µl of chromagen solution was added. After an incubation period of 30min at room temperature in the dark, the absorbance was measured at 450nm (Tecan Sunrise Microtitre plate).

2.13. Flow cytometry

Flow cytometry was used to assess the cell surface levels of APP, β- and γ-secretase on HEK293 cells subsequent to shRNA treatment. The medium from transfected HEK293 cells was aspirated and the cells rinsed with D-PBS (Gibco®). 300µl of 0.25% (w/v) Trypsin- 0.53mM EDTA solution (Gibco®) was added to the cell culture dish and incubated at 37°C for approximately 5min (or until the cell layer was dispersed when viewed under an inverted microscope). The detached cells were resuspended in 2ml of HEK293 complete cell culture medium (see 3.2), transferred to 15ml centrifuge tube, and centrifuged at 4°C for 10min at 120g (Heraeus sepatech RF). The supernatant was discarded and the cells resuspended in 1ml 4% paraformaldehyde (Appendix 1.7.1). The mixture was transferred to a microcentrifuge tube and incubated at 4°C for 10min. The cells were centrifuged at 4°C for 10min at 1700g (Eppendorf 5417C) and the cell pellet resuspended in 1ml EPICS™ Sheath Fluid (Beackman Coulter). 500µl of the cell suspension was transferred to a microcentrifuge tube. Both tubes were centrifuged at 4°C for 10min at 1700g, the supernatant discarded and the cell pellet resuspended in 100µl of either 30µg/ml primary antibody solution or EPICS™ Sheath Fluid (control). After an incubation period of 60min at room temperature, the cells were washed three times with 200µl EPICS™ Sheath Fluid, followed by centrifugation at 4°C for 1min at 2000g in between each wash. 100µl of 20µg/ml FITC-coupled secondary antibody was added to both microcentrifuge tubes and allowed to incubate at room temperature for 60min in the dark. Cells were washed three times with 200µl EPICS™ Sheath Fluid, followed by centrifugation at 4°C for 1min at 2000g in between each wash. The cell pellets were resuspended in 1ml EPICS™ Sheath Fluid before analysis on the Accuri C6 flow cytometer (BD Bioscience).

Cell surface APP levels were ascertained using an anti-APP (rabbit polyclonal IgG) (Abcam) and the corresponding goat anti-rabbit FITC secondary antibody. β-secretase levels were detected using anti-BACE (M-83) (rabbit polyclonal IgG) (Santa Cruz

Biotechnology) and goat anti-rabbit FITC secondary antibody (Cell labs). γ-secretase levels on the surface of the cells were detected by a primary antibody directed against the PEN-2 subunit of the γ-secretase complex (anti-PEN-2 (FL-101) (rabbit polyclonal IgG) (Santa Cruz Biotechnology)), and the corresponding goat anti-rabbit FITC secondary antibody.

2.14 Statistical analysis and Pearson's correlation co-efficient

Statistical analyses were performed using a two-tailed student's *t*-test with a 95% confidence interval (GraphPad Prism 5). p-values less than 0.05 were considered significant. The Pearson's correlation coefficient between LRP downregulation and decrease in Aβ shedding was calculated using the WolframAlpha Pearson's correlation coefficient calculator (http://www.wolframalpha.com/widgets/view.jsp?id=3038cb5ccf72f21a13801d9c78f70937).

CHAPTER 3

3. Results

3.1 Production of LRP-shRNA targeting human LRP mRNA

Nested PCR was employed to amplify LRP-shRNA1, LRP-shRNA4 and LRP-shRNA7 oligonucleotides. Bands at 300bp *(Fig. 4.1a)* and 350bp *(Fig. 4.1b)* represent the PCR products from the first and second round of PCR, respectively. LRP-shRNA1, LRP-shRNA4 and LRP-shRNA7 amplified products from the second round of PCR were ligated into the pTZ57R/T plasmid and subsequently transformed into *E.coli* XL-1Blue. Cultures were plated onto LB-plates containing 50μg/ml ampicillin, 0.1mM IPTG and 40μg/ml X-Gal. Successful ligation and transformation was confirmed by the presence of blue and white colonies for LRP-shRNA1 *(Fig. 4.2a)*, LRP-shRNA4 *(Fig. 4.2b)* and LRP-shRNA7 *(Fig. 4.2c)*. Individual white colonies from each plate were inoculated into LB medium containing 50μg/ml ampicillin and the plasmids isolated. Sequencing of plasmids was performed to ensure integrity of the desired sequences and to check for the directionality of the PCR insert. Sequencing results for LRP-shRNA4 displayed several errors with regards to the expected nucleotide code. Due to the high specificity of RNAi, a single nucleotide mismatch can serve as a negative control[245] and as such subsequent experimentation was performed using only LRP-shRNA1 and LRP-shRNA7.

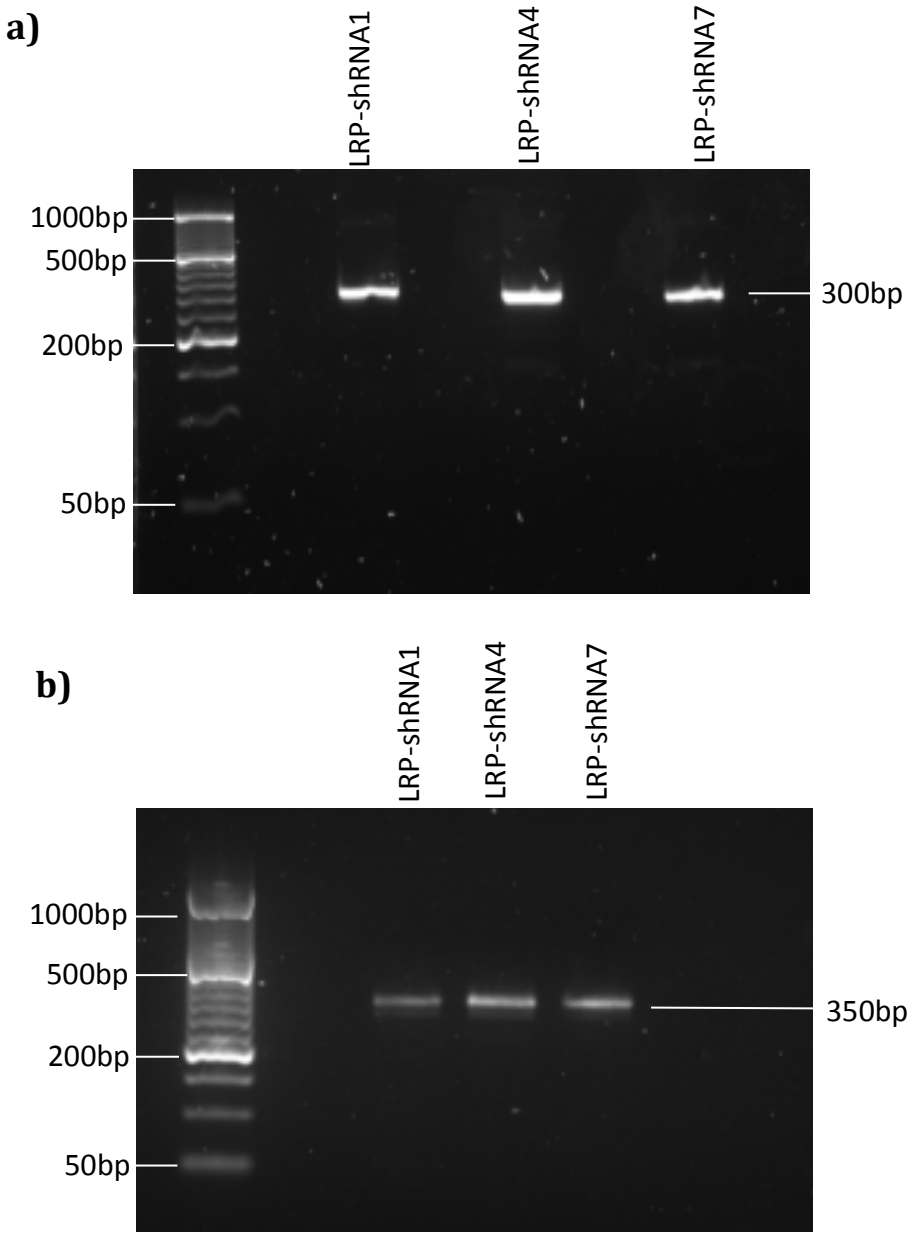

Fig. 3.1| PCR amplified LRP-shRNA oligonucleotides from (a) first round of PCR and (b) second round of PCR. The amplified products from the first and second round of PCR were resolved on a 1% agarose gel. Bands at 300bp and 350bp, respectively, represent the primary and secondary PCR products of LRP-shRNA1, -4 and -7.

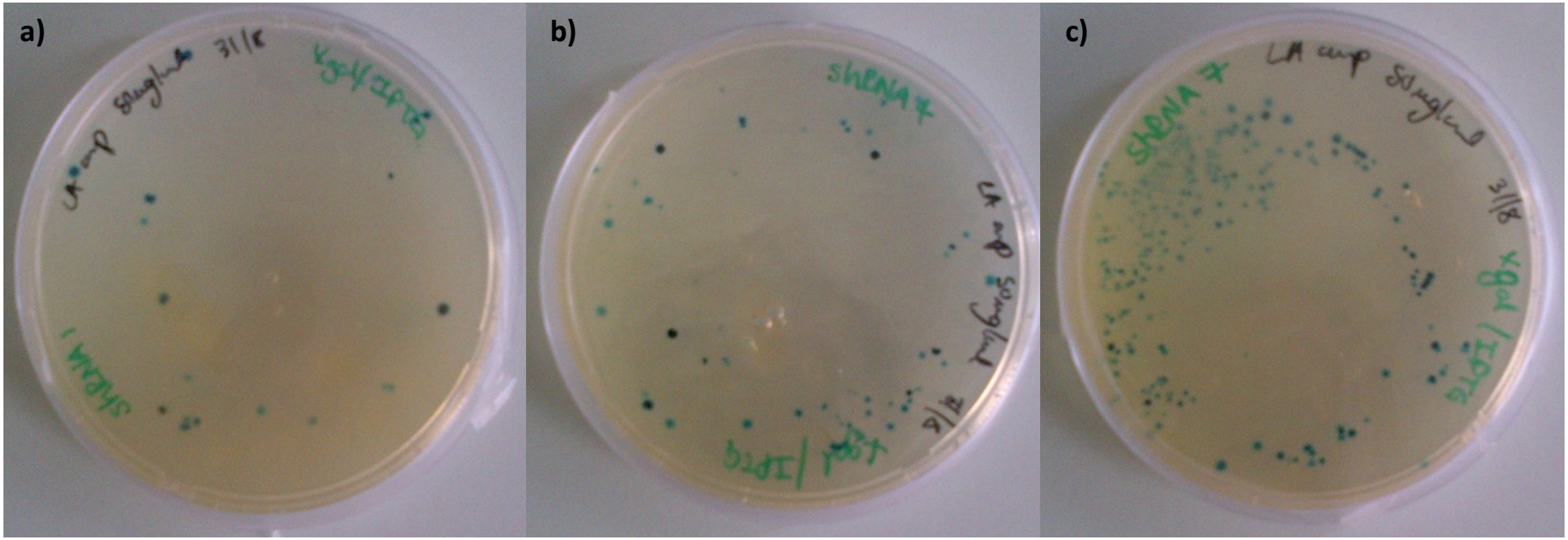

Fig. 3.2| *E.coli* XL-1Blue transformed with (a) LRP-shRNA1, (b) LRP-shRNA4 and (c) LRP-shRNA7. LRP-shRNA1, -4 and -7 PCR amplified products were ligated into the pTZ57R/T plasmid and subsequently transformed into competent *E.coli* XL-1blue for blue-white screening. Cultures were plated onto LB-plates containing 50µg/ml ampicillin, 0.1mM IPTG and 40µg/ml X-Gal.

3.2 HEK293 cells are transfectable using *Trans*IT®-LT1 Transfection Reagent

HEK293 cells were transfected with either pCIneo-GFP *(Fig. 4.3a-c)* or mock transfected (without any plasmid) *(Fig. 4.3 d-f)* using *Trans*IT®-LT1 Transfection Reagent. 24h post transfection, cells were fixed and their nuclei stained with Hoechst 33342. GFP expression of pCIneo-GFP transfected cells is evident *(Fig. 4.3a),* indicative of the transfectability of HEK293 cells using *Trans*IT®-LT1 Transfection Reagent. Absence of GFP expression is noted in the mock-transfected control cells *(Fig. 4.3d)*. Since green fluorescence was observed surrounding the nuclei of each cell, the transfection efficiency of the HEK293 cells was concluded to be 100%.

3.3 N2a cells are transfectable using GenePORTER® 2 Transfection Reagent

N2a cells were transfected with either pCIneo-GFP *(Fig. 4.4a-c)* or mock transfected (without any plasmid) *(Fig. 4.4d-f)* using GenePORTER® 2 Transfection Reagent. 24h post transfection, cells were fixed and their nuclei stained with Hoechst 33342. GFP expression of pCIneo-GFP transfected cells is evident *(Fig. 4.4a),* indicative of the transfectability of N2a cells using GenePORTER® 2 Transfection Reagent. Absence of GFP expression is noted in the mock-transfected control cells *(Fig. 4.4d)*. Since green fluorescence was observed surrounding the nuclei of each cell, the transfection efficiency of the N2a cells was concluded to be 100%.

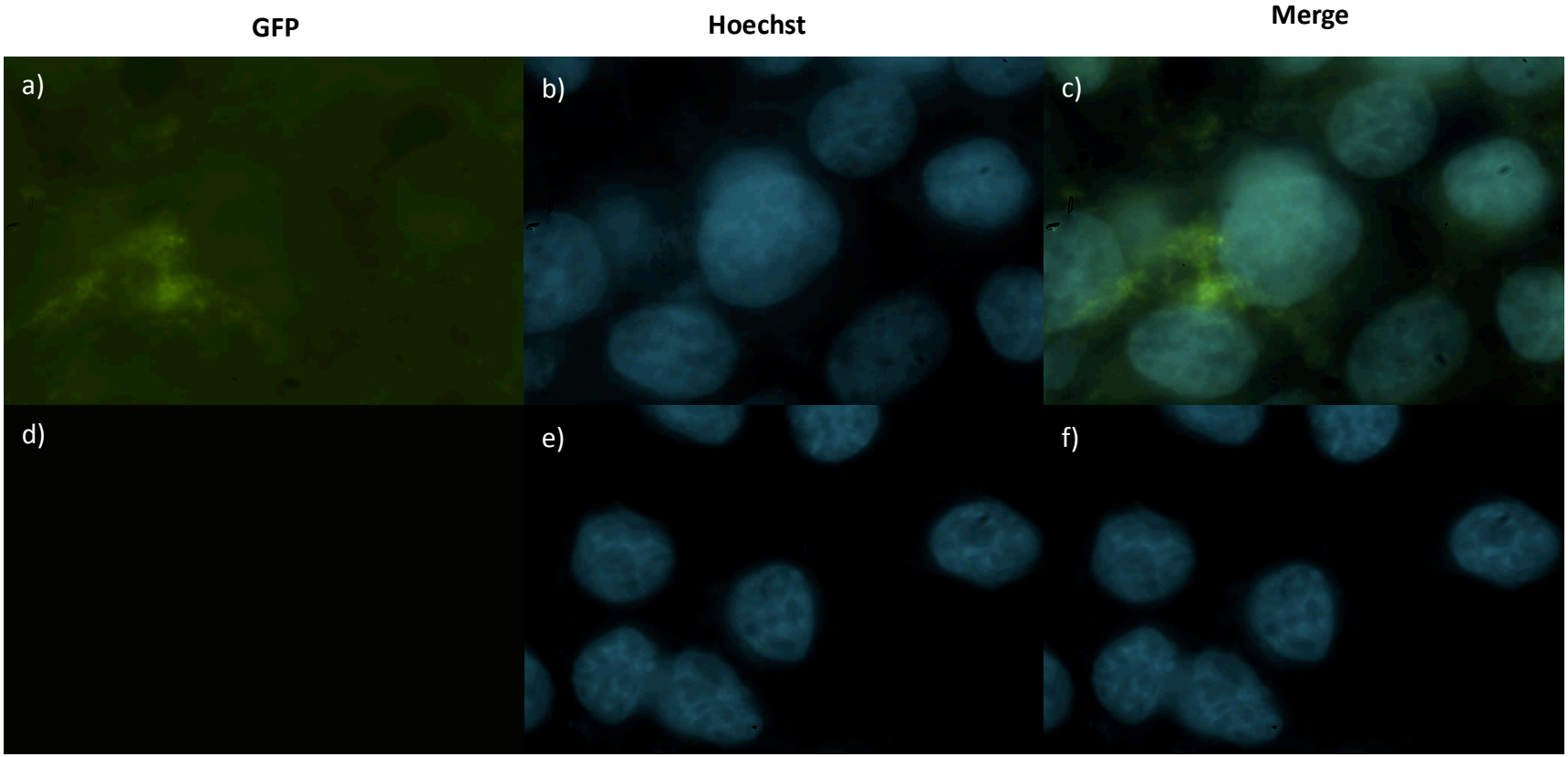

Fig. 3.3| Immunofluorescence microscopy images of HEK293 cells transfected using *Trans*IT®-LT1 Transfection Reagent. HEK293 cells were transfected with **(a-c)** pCIneo-GFP or **(d-f)** mock transfected (without a plasmid) using *Trans*IT®-LT1 Transfection Reagent. 24h post-transfection, cells were fixed and the nuclei stained with Hoechst 33342. **(a)** Green fluorescent protein (GFP) expression was observed in pCIneo-GFP transfected cells, but not in the mock-transfected control **(d)**. **(b, e)** Hoechst-stained nuclei. **(c, f)** Merges between GFP and Hoechst-stained nuclei. Images were obtained using the Olympus IX71 Immunofluorescence Microscope and AnalySIS getIT Software. Hoechst: λ_{ex} = 346nm, λ_{em} = 460nm; GFP: λ_{ex} = 488 nm, λ_{em} = 509nm. Magnification 1000x.

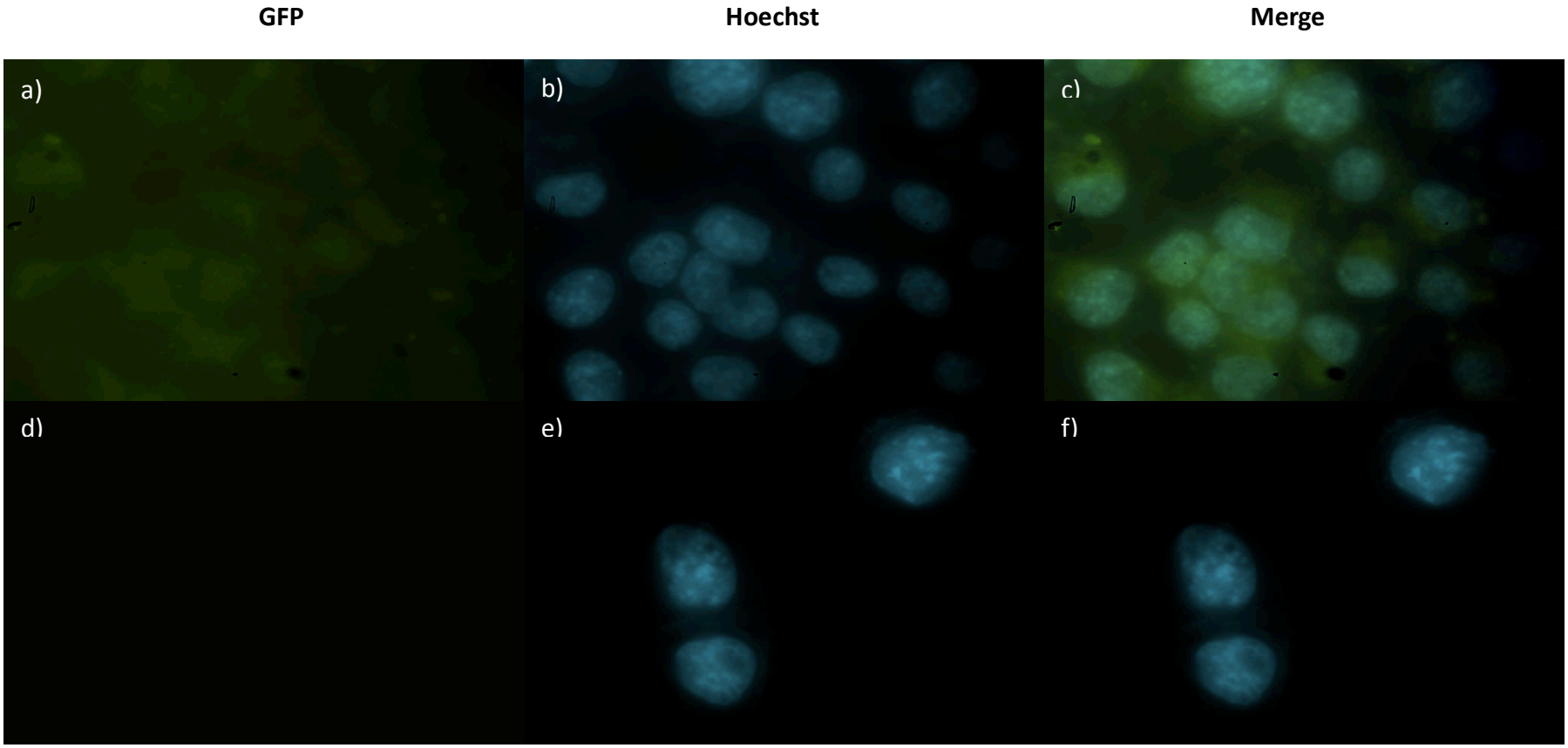

Fig. 3.4| Immunofluorescence microscopy images of N2a cells transfected using GenePORTER® 2 Transfection Reagent. N2a cells were transfected with **(a-c)** pCIneo-GFP or **(d-f)** mock transfected (without a plasmid) using GenePORTER® 2 Transfection Reagent. 24h post-transfection, cells were fixed and the nuclei stained with Hoechst 33342. **(a)** Green fluorescent protein (GFP) expression was observed in pCIneo-GFP transfected cells, but not in the mock-transfected control **(d)**. **(b, e)** Hoechst-stained nuclei. **(c, f)** Merges between GFP and Hoechst-stained nuclei. Images were obtained using the Olympus IX71 Immunofluorescence Microscope and AnalySIS getIT Software. Hoechst: λ_{ex} = 346nm, λ_{em} = 460nm; GFP: λ_{ex} = 488 nm, λ_{em} = 509nm. Magnification 1000x.

3.4 LRP-shRNA treatment of HEK293 cells significantly decreases LRP expression levels

HEK293 cells were transfected with LRP-shRNA1, LRP-shRNA7 and LRP-shRNAscr. 72h post-transfection, cells were lysed and LRP levels assessed by Western blotting. Bands at 37kDa are indicative of LRP *(Fig. 4.5a)*. β-actin, observed at 42kDa, was used as a loading control *(Fig. 4.5a)*. Western blot band intensities from three independent experiments revealed a significant decrease in LRP expression. LRP-shRNA1 and LRP-shRNA7 treated HEK293 cells resulted in a 42.85% and 16.42% reduction in LRP levels, respectively, when compared to the scrambled control (LRP-shRNAscr) *(Fig. 4.5b)*.

3.5 pENTR siRNA-LRP treatment of N2a cells does not significantly downregulate LRP expression

N2a cells were transfected with pENTR siRNA-LRP4, pENTR siRNA-LRP7, pENTR siRNA-LRP9 and LRP-shRNAscr. 72h post-transfection, cells were lysed and LRP expression assessed by immunoblotting. Bands at 37kDa are representative of the 37kDa LRP *(Fig. 4.6a)*. β-actin, seen at 42kDa, was used as a loading control *(Fig. 4.6a)*. Densitometric analysis from three independent experiments does not reveal a significant change in LRP expression levels in pENTR siRNA-LRP treated N2a cells (compared to the LRP-shRNAscr control) *(Fig. 4.6b)*.

3.6 siRNA-LAMR1 treatment of SH-SY5Y cells does not significantly alter LRP levels

SH-SY5Y cells were either transfected with siRNA-LAMR1 or mock-transfected (without any siRNA). 72h post-transfection, cells were lysed and LRP levels assessed by Western blotting. Bands at 37kDa are indicative of LRP *(Fig. 4.7a)*. The β-actin loading control is seen at 42kDa *(Fig. 4.7a)*. Immunoblot banding intensities from three independent experiments does not show a significant change in LRP levels in siRNA-LAMR1 treated SH-SY5Y cells (as compared to the mock-transfected control) *(Fig. 4.7b)*.

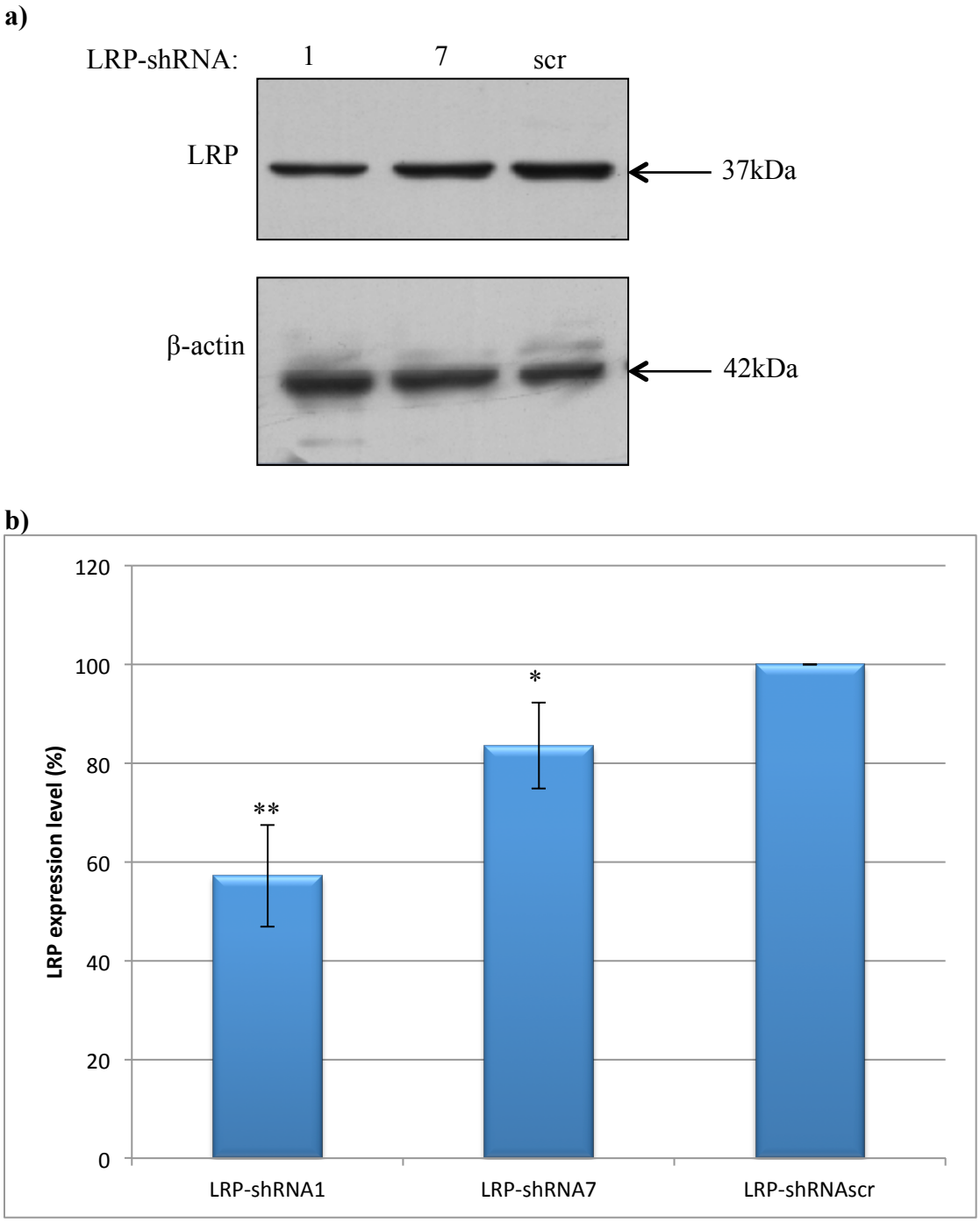

Fig. 3.5| Effect of shRNA treatment on LRP levels in HEK293 cells. (a) HEK293 cells were transfected with LRP-shRNA1, LRP-shRNA7 and LRP-shRNAscr. 72h post-transfection, cells were lysed and LRP levels assessed by Western blotting. β-actin was used as a loading control. **(b)** Western blot band intensities from three independent experiments were quantified using Quanity One 4.5.2 software. Results shown are expressed as percentage changes compared to control levels. *$p<0.05$, **$p<0.01$, Student's *t*-test.

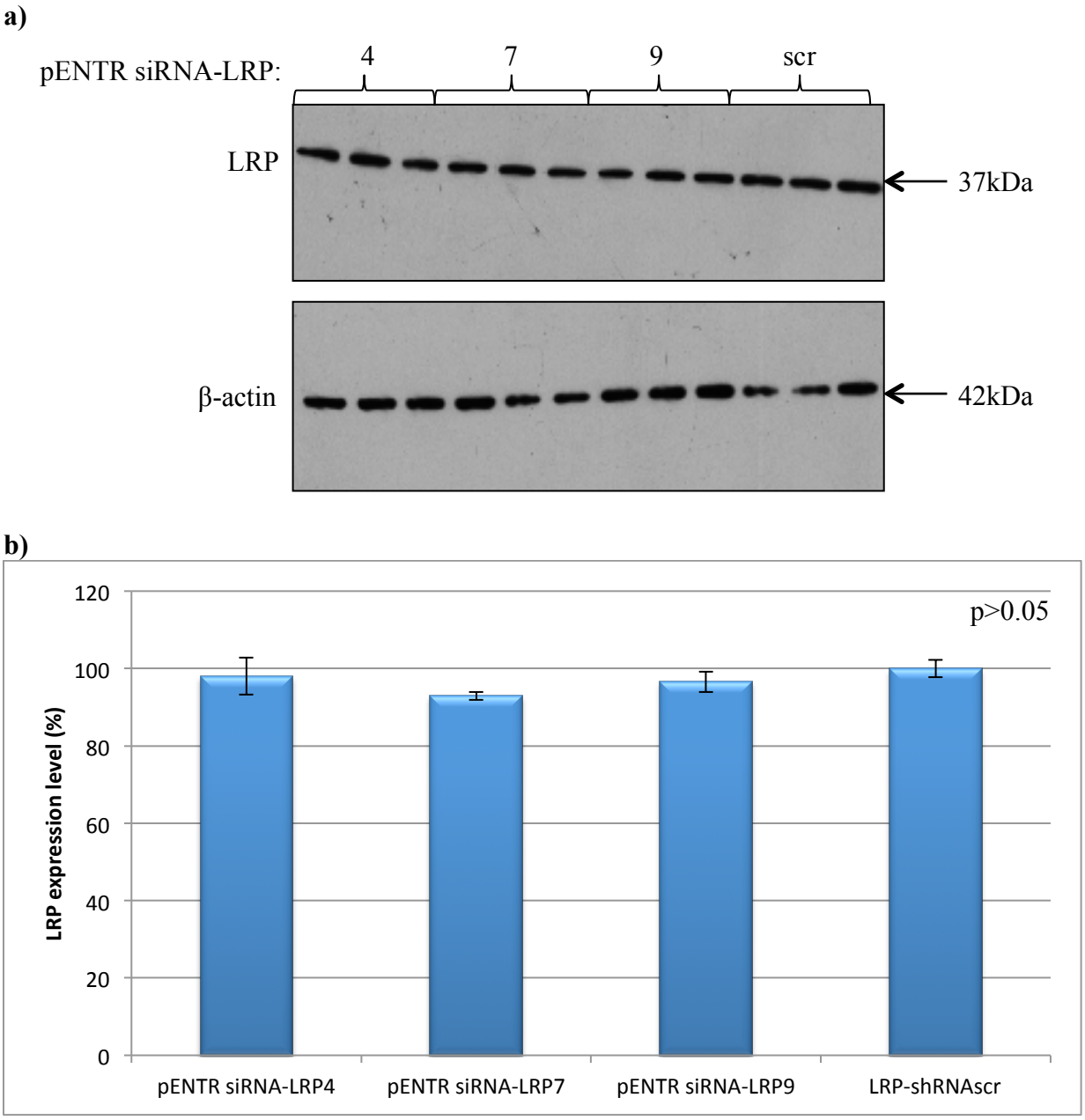

Fig. 3.6| Effect of pENTR siRNA-LRP treatment on LRP levels in N2a cells. (a) N2a cells were transfected with pENTR siRNA-LRP4, pENTR siRNA-LRP7 and pENTR siRNA-LRP9 (as well as a scrambled control, LRP-shRNAscr). 72h post-transfection, cells were lysed and LRP levels assessed by Western blotting. β-actin was used as a loading control. **(b)** Western blot band intensities from three independent experiments were quantified using Quanity One 4.5.2 software. Results shown are expressed as percentage changes compared to control levels. p>0.05, Student's *t*-test.

a)

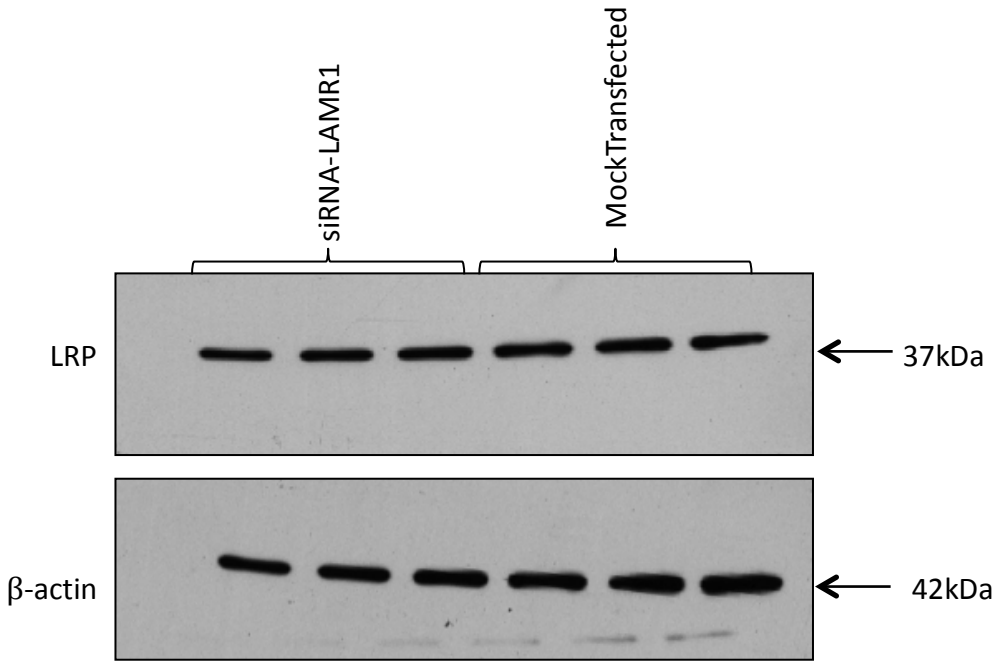

b)

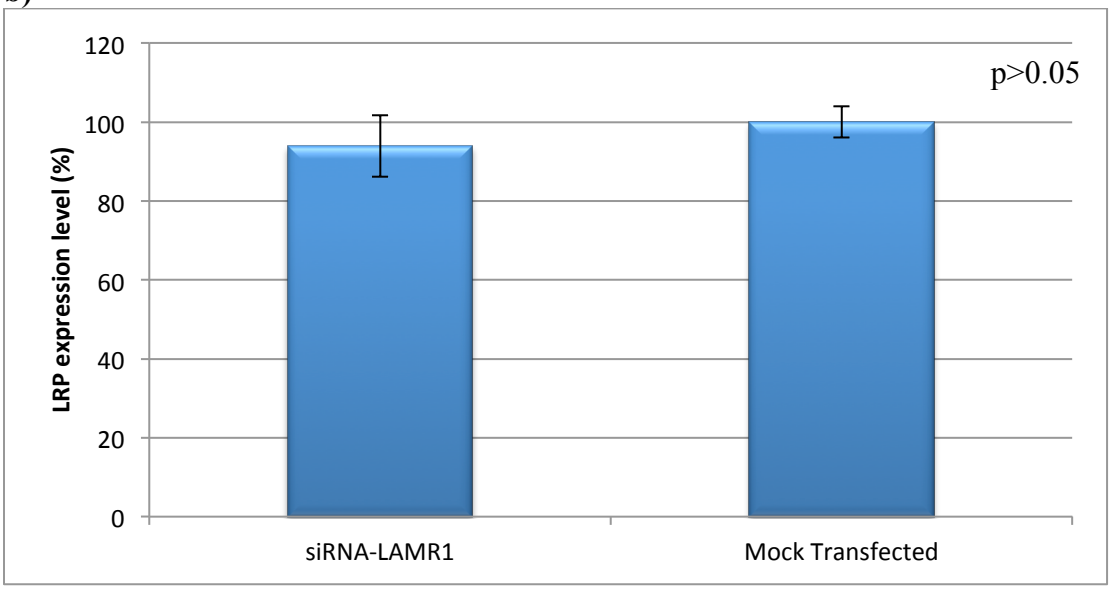

Fig. 3.7| Effect of siRNA-LAMR1 treatment on LRP levels in SH-SY5Y cells. (a) SH-SY5Y cells were either transfected with siRNA-LAMR1 or mock transfected. 72h post-transfection, cells were lysed and LRP levels assessed by Western blotting. β-actin was used as a loading control. **(b)** Western blot band intensities from three independent experiments were quantified using Quanity One 4.5.2 software. Results shown are expressed as percentage changes compared to control levels. $p>0.05$, Student's *t*-test.

3.7 LRP-shRNA treatment of HEK293 cells significantly decreases Aβ shedding

To investigate whether LRP/LR is involved in the amyloidogenic pathway and more specifically Aβ shedding into the extracellular space, HEK293 cells were transfected with LRP-shRNA1, LRP-shRNA7 and the scrambled control, LRP-shRNAscr. 72h post-transfection, the Aβ concentration of the cell culture medium of the transfected cells was analysed using an Aβ ELISA. A 42.85% and 16.42% decrease in LRP expression levels, correlated to a significant 16.88% and 11.95% reduction in Aβ shedding in HEK293 cells (for LRP-shRNA1 and LRP-shRNA7, respectively) *(Fig. 4.8a)*. No significant difference in Aβ concentration was observed in LRP-shRNAscr and mock-transfected HEK293 cells *(Fig. 4.8b)*.

3.8 There is a strong positive correlation between LRP downregulation and reduced Aβ shedding

The Pearson's correlation co-efficient was calculated as a measure of the strength of the relationship between LRP knockdown and decreased Aβ shedding. A Pearson's correlation coefficient value of 1 was obtained between said variables, indicating that there is a strong positive correlation between LRP downregulation and reduced Aβ shedding.

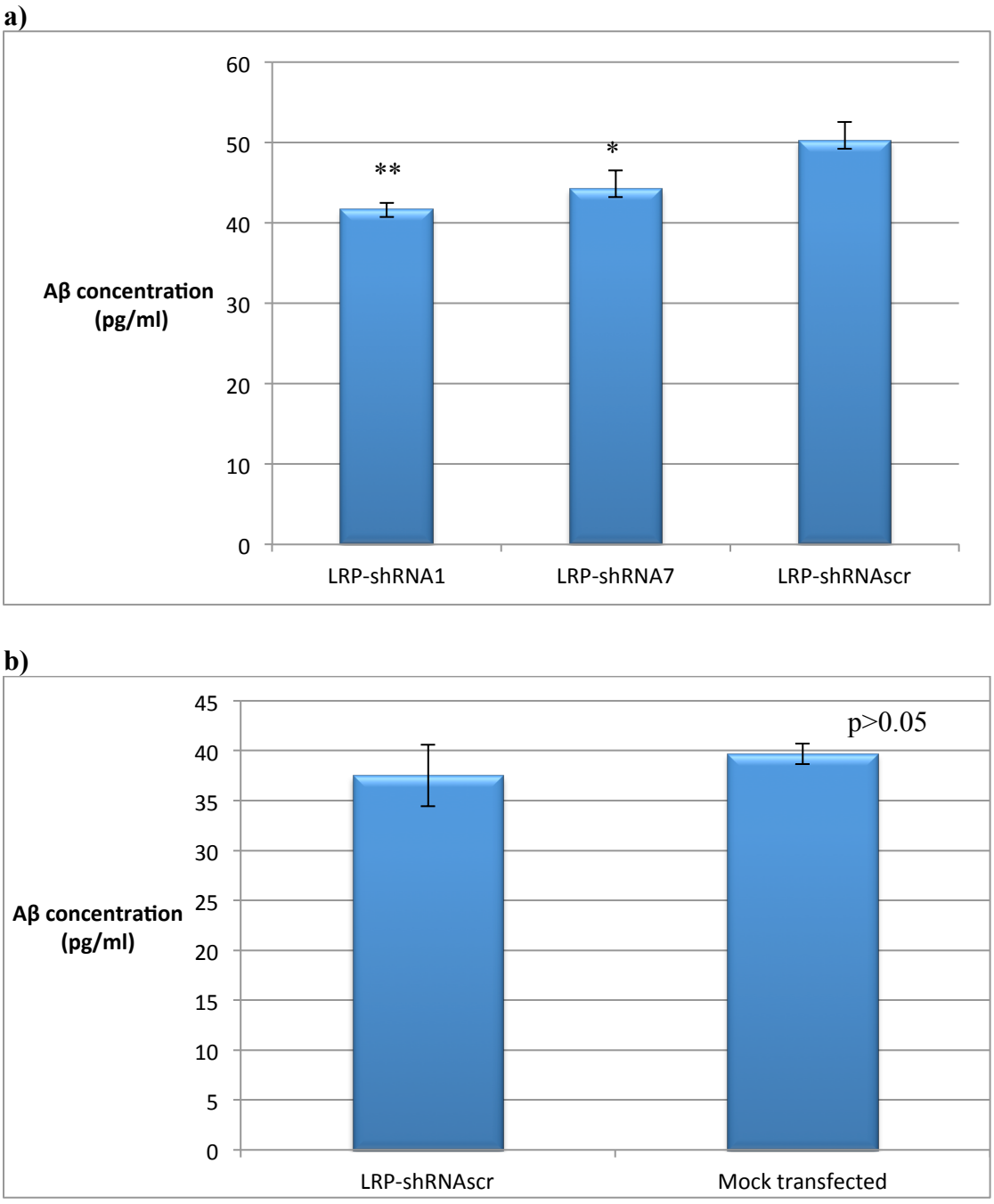

Fig 3.8| Aβ concentration of the cell culture medium of LRP-shRNA transfected HEK293 cells. (a) HEK293 cells were transfected with LRP-shRNA1, LRP-shRNA7 and the scrambled control, LRP-shRNAscr **(b)** HEK293 cells were either transfected with the scrambled control or mock-transfected with no plasmid. 72h post- transfection, the Aβ concentration of the cell culture medium was analysed using an Aβ ELISA. n=3, *p<0.05, **p<0.01, Student's *t*-test.

3.9 LRP-shRNA treatment of HEK293 cells does not alter cell surface expression of APP, β-secretase and γ-secretase

In order to determine whether LRP/LR influences the amyloidogenic pathway through alteration of cell surface expression levels of the AD relevant proteins, flow cytometry was employed. HEK293 cells were either transfected with LRP-shRNA1, LRP-shRNA7, LRP-shRNAscr or mock-transfected without a plasmid. The difference in fluorescence (shift to the right in the flow cytometry histogram overlay plots) of the APP, β-secretase and γ-secretase stained LRP-shRNA-transfected cells relative to that of unstained, mock-transfected control cells reflects the number of HEK293 cells that possessed the aforementioned AD relevant proteins on the cell surface *(Fig. 4.9a)*. Over 99% of all HEK293 cells analysed (for LRP-shRNA1, LRP-shRNA7 and LRP-shRNAscr) revealed APP, β-secretase and γ-secretase on their cell surface *(Fig. 4.9a and b)*. Analysis of three independent experiments showed that LRP-shRNA1 and LRP-shRNA7 treated HEK293 cells did not significantly alter cell surface levels of APP, β-secretase and γ-secretase (compared to the LRP-shRNAscr control) *(Fig. 4.9b)*.

a)

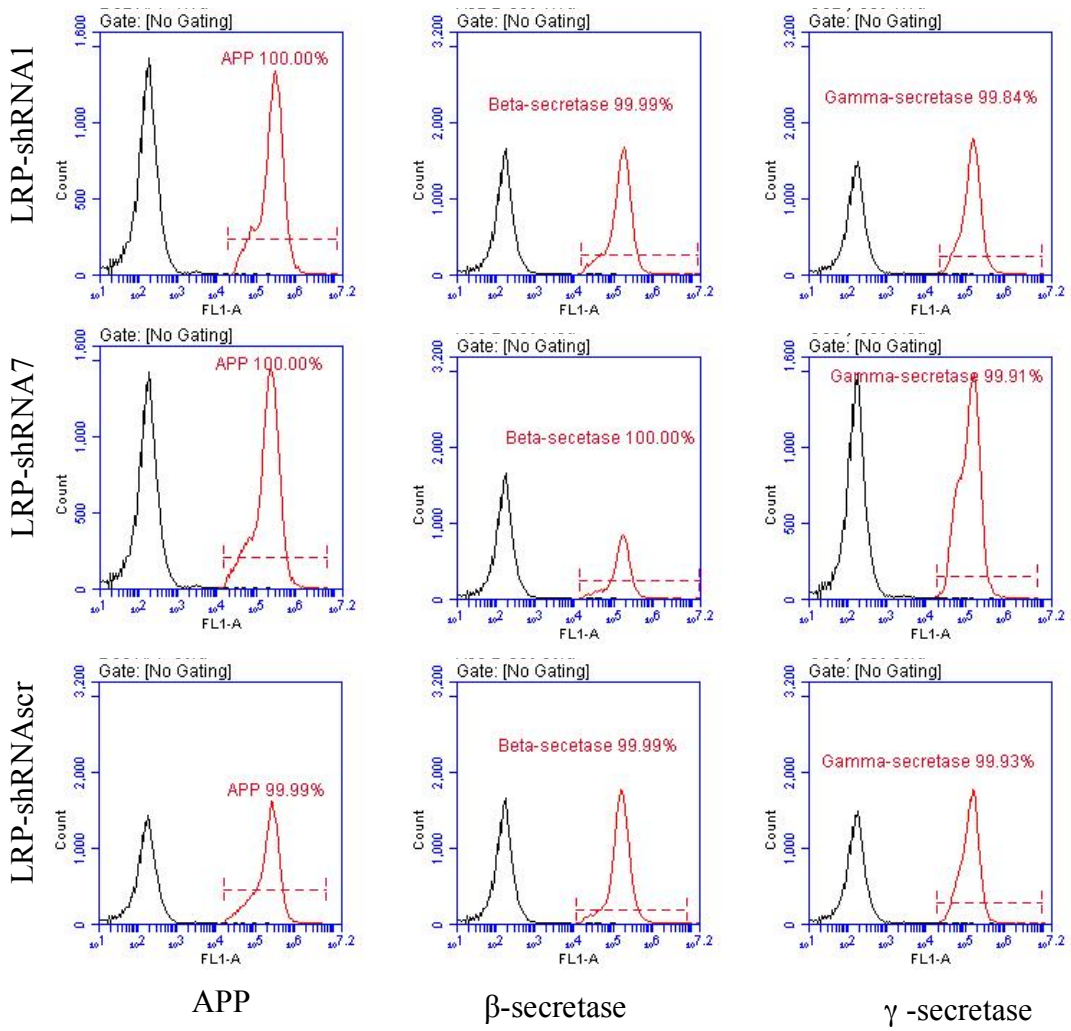
LRP-shRNA1
LRP-shRNA7
LRP-shRNAscr
Gate: [No Gating]
APP 100.00%
Beta-secretase 99.99%
Gamma-secretase 99.84%
APP 100.00%
Beta-secetase 100.00%
Gamma-secretase 99.91%
APP 99.99%
Beta-secetase 99.99%
Gamma-secretase 99.93%
Count
FL1-A
APP
β-secretase
γ -secretase

b)

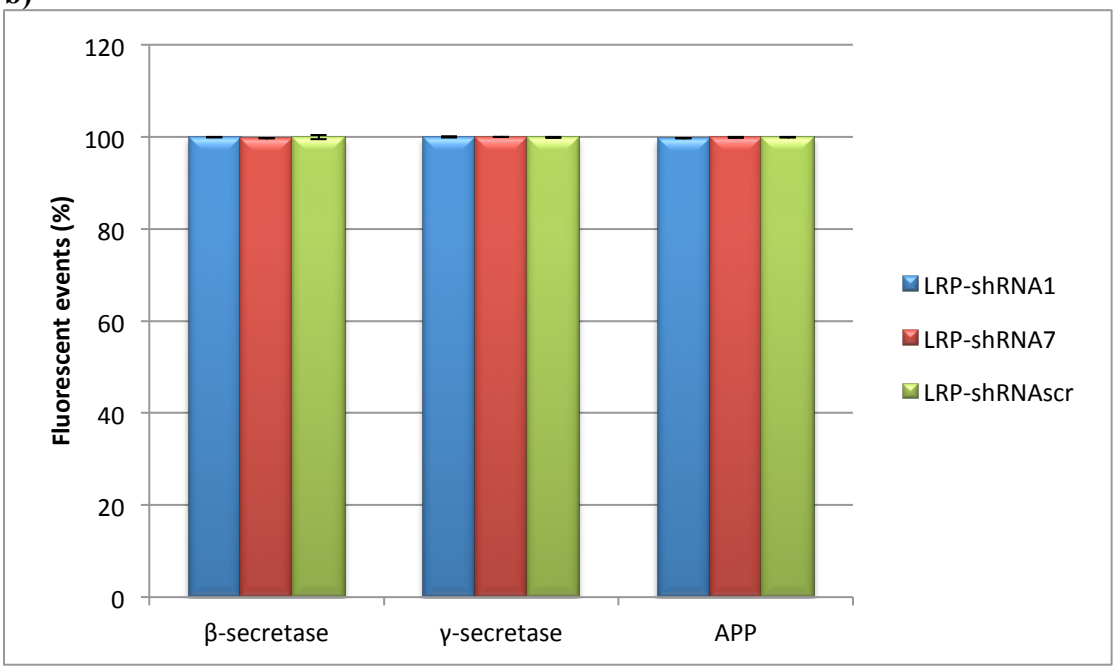

Fig. 3.9| Analysis of APP, β-secretase and γ-secretase levels on the surface of shRNA treated HEK293 cells by flow cytometry. HEK293 cells were transfected with LRP-shRNA1, LRP-shRNA7 and LRP-shRNAscr. 72 hours post transfection, the cell surface levels of APP, β- and γ-secretase were ascertained by flow cytometry (BD Accuri C6). **(a)** Flow cytometry histogram overlay plots. Images shown are a representative of 3 independent experiments. **(b)** Bar chart of cell surface levels of the AD related proteins. n=3, $p>0.05$, Student's *t*-test.

3.10 sAPPβ levels are significantly decreased by LRP-shRNA treatment of HEK293 cells

In an attempt to elucidate the mechanism by which LRP/LR influences the amyloidogenic pathway, sAPPβ levels of the cell culture medium of LRP-shRNA transfected HEK293 cells was analysed by Western blotting. Bands at 110kDa are representative of sAPPβ *(Fig. 4.10a)*. In the absence of a specific and well-accepted protein loading control for secreted proteins, equal loadings were justified by taking equal volumes of cell culture medium from the same number of cells grown under identical conditions[246]. A 22.66% significant reduction in sAPPβ levels was observed in LRP-shRNA1 treated HEK293 cells (compared to the control, LRP-shRNAscr) *(Fig. 4.10b)*. Although a mean reduction of 14.87% in sAPPβ expression was noted in LRP-shRNA7 treated HEK293 cells, this change was deemed non-significant due to large error bars obtained *(Fig. 4.10b)*.

a)

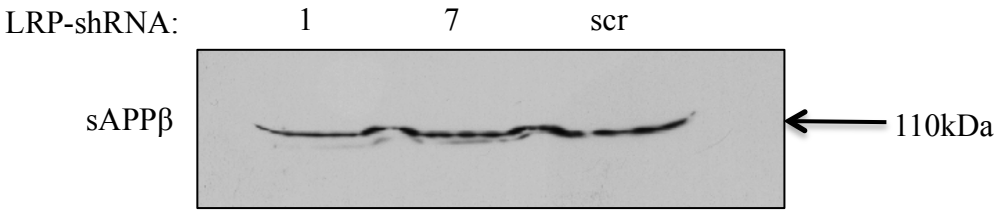

b)

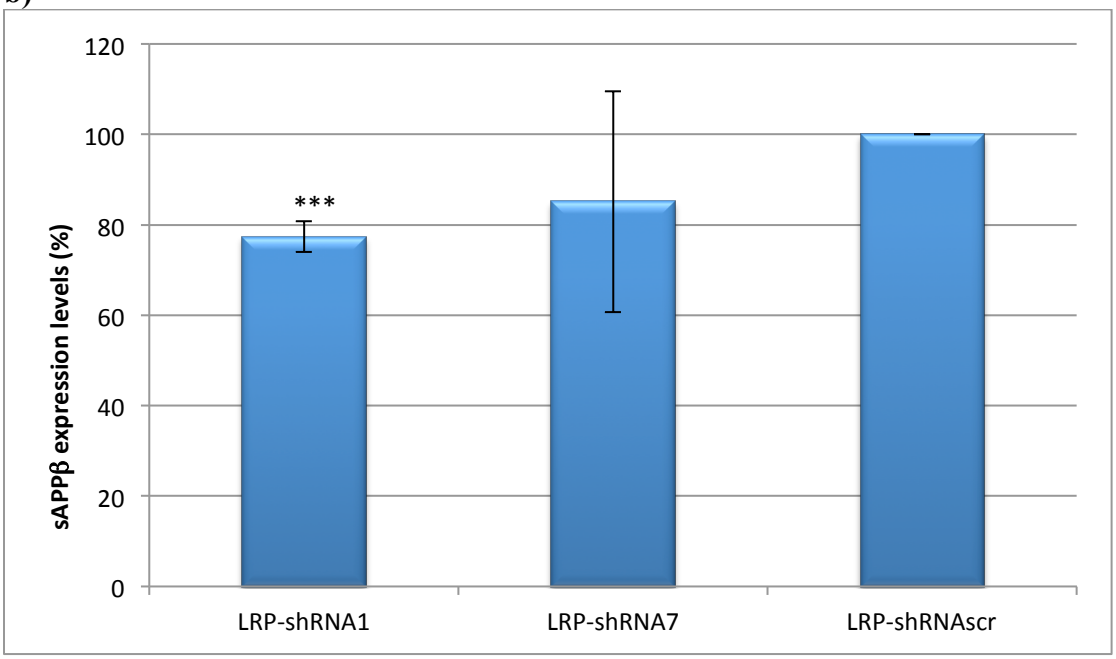

Fig. 3.10| sAPPβ levels of the cell culture medium of LRP-shRNA transfected HE293 cells. **(a)** HEK293 cells were transfected with LRP-shRNA1, LRP-shRNA7 and the scrambled control, LRP-shRNAscr. 72h post- transfection, sAPPβ levels of the cell culture medium was analysed by Western blotting. **(b)** Western blot band intensities from three independent experiments were quantified using Quanity One 4.5.2 software. Results shown are expressed as percentage changes compared to control levels. ***p<0.001, Student's *t*-test.

3.11 LRP/LR co-localises with APP, β-secretase and γ-secretase on the surface of HEK293 cells

Indirect immunofluorescence microscopy was employed to assess the cellular distribution of LRP/LR in relation to the AD relevant proteins APP, β-secretase and γ-secretase. Indirect immunofluorescence microscopy requires the analysis of two colour images (red and green in this instance) for the presence of an overlapping or co-localisation signal. A high degree of co-localisation indicates close proximity of the two-labeled proteins, and therefore suggests an interaction between them[247]. LRP/LR was shown to co-localise with APP (Fig. 4.11a i-iv), β-secretase *(Fig. 4.11a v-viii)* and γ-secretase *(Fig. 4.11a ix-xii)* on the surface of non-permeabilised HEK293 cells, as represented by the yellow merged images *(Fig. 4.11 iii, vii, xi)* and 2D-cytofluorograms *(Fig. 4.11a iv, viii, xii)*. The 2D-cytofluorograms show the joint distribution of the red and green fluorescence, with a yellow diagonal confirming co-localisation between the proteins of interest. An alternate laminin binding receptor, VLA6, was employed as a negative control and failed to co-localise with LRP/LR (as previously observed by [248]) *(Fig. 4.11a xiii-xvi, Table. 4.1)*. Further, Pearson's correlation co-efficients for co-localisation between LRP/LR and the AD relevant proteins are given *(Table 4.1)*. Pearson's co-efficient is not a true quantification of co-localisation but rather an estimate of the strength of association between two proteins. A Pearson's co-efficient value of 1 is indicative of full correlation, while a value of zero is indicative of the absence of correlation[249]. The Pearson's co-efficient values obtained for LRP/LR with APP, β-secretase and γ-secretase were 0.862, 0.915 and 0.938, respectively, representative of a strong correlation between said proteins and thereby confirming co-localisation results obtained above.

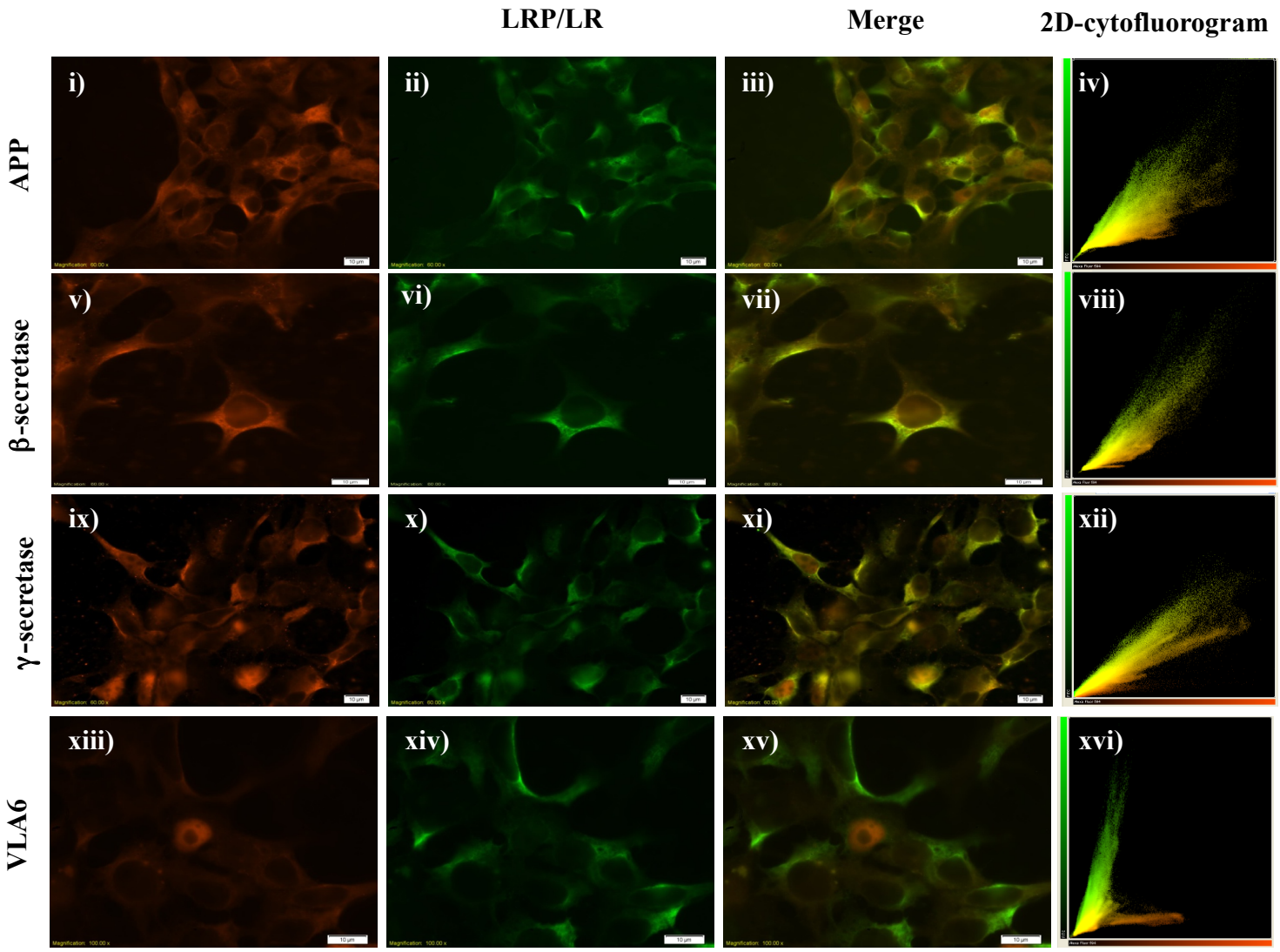
LRP/LR
Merge
2D-cytofluorogram
APP
β-secretase
γ-secretase
VLA6
i)
ii)
iii)
iv)
v)
vi)
vii)
viii)
ix)
x)
xi)
xii)
xiii)
xiv)
xv)
xvi)

Fig. 3.11| Co-localisation between LRP/LR and the AD relevant proteins on the surface of HEK293 cells. HEK293 cells were indirectly immunolabelled for detection using the Olympus IX71 Immunofluorescence Microscope and AnalySIS getIT Software. (**i)** APP (detected by anti-APP). (**v)** β-secretase (detected using anti-BACE (M-83). (**ix)** γ-secretase (detected by anti-PEN-2 (FL-101). **(xiii)** VLA6, a negative control (detected by anti-very late antigen-6 (VLA6) CD49-f). APP, β-secretase, γ-secretase and VLA6 were indirectly labelled with Alexa Fluor® 633, while an anti-human FITC conjugated antibody was used to label LRP/LR (**ii, vi, x, xiv**). The merges between LRP/LR and AD relevant proteins are shown (**iii, vii, xi, xv**) and the corresponding 2D-cytofluorograms (acquired using CellSens Software) have been included to confirm the degree of co-localisation (**iv, viii, xii, xvi).** Alexa Fluor® 633: λ_{ex} = 633nm, λ_{em} = 647nm; FITC: λ_{ex} = 494 nm, λ_{em} = 518nm.

Table 3.1| Pearson's correlation co-efficient of co-localisation between LRP/LR and the AD relevant proteins on the surface of HEK293 cells

	Pearson's correlation co-efficient
LRP/LR + APP	0.862
LRP/LR + β-secretase	0.915
LRP/LR + γ-secretase	0.938
LRP/LR + VLA6	0.583

* Pearson's correlation co-efficient for LRP/LR and the AD related proteins, APP, β-secretase and γ-secretase (as well as VLA6, the negative control). A Pearson's correlation co-efficient value of 1 indicates complete co-localisation, while 0 is indicative of no co-localisation.

CHAPTER 4

4. Discussion

4.1 Failure of LRP downregulation in SH-SY5Y and N2a cells by siRNAs/shRNAs directed against LRP mRNA

Transfection of SH-SY5Y and N2a cells with siRNA-LAMR1 and pENTRsiRNA-LRP4, 7 and 9, respectively, failed to result in significant LRP knockdown. Lipid-based transfection and electroporation are widely used and well-validated techniques for transfection of many standard cell lines. Such methods have often proved ineffective for cell types that are typically refractory to standard lipid-based delivery. Neuronal cells, including N2a and SH-SY5Y cells are such examples[250]. Accell siRNA (Dharmacon) offers the advantage of enabling transfection into difficult-to-transfect cell types without the need for transfection reagents, viral vector or instruments. Accell siRNA has been shown to be effective in SH-SY5Y cells[251], albeit with an alternate gene target to the one used in this dissertation. A single siRNA targeting the LRP gene (siRNA-LAMR1) was selected for use in SH-SY5Y cells; however, a mixture of four siRNA (provided as a single reagent, SMARTpool (Dharmacon)) would provide advantages in both potency and efficacy of gene knockdown. Gene knockdown can be determined by both mRNA and protein knockdown. In this study, protein levels were assessed by Western blotting. Perhaps a more sensitive technique for detecting gene silencing, and one that could be used in future studies, is quantitative real time PCR (QRT-PCR)[250]. While this technique is often perceived as quick and reliable, QRT-PCR is not an established technique within our laboratory and can suffer from poor reproducibility and variability[250].

As previously mentioned, N2a cells, like other neuronal cell lines are notoriously difficult to transfect[250]. However, downregulation of LRP was previously achieved in scrapie infected neuronal cells (ScN2a) using pENTR siRNA-LRP4, pENTR siRNA-LRP7 and pENTR siRNA-LRP9, respectively[252]. Endogenous LRP levels were decreased by 50%, 47% and 54% for pENTR siRNA-LRP4, pENTR siRNA-LRP7 and pENTR siRNA-LRP9, respectively (in comparison to the control). Similar results could not be achieved

in N2a cells using the same plasmids and transfection regent in neither this study nor one from a previous student of the laboratory (unpublished data [253]). The transfectability of N2a cells using GenePORTER® 2 Transfection reagent was confirmed and could not provide a possible explanation for the variance in LRP downregulation. Transfection efficiencies of up to 100% in N2a cells using GenePORTER® 2 Transfection reagent have been previously reported[253]. Further, plasmids were sequenced and their nucleotide sequence confirmed, eliminating point mutations within the plasmid as a potential explanation for the observed lack of LRP downregulation. The difference in cell lines (scrapie infected N2a cells compared to N2a cells) could provide a potential explanation as to the apparent ineffectivity of the pENTR siRNA-LRP constructs. In addition, the effect of passage number on cell line transfection must be considered. It has been demonstrated that although low and high passage cells can be transfected equally well, protein expression in high-passage cells is significantly altered compared to low passage cells[254; 255]. Higher passage N2a cells were used in this study and could provide an alternate explanation as to the inconsistent transfection performance observed.

4.2 Factors affecting the knockdown of LRP expression in HEK293 cells

A number of factors can influence the degree of gene knockdown induced by RNAi and include i) transfection efficiency, ii) transcription rate of the gene of interest, iii) protein stability, iv) efficacy of the siRNA sequence chosen and v) growth characteristics of the cell line[245]. Transfectability of HEK293 cells using *Trans*IT®-LT1 Transfection Reagent has been proved (Fig. 4.3). Given an siRNA target alone, it is not possible to predict the degree of gene knockdown produced [245]. Further, not all siRNAs directed against a target gene are equally effective in suppressing expression of that target gene[245]. Publicly available siRNA design programs typically show success rates of approximately 50% in generating siRNAs that yield over 70% silencing effects (www.ambion.com/RNAi). LRP-shRNA1 and LRP-shRNA7 achieved 42.85% and 16.42% knockdown of LRP compared to the scrambled control (Fig. 4.5). In order to achieve higher levels of gene knockdown, several more siRNA targets would need to be evaluated.

4.3 LRP-shRNA treatment of HEK293 cells significantly decreases Aβ shedding

A 42.85% and 16.42% decrease in LRP expression in HEK293 cells, correlated to a significant 16.88% and 11.95% reduction in Aβ shedding, respectively. These results are the first of its kind to implicate LRP/LR in the amyloidogenic processing of APP and specifically Aβ shedding, pointing to an alternate therapeutic route for the treatment of AD. It would be interesting to investigate the maximum reduction in Aβ shedding attainable through LRP knockdown. However, as stated above, more effective LRP-shRNA targets would need to be investigated in order to achieve LRP knockdown in the range of >90%.

4.4 There is a strong positive correlation between LRP downregulation and reduced Aβ shedding

The Person's correlation coefficient between LRP knockdown and decreased Aβ shedding was calculated to have a value of 1, thus implying that a strong positive correlation between said variable exists. This result further suggests that LRP downregulation and its associated decrease in Aβ shedding could be exploited as an alternative therapeutic route to hamper Aβ shedding and subsequent plaque formation in AD.

4.5 LRP-shRNA treatment of HEK293 cells does not alter cell surface expression of APP, β-secretase and γ-secetase

The cell surface levels of APP, β- and γ-secretase were investigated to allude to a possible mechanism by which LRP knockdown impedes Aβ shedding. Interestingly, LRP downregulation and accompanying hindrance of Aβ shedding did not alter the cell surface expression levels of APP, β-secretase and γ-secretase. That is, the proteins central to the amyloidogenic pathway remained unaffected by a decrease in LRP expression. Thus, the influence of LRP/LR could potentially be as a result of protein interaction. Involvement of LRP/LR in the amyloidogenic pathway is therefore believed to be

independent of gene expression modulation and most likely to involve an interaction (be it direct or indirect) with APP, β-secretase or γ-secretase. This idea is further supported by the co-localisation of LRP/LR with APP, β-secretase and γ-secretase on the surface of HEK293 cells. While co-localisation is not explicitly indicative of an interaction between the proteins of interest, it does imply that a possible protein interaction between LRP/LR and the AD related proteins does exist (co-localisation of LRP/LR with APP, β-secretase and γ-secretase is discussed further under section 4.7). Further studies investigating this interaction, through the use of pull-down assays and fluorescence resonance energy transfer (FRET) for example (see 5.10), would provide valuable insight into the exact mechanism by which LRP/LR influences the amyloidogenic pathway.

4.6 sAPPβ levels are significantly decreased by LRP-shRNA treatment of HEK293 cells

The mechanism by which LRP/LR knockdown impedes Aβ shedding was further investigated through the determination of sAPPβ levels in the cell culture medium of shRNA-treated HEK293 cells. sAPPβ is the initial cleavage product of APP by β-secretase and as such sAPPβ expression levels are an indirect measure of β-secretase activity. Knockdown of LRP levels resulted in a significant decrease in sAPPβ expression, suggesting that downregulation of LRP impedes sAPPβ shedding into the extracellular space. These results implicate LRP/LR in the amyloidogenic processing of APP, and specifically via augmenting the activity of β-secretase.

A significant decrease in sAPPβ expression was only observed as a result of LRP-shRNA1-treatment. Although a mean reduction of 14.87% in sAPPβ expression was noted in LRP-shRNA7 treated HEK293 cells, this change was deemed non-significant due to the large errors attained. Additional experimental repeats would potentially reduce the variability obtained for triplicate value and result in significant data.

The sequential cleavage of APP by β- and γ-secretase are essential for Aβ production, with enhanced activity of either enzyme resulting in increased Aβ shedding and hence plaque formation. The influence of LRP/LR on β-secretase activity has been investigated and clearly implicates LRP/LR in the amyloidogenic pathway through enhanced β-secretase cleavage of APP. Whether, LRP/LR augments the shedding of Aβ through altered γ-secretase activity still needs to be investigated. The contribution of LRP/LR on γ-secretase activity (through the determination of AICD expression) and its potential influence on Aβ shedding cannot as this time be investigated due to the fact that the AICD has eluded detection in cell and tissue lysates, often being regarded as a non-significant by-product of APP processing that is rapidly degraded[256]. An antigen retrieval protocol has recently been employed to detected endogenous AICD by Western blotting; however this technique has only been proved effective for brain tissue samples [256].

4.7 LRP/LR co-localises with APP, β-secretase and γ-secretase on the surface of HEK293 cells

LRP/LR was shown to co-localise with the AD relevant proteins APP, β-secretase and γ-secretase on the surface of HEK293. The Pearson's correlation co-efficients, although not a true quantification of co-localisation, do provide an estimate of the strength of association between the proteins of interest[249]. Taken together, the immunofluorescence images and Pearson's correlation coefficients, allude to a spatial overlap between said proteins on the cell surface. Although these results are not explicitly indicative of an interaction between LRP/LR and APP, β-secretase and γ-secretase, they do imply that a non-random association between LRP/LR and the AD relevant proteins exist. Such use of co-localisation studies as a preliminary indication of protein interaction has been widely used [257]. Further studies to confirm an interaction between LRP/LR and the AD related proteins may include pull-down assays, FRET and live cell imaging (see 5.9).

4.8 Role of LRP/LR in the amyloidogenic processing of APP

The fact that LRP/LR co-localises with β-secretase on the cell surface, taken together with LRP/LR's ability to promote β-secretase activity, has led us to propose a direct interaction between LRP/LR and β-secretase. This interaction would appear to enhance the amyloidogenic processing of APP and hence shedding of Aβ. Further studies validating this interaction would obviously be required to prove this hypothesis.

As mentioned above (see 5.6), the contribution of γ-secretase on the proteolytic processing of APP has not been investigated within this study for various reasons. Co-localisation of LRP/LR with γ-secretase does imply that an interaction between said proteins exists and it hypothesized that the influence of LRP on Aβ shedding may further be augmented by enhanced γ-secretase activity either through a direct or indirect interaction of said proteins. Co-localisation of LRP/LR with APP, through further investigation, may prove to be an important binding partner involved in the amyloidogenic pathway, with an interaction possibly enhancing β-secretase/γ-secretase activity or both.

Alternatively, the observed effects of LRP on the amyloidogenic pathway are potentially through a more indirect route. As LRP/LR is the receptor for PrP^{C} [209], a knockdown of LRP/LR would result in an increased concentration of freely available PrP^{C} on the cell surface. PrP^{C} has been shown to negatively regulate β-secretase activity and hence Aβ shedding [179]. Thus we postulate that the effects observed upon shRNA treatment could potentially be as a result of more freely available PrP^{C} on the cell surface to hamper β-secretase activity. As this is the first investigation implicating LRP/LR in the amyloidogenic processing of APP, there are still many unknowns with regards to the mechanism by which LRP/LR influences Aβ shedding. Further studies will provide valuable insight as to the role of LRP/LR in the proteolytic processing of APP and hence contribution to AD.

4.9 Conclusions

A novel role of LRP/LR in AD and more specifically in the amyloidogenic processing of APP has been identified. Downregulation of LRP though the use of shRNA resulted in a decrease in both sAPPβ and Aβ shedding within the extracellular space. LRP-shRNA treatment has been proposed to exert its effect through inhibiting the activity of β-secretase rather than modulating gene expression of APP, β-secretase and γ-secretase. Further, LRP/LR has been shown to co-localise with the AD relevant proteins APP, β-secretase and γ-secretase on the cell surface, alluding to a possible interaction between said proteins. Owing to LRP/LR's influence in APP processing and Aβ shedding specifically, shRNAs targeted against LRP mRNA could potentially be used as alternative therapeutic tools for the treatment of AD.

4.10 Outlook

The exact mechanism by which LRP/LR influences APP processing still needs to be investigated. Confocal microscopy and specifically z-stacks (which permits one to obtain images of planes at various depths within the sample) will be employed to determine the exact subcellular localisation of LRP/LR in relation to APP, β- and γ-secretase. Pull-down assays between LRP/LR and the AD related proteins will provide valuable information on whether a physical interaction between LRP/LR and APP, β- and γ-secretase exists. Fluorescence resonance energy transfer (FRET) describes the distance-dependent interaction between the electronic excited states of two chromophores (fluorescently tagged LRP/LR and either APP, β-secretase or γ-secretase) in which excitation is transferred from a donor molecule to an acceptor molecule without emission of a photon. When FRET is used as a contrast mechanism, co-localisation of proteins can be imaged with spatial resolution beyond the limits of conventional microscopy. FRET will be employed to determine the co-localisation and hence possible interaction between LRP/LR and the AD-related proteins. Further, live cell imaging will be used to track the movement and possible interaction between fluorescently labeled LRP/LR and the AD-related proteins. This technique will provide more detailed information as to the cellular dynamics involved in the aforementioned interactions. Since shRNAs directed against

LRP mRNA were able to significantly decrease Aβ shedding *in vitro*, its effect *in vivo* warrants investigation. Before transitioning into *in vivo* studies, the mechanism by which LRP/LR exerts its effects in APP processing must be fully elucidated.

REFERENCES

1. Lobo, A., Launer, L. J., Fratiglioni, L., Andersen, K., Di Carlo, A., Breteler, M. M., Copeland, J. R., Dartigues, J. F., Jagger, C., Martinez-Lage, J., Soininen, H. & Hofman, A. (2000). Prevalence of dementia and major subtypes in Europe: A collaborative study of population-based cohorts. Neurologic Diseases in the Elderly Research Group. *Neurology* **54**, S4-9.
2. McKhann, G., Drachman, D., Folstein, M., Katzman, R., Price, D. & Stadlan, E. M. (1984). Clinical diagnosis of Alzheimer's disease: report of the NINCDS-ADRDA Work Group under the auspices of Department of Health and Human Services Task Force on Alzheimer's Disease. *Neurology* **34**, 939-44.
3. Palmer, A. M. (2011). Neuroprotective therapeutics for Alzheimer's disease: progress and prospects. *Trends Pharmacol Sci* **32**, 141-7.
4. Braak, H., Braak, E., Bohl, J. & Bratzke, H. (1998). Evolution of Alzheimer's disease related cortical lesions. *J Neural Transm Suppl* **54**, 97-106.
5. Palmer, A. M. (2002). Pharmacotherapy for Alzheimer's disease: progress and prospects. *Trends Pharmacol Sci* **23**, 426-33.
6. Mayeux, R. & Stern, Y. (2012). Epidemiology of Alzheimer disease. *Cold Spring Harb Perspect Med* **2**.
7. (2010). Alzheimer's association: Alzheimer's Disease Facts and Figures 2010. *Alzheimer's and Dementia*.
8. Thies, W. & Bleiler, L. (2011). 2011 Alzheimer's disease facts and figures. *Alzheimers Dement* **7**, 208-44.
9. Heron, M., Hoyert, D. L., Murphy, S. L., Xu, J., Kochanek, K. D. & Tejada-Vera, B. (2009). Deaths: final data for 2006. *Natl Vital Stat Rep* **57**, 1-134.
10. Bertram, L. & Tanzi, R. E. (2012). The genetics of Alzheimer's disease. *Prog Mol Biol Transl Sci* **107**, 79-100.
11. Tanzi, R. E. & Bertram, L. (2005). Twenty years of the Alzheimer's disease amyloid hypothesis: a genetic perspective. *Cell* **120**, 545-55.
12. Bertram, L. & Tanzi, R. E. (2005). The genetic epidemiology of neurodegenerative disease. *J Clin Invest* **115**, 1449-57.
13. Scheuner, D., Eckman, C., Jensen, M., Song, X., Citron, M., Suzuki, N., Bird, T. D., Hardy, J., Hutton, M., Kukull, W., Larson, E., Levy-Lahad, E., Viitanen, M., Peskind, E., Poorkaj, P., Schellenberg, G., Tanzi, R., Wasco, W., Lannfelt, L., Selkoe, D. & Younkin, S. (1996). Secreted amyloid beta-protein similar to that in the senile plaques of Alzheimer's disease is increased in vivo by the presenilin 1 and 2 and APP mutations linked to familial Alzheimer's disease. *Nat Med* **2**, 864-70.
14. Jarrett, J. T., Berger, E. P. & Lansbury, P. T., Jr. (1993). The carboxy terminus of the beta amyloid protein is critical for the seeding of amyloid formation: implications for the pathogenesis of Alzheimer's disease. *Biochemistry* **32**, 4693-7.

15. Bettens, K., Sleegers, K. & Van Broeckhoven, C. (2010). Current status on Alzheimer disease molecular genetics: from past, to present, to future. *Hum Mol Genet* **19**, R4-R11.
16. Tanzi, R. E. (2012). The genetics of Alzheimer disease. *Cold Spring Harbor perspectives in medicine* **2**.
17. Strittmatter, W. J., Saunders, A. M., Schmechel, D., Pericak-Vance, M., Enghild, J., Salvesen, G. S. & Roses, A. D. (1993). Apolipoprotein E: high-avidity binding to beta-amyloid and increased frequency of type 4 allele in late-onset familial Alzheimer disease. *Proc Natl Acad Sci U S A* **90**, 1977-81.
18. Corder, E. H., Saunders, A. M., Risch, N. J., Strittmatter, W. J., Schmechel, D. E., Gaskell, P. C., Jr., Rimmler, J. B., Locke, P. A., Conneally, P. M., Schmader, K. E. & et al. (1994). Protective effect of apolipoprotein E type 2 allele for late onset Alzheimer disease. *Nat Genet* **7**, 180-4.
19. Serrano-Pozo, A., Frosch, M. P., Masliah, E. & Hyman, B. T. (2011). Neuropathological alterations in Alzheimer disease. *Cold Spring Harb Perspect Med* **1**, a006189.
20. Mandelkow, E. M. & Mandelkow, E. (1998). Tau in Alzheimer's disease. *Trends Cell Biol* **8**, 425-7.
21. Trojanowski, J. Q. & Lee, V. M. (2000). "Fatal attractions" of proteins. A comprehensive hypothetical mechanism underlying Alzheimer's disease and other neurodegenerative disorders. *Ann N Y Acad Sci* **924**, 62-7.
22. Iqbal, K. & Grundke-Iqbal, I. (2002). Neurofibrillary pathology leads to synaptic loss and not the other way around in Alzheimer disease. *J Alzheimers Dis* **4**, 235-8.
23. Crews, L. & Masliah, E. (2010). Molecular mechanisms of neurodegeneration in Alzheimer's disease. *Hum Mol Genet* **19**, R12-20.
24. Beach, T. G., Walker, R. & McGeer, E. G. (1989). Patterns of gliosis in Alzheimer's disease and aging cerebrum. *Glia* **2**, 420-36.
25. Itagaki, S., McGeer, P. L., Akiyama, H., Zhu, S. & Selkoe, D. (1989). Relationship of microglia and astrocytes to amyloid deposits of Alzheimer disease. *J Neuroimmunol* **24**, 173-82.
26. Rogers, J., Luber-Narod, J., Styren, S. D. & Civin, W. H. (1988). Expression of immune system-associated antigens by cells of the human central nervous system: relationship to the pathology of Alzheimer's disease. *Neurobiol Aging* **9**, 339-49.
27. Scheff, S. W., DeKosky, S. T. & Price, D. A. (1990). Quantitative assessment of cortical synaptic density in Alzheimer's disease. *Neurobiol Aging* **11**, 29-37.
28. Scheff, S. W., Price, D. A., Schmitt, F. A. & Mufson, E. J. (2006). Hippocampal synaptic loss in early Alzheimer's disease and mild cognitive impairment. *Neurobiol Aging* **27**, 1372-84.
29. Scheff, S. W., Price, D. A., Schmitt, F. A., DeKosky, S. T. & Mufson, E. J. (2007). Synaptic alterations in CA1 in mild Alzheimer disease and mild cognitive impairment. *Neurology* **68**, 1501-8.
30. DeKosky, S. T. & Scheff, S. W. (1990). Synapse loss in frontal cortex biopsies in Alzheimer's disease: correlation with cognitive severity. *Ann Neurol* **27**, 457-64.

31. Terry, R. D., Masliah, E., Salmon, D. P., Butters, N., DeTeresa, R., Hill, R., Hansen, L. A. & Katzman, R. (1991). Physical basis of cognitive alterations in Alzheimer's disease: synapse loss is the major correlate of cognitive impairment. *Ann Neurol* **30**, 572-80.
32. Gomez-Isla, T., Hollister, R., West, H., Mui, S., Growdon, J. H., Petersen, R. C., Parisi, J. E. & Hyman, B. T. (1997). Neuronal loss correlates with but exceeds neurofibrillary tangles in Alzheimer's disease. *Ann Neurol* **41**, 17-24.
33. Blennow, K., de Leon, M. J. & Zetterberg, H. (2006). Alzheimer's disease. *Lancet* **368**, 387-403.
34. Plant, L. D., Boyle, J. P., Smith, I. F., Peers, C. & Pearson, H. A. (2003). The production of amyloid beta peptide is a critical requirement for the viability of central neurons. *J Neurosci* **23**, 5531-5.
35. Mehta, P. D., Pirttila, T., Patrick, B. A., Barshatzky, M. & Mehta, S. P. (2001). Amyloid beta protein 1-40 and 1-42 levels in matched cerebrospinal fluid and plasma from patients with Alzheimer disease. *Neurosci Lett* **304**, 102-6.
36. Omar, A., Jovanovic, K., Da Costa Dias, B., Gonsalves, D., Moodley, K., Caveney, R., Mbazima, V. & Weiss, S. F. (2011). Patented biological approaches for the therapeutic modulation of the 37 kDa/67 kDa laminin receptor. *Expert Opin Ther Pat* **21**, 35-53.
37. Pimplikar, S. W. (2009). Reassessing the amyloid cascade hypothesis of Alzheimer's disease. *Int J Biochem Cell Biol* **41**, 1261-8.
38. Hardy, J. A. & Higgins, G. A. (1992). Alzheimer's disease: the amyloid cascade hypothesis. *Science* **256**, 184-5.
39. Selkoe, D. J. (1991). The molecular pathology of Alzheimer's disease. *Neuron* **6**, 487-98.
40. Nordberg, A. (2008). Amyloid imaging in Alzheimer's disease. *Neuropsychologia* **46**, 1636-41.
41. Villemagne, V. L., Fodero-Tavoletti, M. T., Pike, K. E., Cappai, R., Masters, C. L. & Rowe, C. C. (2008). The ART of loss: Abeta imaging in the evaluation of Alzheimer's disease and other dementias. *Mol Neurobiol* **38**, 1-15.
42. Caughey, B. & Lansbury, P. T. (2003). Protofibrils, pores, fibrils, and neurodegeneration: separating the responsible protein aggregates from the innocent bystanders. *Annu Rev Neurosci* **26**, 267-98.
43. Younkin, S. G. (1995). Evidence that A beta 42 is the real culprit in Alzheimer's disease. *Ann Neurol* **37**, 287-8.
44. Bentahir, M., Nyabi, O., Verhamme, J., Tolia, A., Horre, K., Wiltfang, J., Esselmann, H. & De Strooper, B. (2006). Presenilin clinical mutations can affect gamma-secretase activity by different mechanisms. *J Neurochem* **96**, 732-42.
45. Glabe, C. C. (2005). Amyloid accumulation and pathogensis of Alzheimer's disease: significance of monomeric, oligomeric and fibrillar Abeta. *Subcell Biochem* **38**, 167-77.
46. Klein, W. L., Krafft, G. A. & Finch, C. E. (2001). Targeting small Abeta oligomers: the solution to an Alzheimer's disease conundrum? *Trends Neurosci* **24**, 219-24.

47. Walsh, D. M. & Selkoe, D. J. (2004). Deciphering the molecular basis of memory failure in Alzheimer's disease. *Neuron* **44**, 181-93.
48. Walsh, D. M. & Selkoe, D. J. (2007). A beta oligomers - a decade of discovery. *J Neurochem* **101**, 1172-84.
49. Lacor, P. N., Buniel, M. C., Furlow, P. W., Clemente, A. S., Velasco, P. T., Wood, M., Viola, K. L. & Klein, W. L. (2007). Abeta oligomer-induced aberrations in synapse composition, shape, and density provide a molecular basis for loss of connectivity in Alzheimer's disease. *J Neurosci* **27**, 796-807.
50. Walsh, D. M. & Selkoe, D. J. (2004). Oligomers on the brain: the emerging role of soluble protein aggregates in neurodegeneration. *Protein Pept Lett* **11**, 213-28.
51. Townsend, M., Shankar, G. M., Mehta, T., Walsh, D. M. & Selkoe, D. J. (2006). Effects of secreted oligomers of amyloid beta-protein on hippocampal synaptic plasticity: a potent role for trimers. *J Physiol* **572**, 477-92.
52. Selkoe, D. J. (2008). Soluble oligomers of the amyloid beta-protein impair synaptic plasticity and behavior. *Behav Brain Res* **192**, 106-13.
53. Shankar, G. M., Li, S., Mehta, T. H., Garcia-Munoz, A., Shepardson, N. E., Smith, I., Brett, F. M., Farrell, M. A., Rowan, M. J., Lemere, C. A., Regan, C. M., Walsh, D. M., Sabatini, B. L. & Selkoe, D. J. (2008). Amyloid-beta protein dimers isolated directly from Alzheimer's brains impair synaptic plasticity and memory. *Nat Med* **14**, 837-42.
54. Mc Donald, J. M., Savva, G. M., Brayne, C., Welzel, A. T., Forster, G., Shankar, G. M., Selkoe, D. J., Ince, P. G. & Walsh, D. M. (2010). The presence of sodium dodecyl sulphate-stable Abeta dimers is strongly associated with Alzheimer-type dementia. *Brain* **133**, 1328-41.
55. Pham, E., Crews, L., Ubhi, K., Hansen, L., Adame, A., Cartier, A., Salmon, D., Galasko, D., Michael, S., Savas, J. N., Yates, J. R., Glabe, C. & Masliah, E. (2010). Progressive accumulation of amyloid-beta oligomers in Alzheimer's disease and in amyloid precursor protein transgenic mice is accompanied by selective alterations in synaptic scaffold proteins. *FEBS J* **277**, 3051-67.
56. Klyubin, I., Betts, V., Welzel, A. T., Blennow, K., Zetterberg, H., Wallin, A., Lemere, C. A., Cullen, W. K., Peng, Y., Wisniewski, T., Selkoe, D. J., Anwyl, R., Walsh, D. M. & Rowan, M. J. (2008). Amyloid beta protein dimer-containing human CSF disrupts synaptic plasticity: prevention by systemic passive immunization. *J Neurosci* **28**, 4231-7.
57. Grundke-Iqbal, I., Iqbal, K., Tung, Y. C., Quinlan, M., Wisniewski, H. M. & Binder, L. I. (1986). Abnormal phosphorylation of the microtubule-associated protein tau (tau) in Alzheimer cytoskeletal pathology. *Proc Natl Acad Sci U S A* **83**, 4913-7.
58. Nukina, N. & Ihara, Y. (1986). One of the antigenic determinants of paired helical filaments is related to tau protein. *J Biochem* **99**, 1541-4.
59. Kidd, M. (1963). Paired helical filaments in electron microscopy of Alzheimer's disease. *Nature* **197**, 192-3.
60. Kidd, M. (1964). Alzheimer's Disease--an Electron Microscopical Study. *Brain* **87**, 307-20.

61. Wisniewski, H. M., Narang, H. K. & Terry, R. D. (1976). Neurofibrillary tangles of paired helical filaments. *J Neurol Sci* **27**, 173-81.
62. Wegmann, S., Jung, Y. J., Chinnathambi, S., Mandelkow, E. M., Mandelkow, E. & Muller, D. J. (2010). Human Tau isoforms assemble into ribbon-like fibrils that display polymorphic structure and stability. *J Biol Chem* **285**, 27302-13.
63. Iqbal, K., Alonso Adel, C., Chen, S., Chohan, M. O., El-Akkad, E., Gong, C. X., Khatoon, S., Li, B., Liu, F., Rahman, A., Tanimukai, H. & Grundke-Iqbal, I. (2005). Tau pathology in Alzheimer disease and other tauopathies. *Biochim Biophys Acta* **1739**, 198-210.
64. Braak, E., Griffing, K., Arai, K., Bohl, J., Bratzke, H. & Braak, H. (1999). Neuropathology of Alzheimer's disease: what is new since A. Alzheimer? *Eur Arch Psychiatry Clin Neurosci* **249 Suppl 3**, 14-22.
65. Braak, H. & Braak, E. (1991). Neuropathological stageing of Alzheimer-related changes. *Acta Neuropathol* **82**, 239-59.
66. Braak, H., Alafuzoff, I., Arzberger, T., Kretzschmar, H. & Del Tredici, K. (2006). Staging of Alzheimer disease-associated neurofibrillary pathology using paraffin sections and immunocytochemistry. *Acta Neuropathol* **112**, 389-404.
67. Arnold, S. E., Hyman, B. T., Flory, J., Damasio, A. R. & Van Hoesen, G. W. (1991). The topographical and neuroanatomical distribution of neurofibrillary tangles and neuritic plaques in the cerebral cortex of patients with Alzheimer's disease. *Cereb Cortex* **1**, 103-16.
68. Arriagada, P. V., Growdon, J. H., Hedley-Whyte, E. T. & Hyman, B. T. (1992). Neurofibrillary tangles but not senile plaques parallel duration and severity of Alzheimer's disease. *Neurology* **42**, 631-9.
69. Bierer, L. M., Hof, P. R., Purohit, D. P., Carlin, L., Schmeidler, J., Davis, K. L. & Perl, D. P. (1995). Neocortical neurofibrillary tangles correlate with dementia severity in Alzheimer's disease. *Arch Neurol* **52**, 81-8.
70. Giannakopoulos, P., Herrmann, F. R., Bussiere, T., Bouras, C., Kovari, E., Perl, D. P., Morrison, J. H., Gold, G. & Hof, P. R. (2003). Tangle and neuron numbers, but not amyloid load, predict cognitive status in Alzheimer's disease. *Neurology* **60**, 1495-500.
71. Ingelsson, M., Fukumoto, H., Newell, K. L., Growdon, J. H., Hedley-Whyte, E. T., Frosch, M. P., Albert, M. S., Hyman, B. T. & Irizarry, M. C. (2004). Early Abeta accumulation and progressive synaptic loss, gliosis, and tangle formation in AD brain. *Neurology* **62**, 925-31.
72. Selkoe, D. J. (2001). Alzheimer's disease: genes, proteins, and therapy. *Physiol Rev* **81**, 741-66.
73. Stanford, P. M., Halliday, G. M., Brooks, W. S., Kwok, J. B., Storey, C. E., Creasey, H., Morris, J. G., Fulham, M. J. & Schofield, P. R. (2000). Progressive supranuclear palsy pathology caused by a novel silent mutation in exon 10 of the tau gene: expansion of the disease phenotype caused by tau gene mutations. *Brain* **123 (Pt 5)**, 880-93.
74. Gorevic, P. D., Goni, F., Pons-Estel, B., Alvarez, F., Peress, N. S. & Frangione, B. (1986). Isolation and partial characterization of neurofibrillary tangles and amyloid plaque core in Alzheimer's disease: immunohistological studies. *J Neuropathol Exp Neurol* **45**, 647-64.

75. Masters, C. L., Simms, G., Weinman, N. A., Multhaup, G., McDonald, B. L. & Beyreuther, K. (1985). Amyloid plaque core protein in Alzheimer disease and Down syndrome. *Proc Natl Acad Sci U S A* **82**, 4245-9.
76. Hung, A. Y. & Selkoe, D. J. (1994). Selective ectodomain phosphorylation and regulated cleavage of beta-amyloid precursor protein. *Embo J* **13**, 534-42.
77. Oltersdorf, T., Ward, P. J., Henriksson, T., Beattie, E. C., Neve, R., Lieberburg, I. & Fritz, L. C. (1990). The Alzheimer amyloid precursor protein. Identification of a stable intermediate in the biosynthetic/degradative pathway. *J Biol Chem* **265**, 4492-7.
78. Weidemann, A., Konig, G., Bunke, D., Fischer, P., Salbaum, J. M., Masters, C. L. & Beyreuther, K. (1989). Identification, biogenesis, and localization of precursors of Alzheimer's disease A4 amyloid protein. *Cell* **57**, 115-26.
79. Walter, J., Capell, A., Hung, A. Y., Langen, H., Schnolzer, M., Thinakaran, G., Sisodia, S. S., Selkoe, D. J. & Haass, C. (1997). Ectodomain phosphorylation of beta-amyloid precursor protein at two distinct cellular locations. *J Biol Chem* **272**, 1896-903.
80. Haass, C., Hung, A. Y. & Selkoe, D. J. (1991). Processing of beta-amyloid precursor protein in microglia and astrocytes favors an internal localization over constitutive secretion. *J Neurosci* **11**, 3783-93.
81. Selkoe, D. J. (1994). Normal and abnormal biology of the beta-amyloid precursor protein. *Annu Rev Neurosci* **17**, 489-517.
82. Haass, C., Kaether, C., Thinakaran, G. & Sisodia, S. (2012). Trafficking and Proteolytic Processing of APP. *Cold Spring Harb Perspect Med* **2**, a006270.
83. Busciglio, J., Gabuzda, D. H., Matsudaira, P. & Yankner, B. A. (1993). Generation of beta-amyloid in the secretory pathway in neuronal and nonneuronal cells. *Proc Natl Acad Sci U S A* **90**, 2092-6.
84. Haass, C., Schlossmacher, M. G., Hung, A. Y., Vigo-Pelfrey, C., Mellon, A., Ostaszewski, B. L., Lieberburg, I., Koo, E. H., Schenk, D., Teplow, D. B. & et al. (1992). Amyloid beta-peptide is produced by cultured cells during normal metabolism. *Nature* **359**, 322-5.
85. Seubert, P., Vigo-Pelfrey, C., Esch, F., Lee, M., Dovey, H., Davis, D., Sinha, S., Schlossmacher, M., Whaley, J., Swindlehurst, C. & et al. (1992). Isolation and quantification of soluble Alzheimer's beta-peptide from biological fluids. *Nature* **359**, 325-7.
86. Shoji, M., Golde, T. E., Ghiso, J., Cheung, T. T., Estus, S., Shaffer, L. M., Cai, X. D., McKay, D. M., Tintner, R., Frangione, B. & et al. (1992). Production of the Alzheimer amyloid beta protein by normal proteolytic processing. *Science* **258**, 126-9.
87. Nitsch, R. M., Slack, B. E., Wurtman, R. J. & Growdon, J. H. (1992). Release of Alzheimer amyloid precursor derivatives stimulated by activation of muscarinic acetylcholine receptors. *Science* **258**, 304-7.
88. Postina, R., Schroeder, A., Dewachter, I., Bohl, J., Schmitt, U., Kojro, E., Prinzen, C., Endres, K., Hiemke, C., Blessing, M., Flamez, P., Dequenne, A., Godaux, E., van Leuven, F. & Fahrenholz, F. (2004). A disintegrin-metalloproteinase prevents amyloid plaque formation and hippocampal defects in an Alzheimer disease mouse model. *J Clin Invest* **113**, 1456-64.

89. Haass, C., Hung, A. Y., Schlossmacher, M. G., Teplow, D. B. & Selkoe, D. J. (1993). beta-Amyloid peptide and a 3-kDa fragment are derived by distinct cellular mechanisms. *J Biol Chem* **268**, 3021-4.
90. Mills, J. & Reiner, P. B. (1999). Regulation of amyloid precursor protein cleavage. *J Neurochem* **72**, 443-60.
91. Sisodia, S. S. (1992). Beta-amyloid precursor protein cleavage by a membrane-bound protease. *Proc Natl Acad Sci U S A* **89**, 6075-9.
92. De Strooper, B., Umans, L., Van Leuven, F. & Van Den Berghe, H. (1993). Study of the synthesis and secretion of normal and artificial mutants of murine amyloid precursor protein (APP): cleavage of APP occurs in a late compartment of the default secretion pathway. *J Cell Biol* **121**, 295-304.
93. Haass, C., Lemere, C. A., Capell, A., Citron, M., Seubert, P., Schenk, D., Lannfelt, L. & Selkoe, D. J. (1995). The Swedish mutation causes early-onset Alzheimer's disease by beta-secretase cleavage within the secretory pathway. *Nat Med* **1**, 1291-6.
94. Fahrenholz, F., Gilbert, S., Kojro, E., Lammich, S. & Postina, R. (2000). Alpha-secretase activity of the disintegrin metalloprotease ADAM 10. Influences of domain structure. *Ann N Y Acad Sci* **920**, 215-22.
95. Asai, M., Hattori, C., Szabo, B., Sasagawa, N., Maruyama, K., Tanuma, S. & Ishiura, S. (2003). Putative function of ADAM9, ADAM10, and ADAM17 as APP alpha-secretase. *Biochem Biophys Res Commun* **301**, 231-5.
96. Tanabe, C., Hotoda, N., Sasagawa, N., Sehara-Fujisawa, A., Maruyama, K. & Ishiura, S. (2007). ADAM19 is tightly associated with constitutive Alzheimer's disease APP alpha-secretase in A172 cells. *Biochem Biophys Res Commun* **352**, 111-7.
97. Seubert, P., Oltersdorf, T., Lee, M. G., Barbour, R., Blomquist, C., Davis, D. L., Bryant, K., Fritz, L. C., Galasko, D., Thal, L. J. & et al. (1993). Secretion of beta-amyloid precursor protein cleaved at the amino terminus of the beta-amyloid peptide. *Nature* **361**, 260-3.
98. Selkoe, D. J. (1999). Translating cell biology into therapeutic advances in Alzheimer's disease. *Nature* **399**, A23-31.
99. Esler, W. P. & Wolfe, M. S. (2001). A portrait of Alzheimer secretases--new features and familiar faces. *Science* **293**, 1449-54.
100. Sastre, M., Steiner, H., Fuchs, K., Capell, A., Multhaup, G., Condron, M. M., Teplow, D. B. & Haass, C. (2001). Presenilin-dependent gamma-secretase processing of beta-amyloid precursor protein at a site corresponding to the S3 cleavage of Notch. *EMBO Rep* **2**, 835-41.
101. Chow, V. W., Mattson, M. P., Wong, P. C. & Gleichmann, M. (2010). An overview of APP processing enzymes and products. *Neuromolecular Med* **12**, 1-12.
102. Gu, Y., Misonou, H., Sato, T., Dohmae, N., Takio, K. & Ihara, Y. (2001). Distinct intramembrane cleavage of the beta-amyloid precursor protein family resembling gamma-secretase-like cleavage of Notch. *J Biol Chem* **276**, 35235-8.

103. Hong, L., Koelsch, G., Lin, X., Wu, S., Terzyan, S., Ghosh, A. K., Zhang, X. C. & Tang, J. (2000). Structure of the protease domain of memapsin 2 (beta-secretase) complexed with inhibitor. *Science* **290**, 150-3.
104. Vassar, R. (2004). BACE1: the beta-secretase enzyme in Alzheimer's disease. *J Mol Neurosci* **23**, 105-14.
105. Vassar, R., Bennett, B. D., Babu-Khan, S., Kahn, S., Mendiaz, E. A., Denis, P., Teplow, D. B., Ross, S., Amarante, P., Loeloff, R., Luo, Y., Fisher, S., Fuller, J., Edenson, S., Lile, J., Jarosinski, M. A., Biere, A. L., Curran, E., Burgess, T., Louis, J. C., Collins, F., Treanor, J., Rogers, G. & Citron, M. (1999). Beta-secretase cleavage of Alzheimer's amyloid precursor protein by the transmembrane aspartic protease BACE. *Science* **286**, 735-41.
106. Cai, H., Wang, Y., McCarthy, D., Wen, H., Borchelt, D. R., Price, D. L. & Wong, P. C. (2001). BACE1 is the major beta-secretase for generation of Abeta peptides by neurons. *Nat Neurosci* **4**, 233-4.
107. Roberds, S. L., Anderson, J., Basi, G., Bienkowski, M. J., Branstetter, D. G., Chen, K. S., Freedman, S. B., Frigon, N. L., Games, D., Hu, K., Johnson-Wood, K., Kappenman, K. E., Kawabe, T. T., Kola, I., Kuehn, R., Lee, M., Liu, W., Motter, R., Nichols, N. F., Power, M., Robertson, D. W., Schenk, D., Schoor, M., Shopp, G. M., Shuck, M. E., Sinha, S., Svensson, K. A., Tatsuno, G., Tintrup, H., Wijsman, J., Wright, S. & McConlogue, L. (2001). BACE knockout mice are healthy despite lacking the primary beta-secretase activity in brain: implications for Alzheimer's disease therapeutics. *Hum Mol Genet* **10**, 1317-24.
108. Bennett, B. D., Babu-Khan, S., Loeloff, R., Louis, J. C., Curran, E., Citron, M. & Vassar, R. (2000). Expression analysis of BACE2 in brain and peripheral tissues. *J Biol Chem* **275**, 20647-51.
109. Farzan, M., Schnitzler, C. E., Vasilieva, N., Leung, D. & Choe, H. (2000). BACE2, a beta -secretase homolog, cleaves at the beta site and within the amyloid-beta region of the amyloid-beta precursor protein. *Proc Natl Acad Sci U S A* **97**, 9712-7.
110. Fluhrer, R., Capell, A., Westmeyer, G., Willem, M., Hartung, B., Condron, M. M., Teplow, D. B., Haass, C. & Walter, J. (2002). A non-amyloidogenic function of BACE-2 in the secretory pathway. *J Neurochem* **81**, 1011-20.
111. Basi, G., Frigon, N., Barbour, R., Doan, T., Gordon, G., McConlogue, L., Sinha, S. & Zeller, M. (2003). Antagonistic effects of beta-site amyloid precursor protein-cleaving enzymes 1 and 2 on beta-amyloid peptide production in cells. *J Biol Chem* **278**, 31512-20.
112. Citron, M. (2004). Beta-secretase inhibition for the treatment of Alzheimer's disease--promise and challenge. *Trends Pharmacol Sci* **25**, 92-7.
113. Birchmeier, C. & Nave, K. A. (2008). Neuregulin-1, a key axonal signal that drives Schwann cell growth and differentiation. *Glia* **56**, 1491-7.
114. Hu, X., Hicks, C. W., He, W., Wong, P., Macklin, W. B., Trapp, B. D. & Yan, R. (2006). Bace1 modulates myelination in the central and peripheral nervous system. *Nat Neurosci* **9**, 1520-5.
115. Willem, M., Garratt, A. N., Novak, B., Citron, M., Kaufmann, S., Rittger, A., DeStrooper, B., Saftig, P., Birchmeier, C. & Haass, C. (2006). Control of

peripheral nerve myelination by the beta-secretase BACE1. *Science* **314**, 664-6.
116. Wolfe, M. S., Xia, W., Ostaszewski, B. L., Diehl, T. S., Kimberly, W. T. & Selkoe, D. J. (1999). Two transmembrane aspartates in presenilin-1 required for presenilin endoproteolysis and gamma-secretase activity. *Nature* **398**, 513-7.
117. Francis, R., McGrath, G., Zhang, J., Ruddy, D. A., Sym, M., Apfeld, J., Nicoll, M., Maxwell, M., Hai, B., Ellis, M. C., Parks, A. L., Xu, W., Li, J., Gurney, M., Myers, R. L., Himes, C. S., Hiebsch, R., Ruble, C., Nye, J. S. & Curtis, D. (2002). aph-1 and pen-2 are required for Notch pathway signaling, gamma-secretase cleavage of betaAPP, and presenilin protein accumulation. *Dev Cell* **3**, 85-97.
118. Yu, G., Nishimura, M., Arawaka, S., Levitan, D., Zhang, L., Tandon, A., Song, Y. Q., Rogaeva, E., Chen, F., Kawarai, T., Supala, A., Levesque, L., Yu, H., Yang, D. S., Holmes, E., Milman, P., Liang, Y., Zhang, D. M., Xu, D. H., Sato, C., Rogaev, E., Smith, M., Janus, C., Zhang, Y., Aebersold, R., Farrer, L. S., Sorbi, S., Bruni, A., Fraser, P. & St George-Hyslop, P. (2000). Nicastrin modulates presenilin-mediated notch/glp-1 signal transduction and betaAPP processing. *Nature* **407**, 48-54.
119. Edbauer, D., Winkler, E., Regula, J. T., Pesold, B., Steiner, H. & Haass, C. (2003). Reconstitution of gamma-secretase activity. *Nat Cell Biol* **5**, 486-8.
120. Shah, S., Lee, S. F., Tabuchi, K., Hao, Y. H., Yu, C., LaPlant, Q., Ball, H., Dann, C. E., 3rd, Sudhof, T. & Yu, G. (2005). Nicastrin functions as a gamma-secretase-substrate receptor. *Cell* **122**, 435-47.
121. Dries, D. R., Shah, S., Han, Y. H., Yu, C., Yu, S., Shearman, M. S. & Yu, G. (2009). Glu-333 of nicastrin directly participates in gamma-secretase activity. *J Biol Chem* **284**, 29714-24.
122. Chavez-Gutierrez, L., Tolia, A., Maes, E., Li, T., Wong, P. C. & de Strooper, B. (2008). Glu(332) in the Nicastrin ectodomain is essential for gamma-secretase complex maturation but not for its activity. *J Biol Chem* **283**, 20096-105.
123. Martin, L., Fluhrer, R. & Haass, C. (2009). Substrate requirements for SPPL2b-dependent regulated intramembrane proteolysis. *J Biol Chem* **284**, 5662-70.
124. Hasegawa, H., Sanjo, N., Chen, F., Gu, Y. J., Shier, C., Petit, A., Kawarai, T., Katayama, T., Schmidt, S. D., Mathews, P. M., Schmitt-Ulms, G., Fraser, P. E. & St George-Hyslop, P. (2004). Both the sequence and length of the C terminus of PEN-2 are critical for intermolecular interactions and function of presenilin complexes. *J Biol Chem* **279**, 46455-63.
125. Prokop, S., Shirotani, K., Edbauer, D., Haass, C. & Steiner, H. (2004). Requirement of PEN-2 for stabilization of the presenilin N-/C-terminal fragment heterodimer within the gamma-secretase complex. *J Biol Chem* **279**, 23255-61.
126. LaVoie, M. J., Fraering, P. C., Ostaszewski, B. L., Ye, W., Kimberly, W. T., Wolfe, M. S. & Selkoe, D. J. (2003). Assembly of the gamma-secretase complex involves early formation of an intermediate subcomplex of Aph-1 and nicastrin. *J Biol Chem* **278**, 37213-22.
127. Oh, E. S., Savonenko, A. V., King, J. F., Fangmark Tucker, S. M., Rudow, G. L., Xu, G., Borchelt, D. R. & Troncoso, J. C. (2009). Amyloid precursor protein

increases cortical neuron size in transgenic mice. *Neurobiol Aging* **30**, 1238-44.
128. Ring, S., Weyer, S. W., Kilian, S. B., Waldron, E., Pietrzik, C. U., Filippov, M. A., Herms, J., Buchholz, C., Eckman, C. B., Korte, M., Wolfer, D. P. & Muller, U. C. (2007). The secreted beta-amyloid precursor protein ectodomain APPs alpha is sufficient to rescue the anatomical, behavioral, and electrophysiological abnormalities of APP-deficient mice. *J Neurosci* **27**, 7817-26.
129. Muller, U. C. & Zheng, H. (2012). Physiological Functions of APP Family Proteins. *Cold Spring Harb Perspect Med* **2**, a006288.
130. Clarris, H. J., Cappai, R., Heffernan, D., Beyreuther, K., Masters, C. L. & Small, D. H. (1997). Identification of heparin-binding domains in the amyloid precursor protein of Alzheimer's disease by deletion mutagenesis and peptide mapping. *J Neurochem* **68**, 1164-72.
131. Mok, S. S., Sberna, G., Heffernan, D., Cappai, R., Galatis, D., Clarris, H. J., Sawyer, W. H., Beyreuther, K., Masters, C. L. & Small, D. H. (1997). Expression and analysis of heparin-binding regions of the amyloid precursor protein of Alzheimer's disease. *FEBS Lett* **415**, 303-7.
132. Kibbey, M. C., Jucker, M., Weeks, B. S., Neve, R. L., Van Nostrand, W. E. & Kleinman, H. K. (1993). beta-Amyloid precursor protein binds to the neurite-promoting IKVAV site of laminin. *Proc Natl Acad Sci U S A* **90**, 10150-3.
133. Beher, D., Hesse, L., Masters, C. L. & Multhaup, G. (1996). Regulation of amyloid protein precursor (APP) binding to collagen and mapping of the binding sites on APP and collagen type I. *J Biol Chem* **271**, 1613-20.
134. Allinquant, B., Hantraye, P., Mailleux, P., Moya, K., Bouillot, C. & Prochiantz, A. (1995). Downregulation of amyloid precursor protein inhibits neurite outgrowth in vitro. *J Cell Biol* **128**, 919-27.
135. Perez, R. G., Zheng, H., Van der Ploeg, L. H. & Koo, E. H. (1997). The beta-amyloid precursor protein of Alzheimer's disease enhances neuron viability and modulates neuronal polarity. *J Neurosci* **17**, 9407-14.
136. Herard, A. S., Besret, L., Dubois, A., Dauguet, J., Delzescaux, T., Hantraye, P., Bonvento, G. & Moya, K. L. (2006). siRNA targeted against amyloid precursor protein impairs synaptic activity in vivo. *Neurobiol Aging* **27**, 1740-50.
137. Mattson, M. P., Cheng, B., Culwell, A. R., Esch, F. S., Lieberburg, I. & Rydel, R. E. (1993). Evidence for excitoprotective and intraneuronal calcium-regulating roles for secreted forms of the beta-amyloid precursor protein. *Neuron* **10**, 243-54.
138. Furukawa, K., Barger, S. W., Blalock, E. M. & Mattson, M. P. (1996). Activation of K+ channels and suppression of neuronal activity by secreted beta-amyloid-precursor protein. *Nature* **379**, 74-8.
139. Mattson, M. P. (1997). Cellular actions of beta-amyloid precursor protein and its soluble and fibrillogenic derivatives. *Physiol Rev* **77**, 1081-132.
140. Gakhar-Koppole, N., Hundeshagen, P., Mandl, C., Weyer, S. W., Allinquant, B., Muller, U. & Ciccolini, F. (2008). Activity requires soluble amyloid precursor protein alpha to promote neurite outgrowth in neural stem cell-derived neurons via activation of the MAPK pathway. *Eur J Neurosci* **28**, 871-82.

141. Nikolaev, A., McLaughlin, T., O'Leary, D. D. & Tessier-Lavigne, M. (2009). APP binds DR6 to trigger axon pruning and neuron death via distinct caspases. *Nature* **457**, 981-9.
142. Kwak, Y. D., Brannen, C. L., Qu, T., Kim, H. M., Dong, X., Soba, P., Majumdar, A., Kaplan, A., Beyreuther, K. & Sugaya, K. (2006). Amyloid precursor protein regulates differentiation of human neural stem cells. *Stem Cells Dev* **15**, 381-9.
143. Kimberly, W. T., Zheng, J. B., Guenette, S. Y. & Selkoe, D. J. (2001). The intracellular domain of the beta-amyloid precursor protein is stabilized by Fe65 and translocates to the nucleus in a notch-like manner. *J Biol Chem* **276**, 40288-92.
144. Cupers, P., Orlans, I., Craessaerts, K., Annaert, W. & De Strooper, B. (2001). The amyloid precursor protein (APP)-cytoplasmic fragment generated by gamma-secretase is rapidly degraded but distributes partially in a nuclear fraction of neurones in culture. *J Neurochem* **78**, 1168-78.
145. Cao, X. & Sudhof, T. C. (2001). A transcriptionally [correction of transcriptively] active complex of APP with Fe65 and histone acetyltransferase Tip60. *Science* **293**, 115-20.
146. Gao, Y. & Pimplikar, S. W. (2001). The gamma -secretase-cleaved C-terminal fragment of amyloid precursor protein mediates signaling to the nucleus. *Proc Natl Acad Sci U S A* **98**, 14979-84.
147. Checler, F., Sunyach, C., Pardossi-Piquard, R., Sevalle, J., Vincent, B., Kawarai, T., Girardot, N., St George-Hyslop, P. & da Costa, C. A. (2007). The gamma/epsilon-secretase-derived APP intracellular domain fragments regulate p53. *Curr Alzheimer Res* **4**, 423-6.
148. Kim, H. S., Kim, E. M., Lee, J. P., Park, C. H., Kim, S., Seo, J. H., Chang, K. A., Yu, E., Jeong, S. J., Chong, Y. H. & Suh, Y. H. (2003). C-terminal fragments of amyloid precursor protein exert neurotoxicity by inducing glycogen synthase kinase-3beta expression. *FASEB J* **17**, 1951-3.
149. Ryan, K. A. & Pimplikar, S. W. (2005). Activation of GSK-3 and phosphorylation of CRMP2 in transgenic mice expressing APP intracellular domain. *J Cell Biol* **171**, 327-35.
150. Pardossi-Piquard, R., Petit, A., Kawarai, T., Sunyach, C., Alves da Costa, C., Vincent, B., Ring, S., D'Adamio, L., Shen, J., Muller, U., St George Hyslop, P. & Checler, F. (2005). Presenilin-dependent transcriptional control of the Abeta-degrading enzyme neprilysin by intracellular domains of betaAPP and APLP. *Neuron* **46**, 541-54.
151. Zhang, Y. W., Wang, R., Liu, Q., Zhang, H., Liao, F. F. & Xu, H. (2007). Presenilin/gamma-secretase-dependent processing of beta-amyloid precursor protein regulates EGF receptor expression. *Proc Natl Acad Sci U S A* **104**, 10613-8.
152. Biasini, E., Turnbaugh, J. A., Unterberger, U. & Harris, D. A. (2012). Prion protein at the crossroads of physiology and disease. *Trends Neurosci* **35**, 92-103.
153. Prusiner, S. B. (1982). Novel proteinaceous infectious particles cause scrapie. *Science* **216**, 136-44.

154. Prusiner, S. B. (1998). Prions. *Proc Natl Acad Sci U S A* **95**, 13363-83.
155. Caughey, B. & Chesebro, B. (2001). Transmissible spongiform encephalopathies and prion protein interconversions. *Adv Virus Res* **56**, 277-311.
156. Collinge, J. (2001). Prion diseases of humans and animals: their causes and molecular basis. *Annu Rev Neurosci* **24**, 519-50.
157. Aguzzi, A. & Polymenidou, M. (2004). Mammalian prion biology: one century of evolving concepts. *Cell* **116**, 313-27.
158. Weissmann, C. (2004). The state of the prion. *Nat Rev Microbiol* **2**, 861-71.
159. Mabbott, N. A. & MacPherson, G. G. (2006). Prions and their lethal journey to the brain. *Nat Rev Microbiol* **4**, 201-11.
160. Cobb, N. J. & Surewicz, W. K. (2009). Prion diseases and their biochemical mechanisms. *Biochemistry* **48**, 2574-85.
161. Taylor, D. R. & Hooper, N. M. (2006). The prion protein and lipid rafts. *Mol Membr Biol* **23**, 89-99.
162. Zahn, R., Liu, A., Luhrs, T., Riek, R., von Schroetter, C., Lopez Garcia, F., Billeter, M., Calzolai, L., Wider, G. & Wuthrich, K. (2000). NMR solution structure of the human prion protein. *Proc Natl Acad Sci U S A* **97**, 145-50.
163. Bremer, J., Baumann, F., Tiberi, C., Wessig, C., Fischer, H., Schwarz, P., Steele, A. D., Toyka, K. V., Nave, K. A., Weis, J. & Aguzzi, A. (2010). Axonal prion protein is required for peripheral myelin maintenance. *Nat Neurosci* **13**, 310-8.
164. Le Pichon, C. E., Valley, M. T., Polymenidou, M., Chesler, A. T., Sagdullaev, B. T., Aguzzi, A. & Firestein, S. (2009). Olfactory behavior and physiology are disrupted in prion protein knockout mice. *Nat Neurosci* **12**, 60-9.
165. Caughey, B. & Baron, G. S. (2006). Prions and their partners in crime. *Nature* **443**, 803-10.
166. Westergard, L., Christensen, H. M. & Harris, D. A. (2007). The cellular prion protein (PrP(C)): its physiological function and role in disease. *Biochim Biophys Acta* **1772**, 629-44.
167. Watts, J. C. & Westaway, D. (2007). The prion protein family: diversity, rivalry, and dysfunction. *Biochim Biophys Acta* **1772**, 654-72.
168. Hainfellner, J. A., Wanschitz, J., Jellinger, K., Liberski, P. P., Gullotta, F. & Budka, H. (1998). Coexistence of Alzheimer-type neuropathology in Creutzfeldt-Jakob disease. *Acta Neuropathol* **96**, 116-22.
169. Voigtlander, T., Kloppel, S., Birner, P., Jarius, C., Flicker, H., Verghese-Nikolakaki, S., Sklaviadis, T., Guentchev, M. & Budka, H. (2001). Marked increase of neuronal prion protein immunoreactivity in Alzheimer's disease and human prion diseases. *Acta Neuropathol* **101**, 417-23.
170. Del Bo, R., Scarlato, M., Ghezzi, S., Martinelli-Boneschi, F., Fenoglio, C., Galimberti, G., Galbiati, S., Virgilio, R., Galimberti, D., Ferrarese, C., Scarpini, E., Bresolin, N. & Comi, G. P. (2006). Is M129V of PRNP gene associated with Alzheimer's disease? A case-control study and a meta-analysis. *Neurobiol Aging* **27**, 770 e1-770 e5.

171. Schwarze-Eicker, K., Keyvani, K., Gortz, N., Westaway, D., Sachser, N. & Paulus, W. (2005). Prion protein (PrPc) promotes beta-amyloid plaque formation. *Neurobiol Aging* **26**, 1177-82.
172. Bertram, L., McQueen, M. B., Mullin, K., Blacker, D. & Tanzi, R. E. (2007). Systematic meta-analyses of Alzheimer disease genetic association studies: the AlzGene database. *Nat Genet* **39**, 17-23.
173. Dermaut, B., Croes, E. A., Rademakers, R., Van den Broeck, M., Cruts, M., Hofman, A., van Duijn, C. M. & Van Broeckhoven, C. (2003). PRNP Val129 homozygosity increases risk for early-onset Alzheimer's disease. *Ann Neurol* **53**, 409-12.
174. Riemenschneider, M., Klopp, N., Xiang, W., Wagenpfeil, S., Vollmert, C., Muller, U., Forstl, H., Illig, T., Kretzschmar, H. & Kurz, A. (2004). Prion protein codon 129 polymorphism and risk of Alzheimer disease. *Neurology* **63**, 364-6.
175. Papassotiropoulos, A., Wollmer, M. A., Aguzzi, A., Hock, C., Nitsch, R. M. & de Quervain, D. J. (2005). The prion gene is associated with human long-term memory. *Hum Mol Genet* **14**, 2241-6.
176. Croes, E. A., Dermaut, B., Houwing-Duistermaat, J. J., Van den Broeck, M., Cruts, M., Breteler, M. M., Hofman, A., van Broeckhoven, C. & van Duijn, C. M. (2003). Early cognitive decline is associated with prion protein codon 129 polymorphism. *Ann Neurol* **54**, 275-6.
177. Meyne, F., Gloeckner, S. F., Ciesielczyk, B., Heinemann, U., Krasnianski, A., Meissner, B. & Zerr, I. (2009). Total prion protein levels in the cerebrospinal fluid are reduced in patients with various neurological disorders. *J Alzheimers Dis* **17**, 863-73.
178. Oda, T., Himeno, R., D, C. H., Chino, K., Kurihara, T., Nagayoshi, T., Kanehisa, H., Fukunaga, T. & Kawakami, Y. (2007). In vivo behavior of muscle fascicles and tendinous tissues in human tibialis anterior muscle during twitch contraction. *J Biomech* **40**, 3114-20.
179. Parkin, E. T., Watt, N. T., Hussain, I., Eckman, E. A., Eckman, C. B., Manson, J. C., Baybutt, H. N., Turner, A. J. & Hooper, N. M. (2007). Cellular prion protein regulates beta-secretase cleavage of the Alzheimer's amyloid precursor protein. *Proc Natl Acad Sci U S A* **104**, 11062-7.
180. Cordy, J. M., Hussain, I., Dingwall, C., Hooper, N. M. & Turner, A. J. (2003). Exclusively targeting beta-secretase to lipid rafts by GPI-anchor addition up-regulates beta-site processing of the amyloid precursor protein. *Proc Natl Acad Sci U S A* **100**, 11735-40.
181. Ehehalt, R., Keller, P., Haass, C., Thiele, C. & Simons, K. (2003). Amyloidogenic processing of the Alzheimer beta-amyloid precursor protein depends on lipid rafts. *J Cell Biol* **160**, 113-23.
182. Griffiths, H. H., Whitehouse, I. J., Baybutt, H., Brown, D., Kellett, K. A., Jackson, C. D., Turner, A. J., Piccardo, P., Manson, J. C. & Hooper, N. M. (2011). Prion protein interacts with BACE1 protein and differentially regulates its activity toward wild type and Swedish mutant amyloid precursor protein. *J Biol Chem* **286**, 33489-500.
183. Hooper, N. M. & Turner, A. J. (2008). A new take on prions: preventing Alzheimer's disease. *Trends Biochem Sci* **33**, 151-5.

184. Vincent, B., Sunyach, C., Orzechowski, H. D., St George-Hyslop, P. & Checler, F. (2009). p53-Dependent transcriptional control of cellular prion by presenilins. *J Neurosci* **29**, 6752-60.
185. Belyaev, N. D., Nalivaeva, N. N., Makova, N. Z. & Turner, A. J. (2009). Neprilysin gene expression requires binding of the amyloid precursor protein intracellular domain to its promoter: implications for Alzheimer disease. *EMBO Rep* **10**, 94-100.
186. Kellett, K. A. & Hooper, N. M. (2009). Prion protein and Alzheimer disease. *Prion* **3**, 190-4.
187. Calella, A. M., Farinelli, M., Nuvolone, M., Mirante, O., Moos, R., Falsig, J., Mansuy, I. M. & Aguzzi, A. (2010). Prion protein and Abeta-related synaptic toxicity impairment. *EMBO Mol Med* **2**, 306-14.
188. Forloni, G. & Balducci, C. (2011). beta-amyloid oligomers and prion protein: Fatal attraction? *Prion* **5**, 10-5.
189. Lauren, J., Gimbel, D. A., Nygaard, H. B., Gilbert, J. W. & Strittmatter, S. M. (2009). Cellular prion protein mediates impairment of synaptic plasticity by amyloid-beta oligomers. *Nature* **457**, 1128-32.
190. Balducci, C., Beeg, M., Stravalaci, M., Bastone, A., Sclip, A., Biasini, E., Tapella, L., Colombo, L., Manzoni, C., Borsello, T., Chiesa, R., Gobbi, M., Salmona, M. & Forloni, G. (2010). Synthetic amyloid-beta oligomers impair long-term memory independently of cellular prion protein. *Proc Natl Acad Sci U S A* **107**, 2295-300.
191. Kessels, H. W., Nguyen, L. N., Nabavi, S. & Malinow, R. (2010). The prion protein as a receptor for amyloid-beta. *Nature* **466**, E3-4; discussion E4-5.
192. Riopelle, R. J. & Dow, K. E. (1990). Functional interactions of neuronal heparan sulphate proteoglycans with laminin. *Brain Res* **525**, 92-100.
193. Sakashita, S., Engvall, E. & Ruoslahti, E. (1980). Basement membrane glycoprotein laminin binds to heparin. *FEBS Lett* **116**, 243-6.
194. Terranova, V. P., Rohrbach, D. H. & Martin, G. R. (1980). Role of laminin in the attachment of PAM 212 (epithelial) cells to basement membrane collagen. *Cell* **22**, 719-26.
195. Burgeson, R. E., Chiquet, M., Deutzmann, R., Ekblom, P., Engel, J., Kleinman, H., Martin, G. R., Meneguzzi, G., Paulsson, M., Sanes, J. & et al. (1994). A new nomenclature for the laminins. *Matrix Biol* **14**, 209-11.
196. Engel, J. (1992). Laminins and other strange proteins. *Biochemistry* **31**, 10643-51.
197. Liesi, P., Narvanen, A., Soos, J., Sariola, H. & Snounou, G. (1989). Identification of a neurite outgrowth-promoting domain of laminin using synthetic peptides. *FEBS Lett* **244**, 141-8.
198. Venstrom, K. A. & Reichardt, L. F. (1993). Extracellular matrix. 2: Role of extracellular matrix molecules and their receptors in the nervous system. *FASEB J* **7**, 996-1003.
199. Liesi, P., Kaakkola, S., Dahl, D. & Vaheri, A. (1984). Laminin is induced in astrocytes of adult brain by injury. *Embo J* **3**, 683-6.
200. Murtomaki, S., Risteli, J., Risteli, L., Koivisto, U. M., Johansson, S. & Liesi, P. (1992). Laminin and its neurite outgrowth-promoting domain in the brain in

Alzheimer's disease and Down's syndrome patients. *J Neurosci Res* **32**, 261-73.
201. Narindrasorasak, S., Lowery, D., Gonzalez-DeWhitt, P., Poorman, R. A., Greenberg, B. & Kisilevsky, R. (1991). High affinity interactions between the Alzheimer's beta-amyloid precursor proteins and the basement membrane form of heparan sulfate proteoglycan. *J Biol Chem* **266**, 12878-83.
202. Bronfman, F. C., Garrido, J., Alvarez, A., Morgan, C. & Inestrosa, N. C. (1996). Laminin inhibits amyloid-beta-peptide fibrillation. *Neurosci Lett* **218**, 201-3.
203. Castillo, G. M., Lukito, W., Peskind, E., Raskind, M., Kirschner, D. A., Yee, A. G. & Snow, A. D. (2000). Laminin inhibition of beta-amyloid protein (Abeta) fibrillogenesis and identification of an Abeta binding site localized to the globular domain repeats on the laminin a chain. *J Neurosci Res* **62**, 451-62.
204. Drouet, B., Pincon-Raymond, M., Chambaz, J. & Pillot, T. (1999). Laminin 1 attenuates beta-amyloid peptide Abeta(1-40) neurotoxicity of cultured fetal rat cortical neurons. *J Neurochem* **73**, 742-9.
205. Mbazima, V., Da Costa Dias, B., Omar, A., Jovanovic, K. & Weiss, S. F. (2010). Interactions between PrP(c) and other ligands with the 37-kDa/67-kDa laminin receptor. *Front Biosci* **15**, 1150-63.
206. Hundt, C., Peyrin, J. M., Haik, S., Gauczynski, S., Leucht, C., Rieger, R., Riley, M. L., Deslys, J. P., Dormont, D., Lasmezas, C. I. & Weiss, S. (2001). Identification of interaction domains of the prion protein with its 37-kDa/67-kDa laminin receptor. *Embo J* **20**, 5876-86.
207. Landowski, T. H., Dratz, E. A. & Starkey, J. R. (1995). Studies of the structure of the metastasis-associated 67 kDa laminin binding protein: fatty acid acylation and evidence supporting dimerization of the 32 kDa gene product to form the mature protein. *Biochemistry* **34**, 11276-87.
208. Buto, S., Tagliabue, E., Ardini, E., Magnifico, A., Ghirelli, C., van den Brule, F., Castronovo, V., Colnaghi, M. I., Sobel, M. E. & Menard, S. (1998). Formation of the 67-kDa laminin receptor by acylation of the precursor. *J Cell Biochem* **69**, 244-51.
209. Gauczynski, S., Peyrin, J. M., Haik, S., Leucht, C., Hundt, C., Rieger, R., Krasemann, S., Deslys, J. P., Dormont, D., Lasmezas, C. I. & Weiss, S. (2001). The 37-kDa/67-kDa laminin receptor acts as the cell-surface receptor for the cellular prion protein. *Embo J* **20**, 5863-75.
210. Vana, K., Zuber, C., Nikles, D. & Weiss, S. (2007). Novel aspects of prions, their receptor molecules, and innovative approaches for TSE therapy. *Cell Mol Neurobiol* **27**, 107-28.
211. Zuber, C., Ludewigs, H. & Weiss, S. (2007). Therapeutic approaches targeting the prion receptor LRP/LR. *Vet Microbiol* **123**, 387-93.
212. Vana, K., Zuber, C., Pflanz, H., Kolodziejczak, D., Zemora, G., Bergmann, A. K. & Weiss, S. (2009). LRP/LR as an alternative promising target in therapy of prion diseases, Alzheimer's disease and cancer. *Infect Disord Drug Targets* **9**, 69-80.
213. Ludewigs, H., Zuber, C., Vana, K., Nikles, D., Zerr, I. & Weiss, S. (2007). Therapeutic approaches for prion disorders. *Expert Rev Anti Infect Ther* **5**, 613-30.

214. Zuber, C., Knackmuss, S., Zemora, G., Reusch, U., Vlasova, E., Diehl, D., Mick, V., Hoffmann, K., Nikles, D., Frohlich, T., Arnold, G. J., Brenig, B., Wolf, E., Lahm, H., Little, M. & Weiss, S. (2008). Invasion of tumorigenic HT1080 cells is impeded by blocking or downregulating the 37-kDa/67-kDa laminin receptor. *J Mol Biol* **378**, 530-9.
215. Menard, S., Tagliabue, E. & Colnaghi, M. I. (1998). The 67 kDa laminin receptor as a prognostic factor in human cancer. *Breast Cancer Res Treat* **52**, 137-45.
216. Satoh, K., Narumi, K., Abe, T., Sakai, T., Kikuchi, T., Tanaka, M., Shimo-Oka, T., Uchida, M., Tezuka, F., Isemura, M. & Nukiwa, T. (1999). Diminution of 37-kDa laminin binding protein expression reduces tumour formation of murine lung cancer cells. *Br J Cancer* **80**, 1115-22.
217. Umeda, D., Yano, S., Yamada, K. & Tachibana, H. (2008). Involvement of 67-kDa laminin receptor-mediated myosin phosphatase activation in antiproliferative effect of epigallocatechin-3-O-gallate at a physiological concentration on Caco-2 colon cancer cells. *Biochem Biophys Res Commun* **371**, 172-6.
218. Ardini, E., Pesole, G., Tagliabue, E., Magnifico, A., Castronovo, V., Sobel, M. E., Colnaghi, M. I. & Menard, S. (1998). The 67-kDa laminin receptor originated from a ribosomal protein that acquired a dual function during evolution. *Mol Biol Evol* **15**, 1017-25.
219. Gauczynski, S., Nikles, D., El-Gogo, S., Papy-Garcia, D., Rey, C., Alban, S., Barritault, D., Lasmezas, C. I. & Weiss, S. (2006). The 37-kDa/67-kDa laminin receptor acts as a receptor for infectious prions and is inhibited by polysulfated glycanes. *J Infect Dis* **194**, 702-9.
220. Kirkpatrick, C. A. & Selleck, S. B. (2007). Heparan sulfate proteoglycans at a glance. *J Cell Sci* **120**, 1829-32.
221. Urbinati, C., Nicoli, S., Giacca, M., David, G., Fiorentini, S., Caruso, A., Alfano, M., Cassetta, L., Presta, M. & Rusnati, M. (2009). HIV-1 Tat and heparan sulfate proteoglycan interaction: a novel mechanism of lymphocyte adhesion and migration across the endothelium. *Blood* **114**, 3335-42.
222. Snow, A. D., Sekiguchi, R. T., Nochlin, D., Kalaria, R. N. & Kimata, K. (1994). Heparan sulfate proteoglycan in diffuse plaques of hippocampus but not of cerebellum in Alzheimer's disease brain. *Am J Pathol* **144**, 337-47.
223. Tachibana, H., Koga, K., Fujimura, Y. & Yamada, K. (2004). A receptor for green tea polyphenol EGCG. *Nat Struct Mol Biol* **11**, 380-1.
224. Susantad, T. & Smith, D. R. (2008). siRNA-mediated silencing of the 37/67-kDa high affinity laminin receptor in Hep3B cells induces apoptosis. *Cell Mol Biol Lett* **13**, 452-64.
225. Thepparit, C. & Smith, D. R. (2004). Serotype-specific entry of dengue virus into liver cells: identification of the 37-kilodalton/67-kilodalton high-affinity laminin receptor as a dengue virus serotype 1 receptor. *J Virol* **78**, 12647-56.
226. Tio, P. H., Jong, W. W. & Cardosa, M. J. (2005). Two dimensional VOPBA reveals laminin receptor (LAMR1) interaction with dengue virus serotypes 1, 2 and 3. *Virol J* **2**, 25.

227. Wang, K. S., Kuhn, R. J., Strauss, E. G., Ou, S. & Strauss, J. H. (1992). High-affinity laminin receptor is a receptor for Sindbis virus in mammalian cells. *J Virol* **66**, 4992-5001.
228. Ludwig, G. V., Kondig, J. P. & Smith, J. F. (1996). A putative receptor for Venezuelan equine encephalitis virus from mosquito cells. *J Virol* **70**, 5592-9.
229. Akache, B., Grimm, D., Pandey, K., Yant, S. R., Xu, H. & Kay, M. A. (2006). The 37/67-kilodalton laminin receptor is a receptor for adeno-associated virus serotypes 8, 2, 3, and 9. *J Virol* **80**, 9831-6.
230. Scheiman, J., Tseng, J. C., Zheng, Y. & Meruelo, D. (2010). Multiple functions of the 37/67-kd laminin receptor make it a suitable target for novel cancer gene therapy. *Mol Ther* **18**, 63-74.
231. Auth, D. & Brawerman, G. (1992). A 33-kDa polypeptide with homology to the laminin receptor: component of translation machinery. *Proc Natl Acad Sci U S A* **89**, 4368-72.
232. Nikles, D., Vana, K., Gauczynski, S., Knetsch, H., Ludewigs, H. & Weiss, S. (2008). Subcellular localization of prion proteins and the 37 kDa/67 kDa laminin receptor fused to fluorescent proteins. *Biochim Biophys Acta* **1782**, 335-40.
233. Sato, M., Kinoshita, K., Kaneda, Y., Saeki, Y., Iwamatsu, A. & Tanaka, K. (1996). Analysis of nuclear localization of laminin binding protein precursor p40 (LBP/p40). *Biochem Biophys Res Commun* **229**, 896-901.
234. Kurreck, J. (2009). RNA interference: from basic research to therapeutic applications. *Angewandte Chemie* **48**, 1378-98.
235. Napoli, C., Lemieux, C. & Jorgensen, R. (1990). Introduction of a Chimeric Chalcone Synthase Gene into Petunia Results in Reversible Co-Suppression of Homologous Genes in trans. *The Plant cell* **2**, 279-289.
236. Fire, A., Xu, S., Montgomery, M. K., Kostas, S. A., Driver, S. E. & Mello, C. C. (1998). Potent and specific genetic interference by double-stranded RNA in Caenorhabditis elegans. *Nature* **391**, 806-11.
237. Elbashir, S. M., Martinez, J., Patkaniowska, A., Lendeckel, W. & Tuschl, T. (2001). Functional anatomy of siRNAs for mediating efficient RNAi in Drosophila melanogaster embryo lysate. *The EMBO journal* **20**, 6877-88.
238. Liu, J., Carmell, M. A., Rivas, F. V., Marsden, C. G., Thomson, J. M., Song, J. J., Hammond, S. M., Joshua-Tor, L. & Hannon, G. J. (2004). Argonaute2 is the catalytic engine of mammalian RNAi. *Science* **305**, 1437-41.
239. Matranga, C., Tomari, Y., Shin, C., Bartel, D. P. & Zamore, P. D. (2005). Passenger-strand cleavage facilitates assembly of siRNA into Ago2-containing RNAi enzyme complexes. *Cell* **123**, 607-20.
240. Rand, T. A., Petersen, S., Du, F. & Wang, X. (2005). Argonaute2 cleaves the anti-guide strand of siRNA during RISC activation. *Cell* **123**, 621-9.
241. Pecot, C. V., Calin, G. A., Coleman, R. L., Lopez-Berestein, G. & Sood, A. K. (2011). RNA interference in the clinic: challenges and future directions. *Nature reviews. Cancer* **11**, 59-67.
242. Pflanz, H., Vana, K., Mitteregger, G., Pace, C., Messow, D., Sedlaczek, C., Nikles, D., Kretzschmar, H. A. & Weiss, S. F. (2009). Microinjection of lentiviral vectors expressing small interfering RNAs directed against laminin receptor

precursor mRNA prolongs the pre-clinical phase in scrapie-infected mice. *J Gen Virol* **90**, 269-74.
243. Farina, A. R., Tacconelli, A., Cappabianca, L., Cea, G., Chioda, A., Romanelli, A., Pensato, S., Pedone, C., Gulino, A. & Mackay, A. R. (2009). The neuroblastoma tumour-suppressor TrkAI and its oncogenic alternative TrkAIII splice variant exhibit geldanamycin-sensitive interactions with Hsp90 in human neuroblastoma cells. *Oncogene* **28**, 4075-94.
244. Laemmli, U. K. (1970). Cleavage of structural proteins during the assembly of the head of bacteriophage T4. *Nature* **227**, 680-5.
245. Mocellin, S. & Provenzano, M. (2004). RNA interference: learning gene knock-down from cell physiology. *Journal of translational medicine* **2**, 39.
246. Sahu, D., Zhao, Z., Tsen, F., Cheng, C. F., Park, R., Situ, A. J., Dai, J., Eginli, A., Shams, S., Chen, M., Ulmer, T. S., Conti, P., Woodley, D. T. & Li, W. (2012). A potentially common peptide target in secreted heat shock protein-90alpha for hypoxia-inducible factor-1alpha-positive tumors. *Molecular biology of the cell* **23**, 602-13.
247. Comeau, J. W., Costantino, S. & Wiseman, P. W. (2006). A guide to accurate fluorescence microscopy colocalization measurements. *Biophysical journal* **91**, 4611-22.
248. Gauczynski, S., Peyrin, J. M., Haik, S., Leucht, C., Hundt, C., Rieger, R., Krasemann, S., Deslys, J. P., Dormont, D., Lasmezas, C. I. & Weiss, S. (2001). The 37-kDa/67-kDa laminin receptor acts as the cell-surface receptor for the cellular prion protein. *The EMBO journal* **20**, 5863-75.
249. Bolte, S. & Cordelieres, F. P. (2006). A guided tour into subcellular colocalization analysis in light microscopy. *Journal of microscopy* **224**, 213-32.
250. St. Amand, A., Smith, Q. & Vermeulen, A. (2010). Successful RNA interference experiments in difficult-to-transfect cell lines.
251. Dreses-Werringloer, U., Lambert, J. C., Vingtdeux, V., Zhao, H., Vais, H., Siebert, A., Jain, A., Koppel, J., Rovelet-Lecrux, A., Hannequin, D., Pasquier, F., Galimberti, D., Scarpini, E., Mann, D., Lendon, C., Campion, D., Amouyel, P., Davies, P., Foskett, J. K., Campagne, F. & Marambaud, P. (2008). A polymorphism in CALHM1 influences Ca2+ homeostasis, Abeta levels, and Alzheimer's disease risk. *Cell* **133**, 1149-61.
252. Pflanz, H., Vana, K., Mitteregger, G., Pace, C., Messow, D., Sedlaczek, C., Nikles, D., Kretzschmar, H. A. & Weiss, S. F. (2009). Microinjection of lentiviral vectors expressing small interfering RNAs directed against laminin receptor precursor mRNA prolongs the pre-clinical phase in scrapie-infected mice. *The Journal of general virology* **90**, 269-74.
253. Topper, D. (2005). Generation of recombinant lentiviruses encoding siRNAs directed against the 37kDa/67kDa laminin recptor mRNA for treatment of prion disease, Ludwig-Maximilians-University.
254. Jacobsen, L. & Hughes, P. (2007). Effects of passage number on cell line transfection. *Biochemica* **3**, 32.

255. Yu, H., Cook, T. J. & Sinko, P. J. (1997). Evidence for diminished functional expression of intestinal transporters in Caco-2 cell monolayers at high passages. *Pharmaceutical research* **14**, 757-62.
256. Pimplikar, S. W. & Suryanarayana, A. (2011). Detection of APP intracellular domain in brain tissue. *Methods in molecular biology* **670**, 85-91.
257. Kolodziejczak, D., Da Costa Dias, B., Zuber, C., Jovanovic, K., Omar, A., Beck, J., Vana, K., Mbazima, V., Richt, J., Brenig, B. & Weiss, S. F. (2010). Prion interaction with the 37-kDa/67-kDa laminin receptor on enterocytes as a cellular model for intestinal uptake of prions. *Journal of molecular biology* **402**, 293-300.

APPENDIX

1.1 LRP-shRNA1, 7 and 9 design

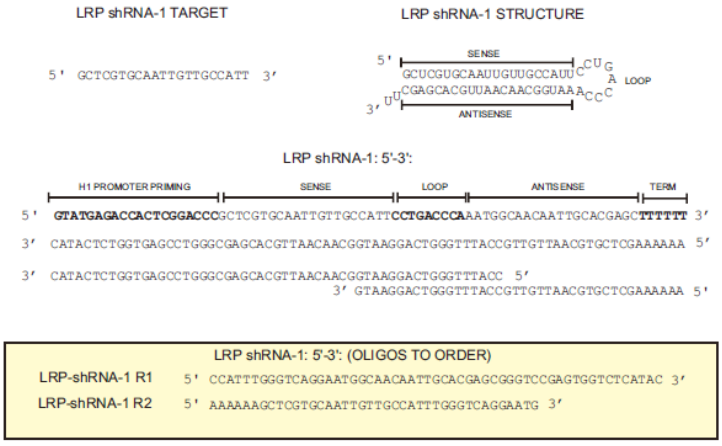

LRP shRNA-1: 5'-3': (OLIGOS TO ORDER)	
LRP-shRNA-1 R1	5' CCATTTGGGTCAGGAATGGCAACAATTGCACGAGCGGGTCCGAGTGGTCTCATAC 3'
LRP-shRNA-1 R2	5' AAAAAAGCTCGTGCAATTGTTGCCATTTGGGTCAGGAATG 3'

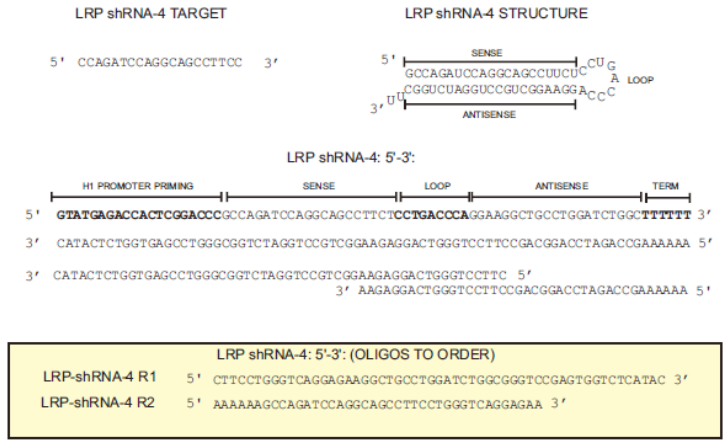

LRP shRNA-4: 5'-3': (OLIGOS TO ORDER)	
LRP-shRNA-4 R1	5' CTTCCTGGGTCAGGAGAAGGCTGCCTGGATCTGGCGGGTCCGAGTGGTCTCATAC 3'
LRP-shRNA-4 R2	5' AAAAAAGCCAGATCCAGGCAGCCTTCCTGGGTCAGGAGAA 3'

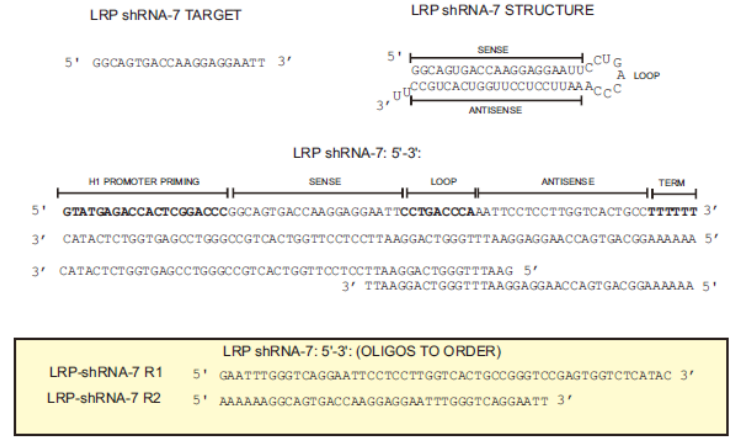

LRP shRNA-7: 5'-3': (OLIGOS TO ORDER)	
LRP-shRNA-7 R1	5' GAATTTGGGTCAGGAATTCCTCCTTGGTCACTGCCGGGTCCGAGTGGTCTCATAC 3'
LRP-shRNA-7 R2	5' AAAAAAGGCAGTGACCAAGGAGGAATTTGGGTCAGGAATT 3'

1.2 pENTRsiRNA-LRP4, 7 and 9 target sequences

auguccggag cccuugacgu ccugcagaug aaggaggagg auguccucaa auuccuugcu
gcgggaaccc acuuaggugg caccaaccuu gacuuucaga uggagcagua caucuacaaa
aggaaaagug acgguaucua caucauaaac cugaagagga ccugggagaa gcuguugcuc
gcagcucgag cuauuguugc caucga**gaau ccugcugacg ucagc**gucau cuccuccagg **siRNA-LRP 9**
aacacuggcc agcgagcugu gcugaaguuu gcugcugcca caggagccac uccgaucgcu
ggccgcuuca caccugggac cuucacuaa**c cagauccaag cagccuuc**ag ggagccacgg **siRNA-LRP 4**
cuucuagugg ugaccgaucc cagggcugac caucagccac ucacagaggc cucuuauguc
aaccugccca ccauugcucu guguaacaca gauucucccc ugcgcuaugu ggacauugcc
aucccaugca acaacaaggg agcucacuca gugggucuga ugugguggau gcuggccagg
gaaguacucc gcaugcgagg uacuaucucc cgugagcacc ccugggaggu caugccugau
cuuuacuucu acagagaccc agaggagauu gagaaggagg agcaggcugc ugcugagaa**g**
gcugugacca aggaggaauu ccagggugaa uggaccgcac cagcuccuga guucacugcu **siRNA-LRP 7**
gcucagccug agguggccga cugguaugag ggugugcagg uucccucugu gcccauccag
caguucccca cggaagacug gagugcacag ccagccacug aggauugguc agcagcuccc
acagcgcagg ccacugagug gguuggagcc accacugagu gguccuga

1.3 Electrophoresis: Agarose gel

1.3.1 Agarose gel (1%)

0.7g Agarose
Make up to 70ml with 1X TBE buffer
Heat until agarose dissolves
Add 5µl ethidium bromide
Pour gel and allow to set

1.3.2 TBE buffer (10X), pH8.3

890mM Tris
890mM Boric acid
20mM EDTA
Adjust pH to 8.3
Make up to a final volume of 1000ml with dH_2O

1.4 Ligation reaction

1.4.1 Map of pTZ57R/T cloning vector

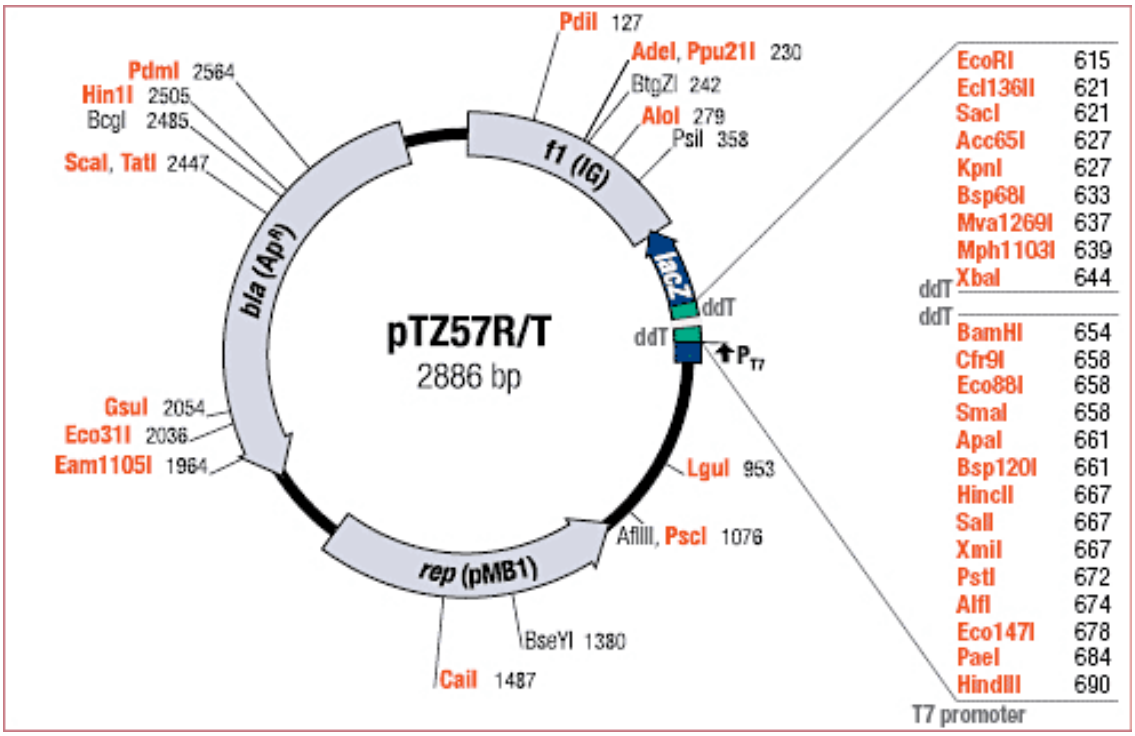

1.5 Preparation of competent bacteria

1.5.1 T-solution

250µl T-solution (A) (Fermentas)
250µl T-solution (B) (Fermentas)
Combine
Store on ice

1.5.2 LB medium

1% Sodium chloride
0.5% Yeast extract
1% Tryptone
Make up to final volume with dH2O
Sterilise for 20 min at 151 lbq
Store at 4°C

1.6 Transformation

1.6.1 0.1M IPTG stock solution

1.2g IPTG
Add dH_2O to a final volume of 50ml
Filter sterilize through a 0.2µm filter unit
Store at 4°C

1.6.2 50mg/ml X-Gal stock solution

50mg X-Gal
Add dimethylformamide to a final volume of 1ml
Filter sterilize through a 0.2µm filter unit
Store at -20°C

1.6.3 LB plates containing 50µg/ml ampicillin

1.5% Bacto-agar
In LB medium (Appendix 1.4.2)
Sterilise for 20min at 151 lbq
Cool to 55°C
Add ampicillin to a final concentration of 50µg/ml
Pour approximately 25ml of solution into separate 100mm Petri-dishes
Allow liquid agar to solidify
Seal Petri-dishes with parafilm
Store at 4°C

1.6.4 LB plates containing 50µg/ml ampicillin, 05mM IPTG and 40µg/ml X-Gal

LB plates containing 50µg/ml ampicillin (Appendix 1.4.4)
100µl 0.1M IPTG stock solution (Appendix 1.4.1)
20µl 50mg/ml X-Gal stock solution (Appendix 1.4.2)
Spread the IPTG and X-Gal onto the LB-ampicillin plates
Allow the components to absorb for 30min at 37°C prior to plating of cells

1.6.5 2M Mg^{2+} stock

20.33g $MgCl_2.6H_2O$
24.65g $MgSO_4.7H_2O$
Add distilled water to a final volume of 100ml
Filter sterilize

1.6.6 SOC medium

2g Tryptone
0.5g Yeast extract
1ml 1M NaCl
0.25ml 1M KCl
1ml 2M Mg^{2+} stock, filter sterilized (Appendix 1.5.5)
1ml 2M glucose, filter sterilized
Add tryptone, yeast extract, NaCl and KCl to 97ml distilled water.
Sterilise for 20min at 151 lbq
Cool to room temperature
Add 2M Mg^{2+} and 2M glucose, each to a final concentration of 20mM
Add distilled water to a final volume of 100ml
Store at 4°C

1.6.7 LB plates containing 50µg/ml kanomycin

1.5% Bacto-agar
In LB medium (Appendix 1.4.2)
Sterilise for 20min at 151 lbq
Cool to 55°C
Add kanomycin to a final concentration of 50µg/ml
Pour approximately 25ml of solution into separate 100mm Petri-dishes
Allow liquid agar to solidify
Seal Petri-dishes with parafilm
Store at 4°C

1.7 Immunofluorescence

1.7.1 Paraformaldehyde (4%)

Solution A
0.14M Sodium dihydrogen orthophosphate (anhydrous)
Make up to final volume with distilled water

Solution B
0.63M Sodium hydroxide
Make up to final volume with distilled water

Dissolve:
4 % Paraformaldehyde in
83% Solution A
17% Solution B

Make up to final volume with distilled water
Heat to approximately 80°C until solution clears
Filter and store at 4°C

1.7.2 Phosphate Buffered Saline (PBS): 1X
136.9mM Sodium chloride
2.68mM Potassium chloride
10.1mM Disodium hydrogen phosphate dodecahydrate
1.76mM Potassium dihydrogen phosphate
Adjust pH to 7.3
Make up to final volume with distilled water
Sterilise for 20 min at 151 lbq
Store at 4°C

1.7.3 0.5% Bovine serum albumin (BSA)
0.5% BSA
In PBS (Appendix 1.6.2)
Store at 4°C

1.7.4 0.25% Triton X-100 + 0.5%BSA
0.25% Triton X-100
In 0.5% BSA (Appendix 1.6.3)
Store at 4°C

1.8 Cell lysis

1.8.1 Lysis buffer

10mM	Tris-HCl (pH7.5)
100mM	NaCl
10mM	Ethylenediaminetetraacetic acid (EDTA)
0.5%	Nonidet-P40
0.05%	Deoxycholate

Make up to final volume with distilled water
Store at 4°C

1.9 Protein Quantification

1.9.1 BCA reagent (Sigma-Aldrich)

Reagent A: Bicinchoninic acid solution
Reagent B: Copper (II) sulphate solution
Mix Reagent A and B in a 1:50 ratio immediately before use

1.10 Electrophoresis: SDS-PAGE

1.10.1 5x Laemmli sample buffer

60mM	Tris-HCl (pH 6.8)
2%	SDS
10%	Glycerol
5%	β-mercaptoethanol
0.01%	Bromophenol blue

Make up to final volume with distilled water
Aliquot and store at -20°C

1.10.2 12% SDS-PAGE gel

1.10.2.1 Separating gel

12%	Acrylamide
0.1%	NN‟-methylenebisacrylamide
375mM	Tris-HCl (pH 8.8)
0.2%	SDS

Make up to final volume with distilled water

Just before use add:

1mM	Ammonium persulphate
0.25%	N,N,N‟N‟-tetramethylenediamine (TEMED)

1.10.2.2 Stacking gel

12%	Acrylamide
0.1%	NN‟-methylenebisacrylamide
125mM	Tris-HCl (pH 6.8)
0.2%	SDS

Make up to final volume with distilled water

Just before use add:

1mM	Ammonium persulphate
0.25%	TEMED

1.10.3 Electrophoresis buffer

25mM	Tris (pH8.3)
192mM	Glycine
0.1%	SDS

Make up to final volume with distilled water

1.11 Western Blotting

1.11.1 Transfer buffer

25mM	Tris-HCl (pH 8.3)
192mM	Glycine
20%	Methanol

Make up to final volume with distilled water
Store at -4°C

1.11.2 PBS-Tween

0.1%	Tween® 20
In	PBS (Appendix 1.6.2)

Store at 4°C

1.11.3 Blocking buffer

3%	Bovine serum albumin (BSA)
In	PBS-Tween (Appendix 1.10.2)

1.11.4 SuperSignal West Pico Chemiluminscent Substrate kit (Pearce): working solution

Before use mix:

50%	Luminol/Enhancer solution
50%	Stable peroxidase buffer

Store in the dark